Variability in the macro- and microstructure of the human brain and its importance to the investigation of neurological disorders

PhD Thesis

András Király M.D.

Szeged

2019

Variability in the macro- and microstructure of the human brain and its importance to the investigation of neurological disorders

PhD Thesis

András Király M.D.

Clinical and Experimental Neuroscience Program,

Doctoral School of Clinical Medicine,

Faculty of Medicine, University of Szeged

Supervisor:

Zsigmond Tamás Kincses, M.D., Ph.D.

Department of Neurology, Albert Szent-Györgyi Clinical Center,

University of Szeged

Szeged

2019

Table of Contents

Publications

Original publications related to the thesis

I.   **András Király**, Nikoletta Szabó, Eszter Tóth, Csete, Péter Faragó, Krisztián Kocsis, Anita Must, László Vécsei, Zsigmond Tamás Kincses: *Male brain ages faster: the age and gender dependence of subcortical volumes.*
Brain imaging and behavior. 2016 Sep; 10(3): 901-10.
IF: 3.985

II.   **András Király**, Nikoletta Szabó, Árpád Párdutz, Eszter Tóth, János Tajti, Gergő Csete, Péter Faragó, Péter Bodnár, Délia Szok, Bernadett Tuka, Éva Pálinkás, Csaba Ertsey, László Vécsei, Zsigmond Tamás Kincses: *Macro- and microstructural alterations of the subcortical structures in episodic cluster headache.*
Cephalalgia. 2018 Apr; 38(4):662-673. Epub 2017 Apr 20.
IF: 3.882

III.   **András Király**, Zsigmond Tamás Kincses, Nikoletta Szabó, Eszter Tóth, Gergő Csete, Péter Faragó, László Vécsei: Gray matter atrophy in presymptomatic Huntington's patients.
Ideggyógyászati szemle. 2016 Jul 30; 69(7-8):261-7.
IF: 0.376

IV.   Zsigmond Tamás Kincses, Nikoletta Szabó, István Valálik, Zsolt Kopniczky, Lívia Dézsi, Péter Klivényi, Mark Jenkinson, **András Király**, Magor Babos, Erika Vörös, Pál Barzó, László Vécsei: *Target identification for stereotactic thalamotomy using diffusion tractography.*
PLoS One. 2012 Jan 4; 7(1): e29969. Epub 2012 Jan 4.
IF: 3.73

Original publications not directly related to the thesis

V.   Nikoletta Szabó, Zsigmond Tamás Kincses, Árpád Párdutz, János Tajti, Délia Szok, Bernadett Tuka, **András Király**, Magor Babos, Erika Vörös, Giuseppe Bomboi, Francesco Orzi, László Vécsei: White matter microstructural alterations in migraine: a diffusion weighted MRI study.
Pain. 2012 Mar; 153(3):651-6. Epub 2012 Jan 13.
IF: 5.644

VI. Zsigmond Tamás Kincses, Eszter Tóth, Nóra Bankó, Dániel Veréb, Nikoletta Szabó, Gergő Csete, Péter Faragó, **András Király**, Krisztina Bencsik, László Vécsei: Grey matter atrophy in patients suffering from multiple sclerosis.

Ideggyógyászati szemle. 2014 Sep 30; 67(9-10):293-300.

IF: 0.343

VII. Amit Khairnar, Jana Ruda-Kucerova, Eva Drazanova, Nikoletta Szabó, Peter Latta, Anas Arab, Birgit Hutter, Paier Daniel, Havas Manfred, Windisch Alexandra-Sulcova, Zenon Starcuk Jr., **András Király**, Irena Rektorova: Late-stage alpha-synuclein accumulation in TNWT-61 mouse model of Parkinson's disease detected by diffusion kurtosis imaging.

Journal of Neurochemistry. 2015 Dec 19.

IF: 4.083

VIII. Péter Faragó, Nikoletta Szabó, Eszter Tóth, Bernadett Tuka, **András Király**, Gergő Csete, Árpád Párdutz, Délia Szok, János Tajti, Csaba Ertsey, László Vécsei, Zsigmond Tamás Kincses: Ipsilateral alteration of resting state activity suggests that cortical dysfunction contributes to the pathogenesis of cluster headache.

Brain Topography. 2017 Mar; 30(2):281-289.

IF: 3.394

IX. Péter Faragó, Bernadett Tuka, Eszter Tóth, Nikoletta Szabó, **András Király**, Gergő Csete, Délia Szok, János Tajti, Árpád Párdutz, László Vécsei, Zsigmond Tamás Kincses: Interictal brain activity differs in migraine with and without aura: resting state fMRI study.

The Journal of Headache and Pain. 2017 Dec;18(1):8.

IF: 3.580

X. Eszter Tóth, Nikoletta Szabó, Gergő Csete, **András Király**, Péter Faragó, Tamás, Spisák, Krisztina Bencsik, László Vécsei, Zsigmond Tamás Kincses: Gray matter atrophy is primarily related to demyelination of lesions in multiple sclerosis: a diffusion tensor imaging MRI study.

Frontiers in Neuroanatomy. 2017 Mar 29;11:23.

IF: 3.267

XI. Ivan Rektor, Alena Svátková, Lubomir Vojtišek, Iva Zikmundová, Jirí Vaníček, **András Király**, Nikoletta Szabó: White matter alterations in Parkinson's disease with normal cognition precede grey matter atrophy.

PlosONE. 2018 Jan 5;13(1):e0187939.

IF: 2.806

XII. Nikoletta Szabó, Péter Faragó, **András Király**, Dániel Veréb, Gergő Csete, Eszter Tóth, Krisztián Kocsis, Bálint Kincses, Bernadett Tuka, Árpád Párdutz, Délia Szok, János Tajti, László Vécsei, Zsigmond Tamás Kincses: Evidence for plastic processes in migraine with aura: a diffusion weighted MRI study.

Frontiers in Neuroanatomy. 2018 Jan 17;11:138.

IF: 3.267

Review publications

I. Kincses Zsigmond Tamás, **András Király**, Dániel Veréb, László Vécsei: Structural magnetic resonance imaging markers of Alzheimer's disease and its retranslation to rodent models.

Journal of Alzheimer's Disease. 2015;47(2):277-90.

IF**: 3.920**

II. Viola Luca Németh, Anita Must, Szatmár Horváth, **András Király**, Kincses Zsigmond Tamás, László Vécsei: Gender-specific degeneration of dementia-related subcortical structures throughout the lifespan.

Journal of Alzheimer's Disease. 2017;55(3):865-880.

IF: 3.731

Scientometry

Impact factor (related to the thesis): 11.973

Impact factor (total): 46.008

H-index: 5

Abbreviations

AD	Axial diffusivity
BET	Brain Extraction Tool
CH	Cluster headache
DOF	Degrees of freedom
DTI	Diffusion tensor imaging
FA	Fractional anisotropy
FAST	FMRIB's Automated Segmentation Tool
FDT	FMRIB's Diffusion Toolbox
FIRST	FMRIB's Integrated Registration and Segmentation Tool
FLIRT	FMRIB's Linear Registration Tool
FSL	FMRIB's Software Library
GLM	General linear model
MD	Mean diffusivity
MRI	Magnetic resonance imaging
RD	Radial diffusivity
ROI	Region-of-interest
SIENAX	Structural Image Evaluation, using Normalization, of Atrophy (single-time-point estimation)
SPSS	Statistical Package for Social Sciences
TFCE	Threshold free cluster enhancing approach
VBM	Voxel-based morphometry
Vim	Ventral intermedial nucleus of the thalamus
Vop	Ventral oral posterior nucleus of the thalamus

1. Introduction

The exact shape of every human brain - including its micro- and macroscopic features - is as unique as a human fingerprint, resulting in inter-individual anatomical variability. In the past two decades, the understanding of this variability advanced dramatically not only at the level of sulcal/gyral patterns, anatomical features (e.g. cortical thickness, volume and shape) and extent of cytoarchitectonic areas defined at the microscopic level, but also in the anatomical and functional connectivity of the brain. The core concept within the field of brain mapping is the use of a standardized 3D coordinate frame for data analysis and reporting of findings from neuroimaging experiments. This simple construct allows brain researchers to combine (even structural or functional) data from many subjects to create group-averaged signals. Also, where the signal is robust enough to be detected in individuals, it allows for the exploration of inter-individual variance in the location of that signal. Spatial standardization requires two basic components: (i) the specification of the 3D standard coordinate space, and (ii) a mapping function that transforms a 3D brain image from "native" space to that standard space. The first component is usually expressed by the choice of a representative 3D MR image that serves as target (template or atlas). The native image is re-sampled to standard space under the mapping function that may have few or many degrees of freedom, depending upon the experimental design. The optimal choice of atlas template and mapping function depends upon considerations of age, gender, hemispheric asymmetry, anatomical correspondence, spatial normalization methodology and disease-specificity (1).

In our studies we investigated some of these aspects, e.g. 1) how gender and normal aging influences brain morphology, 2) how normal hemispheric asymmetry plays a role in lateralized neurological diseases, such as cluster headache, 3) how progressive neurodegenerative disorders, such as Huntington's disease affect the brain structure, or 4) how we can deal with inter-individual variability in case of neurosurgical interventions, such as thalamotomy in the therapy of medication resistant tremor.

1.1. *Gender differences*

Several normal functions and disorders of neuropsychiatric and developmental origin – e.g. motor control (2, 3), emotional memory (4), addiction (5, 6), attention deficit hyperactivity disorder (ADHD) (7), Parkinson's disease (8-10), Alzheimer's dementia (11), headache disorders (12), multiple sclerosis (13), major depression and bipolar disorder (14) or suicidal

behavior (15) - manifest differently in males and females. Because cognitive processes are rooted in neuronal architecture, the identification of neurological structures underlying sexually dimorphism may provide important insight into disease etiology and potential targets for treatment (16, 17). Accordingly, the sexual dimorphism of the human brain anatomy has gained attention with neuroimaging methods being widely used to detect these differences (18-21). Whereas studies are converging upon males having larger absolute cerebral volume and head size (16, 22-26) and females generally have a thicker cortex in several regions of the brain (23, 27).

There is much less evidence on the sexual dimorphism of subcortical gray matter (GM) structures including the amygdala, caudate nucleus, accumbens, hippocampus, amygdala, pallidum, putamen and thalamus (28, 29). Considering that basal ganglia nuclei possess a high density of sex steroid receptors (for reviews, see: (30), (31)), the effect of gender on the volume of these structures might be crucial. Nevertheless, results are somewhat contradictory, with several studies reporting larger volumes of the caudate nuclei (32), hippocampus (33) and thalamus in females (33, 34), and some with opposing results (35, 36). The amygdala (37), pallidum and putamen (36) have been consistently found to be larger in males.

1.2.   *Aging*

Even in a cognitively normal, „healthy" brain, a variety of underlying neurodegenerative processes may be present (38), which may cause small, but detectable differences on MRI that could suggest e.g. increased risk for later cognitive decline (39, 40). Detecting these subtle differences and relating them to physical or cognitive (dys)functions during the aging process will allow us to understand the biological basis of differences in normal aging of the brain. Numerous cross-sectional MRI studies have characterized age-related differences in regional brain volumes that differ with structure and tissue type. In general, recent research evidences are consistent in reporting that "normal" aging is associated with the enlargement of cerebro-spinal fluid (CSF) filled structures and decreased whole-brain and gray matter volumes (which is more prominent in the cortical and allocortical gray matter than in the centrum semiovale or callosal white matter), as well as thinner cortical gray matter in several regions (mainly in the frontal and temporal lobe) (23, 24, 41-55). However, age-related shrinkage of selective subcortical structures is more controversial, e.g. (35, 43, 51, 56-59). Studies investigating the effects of aging on white matter (WM) volume are inconsistent: some studies did not find a significant effect of aging on WM changes (43, 48), while others

reported an increase in volume until middle adulthood, followed by a decline (41, 42, 49, 55) and yet others concluded that there was a steady decline with progressing age (44, 60, 61). Two studies using voxel-based techniques that reported no overall significant effect of aging on WM volume did reveal a decline with age in some areas (43, 48).

The combined effects of age and gender on the human brain have been assessed suggesting a more profound decline in GM volume in males (42, 46, 48, 62). However, research evidence is inconsistent on one hand (60) and sparse on the other, especially considering subcortical GM structures. Discrepancies between studies could be due to using different age ranges or different sample sizes, as well as using different image processing and statistical (mostly univariate) methods. Most of the studies focusing on subcortical nuclei applied a voxel-based morphometric approach to identify gender differences. The segmentation approach based on deformable surface models offers advantages over intensity-based procedures, especially in regions with low tissue contrast. While age, gender and head size (intracranial volume) are the most commonly included "nuisance" variables when performing neuroimaging analysis, studies vary as to which of these variables are included and which method is used for correction (63).

In our first study, we investigated the effect of aging and gender on the size of the subcortical structures with special attention to the interactions of those factors.

1.3. *Lateralization*

The asymmetry of inter-regional structural connectivity (even large-scale connection patterns or small-world attributes) in the two hemispheres is an important topic in the study of the neural basis of brain functional asymmetries. We know that in some neurological disorders symptoms occur only on one side of the body or start on one side and propagate to the other with time. A typical example for the first case is cluster headache and Parkinson's disease best represents the second. In neuroimaging studies investigating unilateral processes - to boost the number of observations - it is common to flip the data about the midsagittal axis to have hemispheres/structures aligned according to the affected side (64-66). This approach is used despite evidence that there is a normal asymmetry in white matter diffusion parameters (67). Previously asymmetry was most consistently found in the arcuate fasciculus and in the cingulum (67-69). Similarly, the diffusion parameters of subcortical structures were reported to be asymmetric in healthy subjects (70).

Neuroimaging studies have demonstrated structural alterations in the striatum and the thalamus in chronic pain syndromes (71), migraine (72) and cluster headache (73). These disease-related structural alterations could possibly be captured as size changes or as disintegration of the highly organized microstructure. The latter makes them readily available to study with diffusion weighted MRI. The two features might show parallel alterations, but since the histological background of diffusion alterations in the gray matter is not well understood, independency of micro- and macrostructural alterations may also occur. The basal ganglia and subcortical structures in general have recently been proposed to have a central role – among others - in nociception. The facts that they receive input directly from the spinal cord and also via the thalamus and exhibit connections with various cortical regions involved in pain processing suggest that this system is ideal for the integration of various aspects of pain-related information (for an in-depth review, see (74) and (75)). Furthermore, it has been shown that basal ganglia structures are activated during painful stimuli (76) and putaminal and pallidal neurons are able to encode the intensity of noxious thermal stimuli (77, 78). Putaminal lesions were also shown to alter the processing of nociceptive information (79).

In our second study, we investigated the normal and altered lateralization in the diffusion data of subcortical gray matter structures through episodic cluster headache (CH), which is a primary headache disorder with prominent features including extremely severe unilateral, periorbital headache attacks accompanied by ipsilateral autonomic symptoms and occurring in clusters usually lasting some weeks, followed by much longer headache-free periods (80, 81).

1.4. *Huntington's disease*

Huntington's disease (HD) is a neurodegenerative disorder with autosomal dominant inheritance. The expansion of CAG triplets in the Huntingtin gene (IT15), which is coded on the 4th chromosome, causes loss of neurons mainly in the striatum. Although the exact behavior of the mutated Huntingtin protein is not completely understood, it seems that toxic (or ineffective defensive) mechanisms, which may already start to operate in the intrauterine life (82), are in the background of this cell loss. Early symptoms are attributable to the function and connections of the striatum (movement control, mood, higher cognitive functions) (83-87). Symptom onset, which is heavily dependent on the number of CAG repeats, usually happens during mid-adulthood (88), but neurodegenerative changes begin

years earlier (82, 89, 90). Diagnosis is based on the symptoms and the family history confirmed by genetic testing. The length of CAG repeats accounts for 60% of the variation in the time of symptom onset and the rate of progression. A longer repeat results in earlier onset and a faster progression of symptoms (91). The remaining variation is due to environmental factors and other genes that influence the mechanism of the disease. With medical imaging techniques, such as CT and MRI, atrophy of the caudate nuclei in the early, and cerebral atrophy in the advanced stages of the disease can be seen. However information about the pattern of the atrophy is very sparse (92-105).

In our third study, we investigated the rate of brain atrophy over 24 months in presymptomatic Huntington's patients.

1.5. *Inter-individual variability*

Replacing selective stereotactic lesioning, electrical stimulation of the ventral intermedial nucleus of the thalamus (*Vim*) is used in the treatment of medication resistant tremor nowadays. In the ideal case, this procedure is performed under local anesthesia, with the patient awake. After the patient's head is secured in a metal frame, the surgeon maps the patient's brain to locate the thalamus. A small hole is drilled through the skull and a temperature-controlled electrode is inserted into the thalamus. A low-frequency current is passed through the electrode to activate the tremor and to confirm proper placement (106-108). In the case of lesioning, once the site has been confirmed, the electrode is heated to create a temporary lesion. Testing is done to examine speech, language, coordination, and tremor activation, if any. If no unwanted effect occurs, the probe is heated again to create an about 3-mm permanent lesion. The probe, when cooled to body temperature, is withdrawn and the skull hole is covered. Ideally, the lesion causes the tremor to permanently disappear without disrupting sensory or motor control.

Precise targeting within the brain is of crucial importance for successful surgical intervention. Targeting the desired thalamic nucleus is usually carried out by using stereotactic coordinates, specified in relation to a point on the anterior commissure – posterior commissure (AC-PC) line (109-111). Other methods try to establish population-based stereotactic coordinates of the target nuclei based on postmortem histological data or intraoperative stimulation techniques (106-108). While achieving reasonable results, these methods neglect individual anatomical variations. Since the identification of thalamic nuclei on conventional imaging modalities is difficult, several novel approaches were proposed to

aid the visualization of the functionally important thalamic nuclei. It is now possible to segregate major thalamic structures using MR relaxometry, even in a clinically acceptable time window (112, 113). Recently, probabilistic tractography was successfully used to investigate the connectivity profile of two major thalamic target nuclei for functional neurosurgery: the ventral intermedial (*Vim*) and ventral oral posterior nuclei (*Vop*) (114). In addition, it is possible to segment thalamic nuclei based on connectivity patterns defined by MR diffusion tractography (115, 116).

In our fourth study, we investigated the normal spatial variability of thalamic nuclei targets for functional neurosurgery.

1.6. *Methodological overview*

1.6.1. *Volume measurement*

During the last decades, magnetic resonance imaging (MRI) has become the method of choice for the examination of macroscopic neuroanatomy *in vivo*, due to excellent image resolution and between-tissue contrast. In brain imaging, the precise and quantitative measurement of the volume and shape of brain compartments is important, as well as measuring the temporal evolution of these parameters. However, achieving accurate and robust segmentation of cortical and subcortical areas is a great challenge for both manual and automated methods. There are two primary methods for manual quantification of brain compartment volume, namely stereology in conjunction with point counting (117, 118) and tracing methods (119). In case of stereology, a set of parallel and equidistant MR images of the brain is randomly selected, and the area of interest is directly estimated on each image by randomly superimposing a grid of points, and subsequently counting the number of points that fall within the region of interest. Rather than counting the number of points within the structure transect area, tracing methods require the investigator to trace the brain region of interest using a mouse driven cursor throughout a defined number of MR sections. The transect areas, determined by pixel counting within the traced region, are summed and multiplied by the distance between the consecutive sections traced to estimate the volume. Unlike manual quantitative region of interest methods, semi-automated and automated methods do not require manual delineation of brain structures through determined number of MR sections. Although these methods sometimes use different mathematical approaches for the same purpose, they also share some common features, such as various geometric parameters with reference to a stereotaxic template for spatial normalization, and either a

combination of between-tissue signal intensity differences and reference to a stereotaxic template or just signal intensity differences for segmentation. These spatial transformations enable cohort comparisons given that homologous brain regions can be compared between brains, or between hemispheres in analyses of cerebral asymmetry. Also, various methods have been proposed and implemented for cross-sectional (single time point) or longitudinal (multiple time points) analysis of brain atrophy (changes in brain size and shape). Cross-sectional methods work by measuring brain tissue volume (usually white and gray matter together) and comparing this against a normalization volume (either brain tissue plus cerebrospinal fluid (CSF) volume, or intracranial volume). Longitudinal methods typically align two scans separated in time and find regions of change.

Nowadays, there are many software packages available (e.g. FSL, FreeSurfer, SPM, AFNI, 3D Slicer, BrainSuite, Caret, ExploreDTI, NITRC, LONI Pipeline etc.) for quantitative image analysis. In our studies we used the automated methods (FIRST, SIENAX and VBM) included in FSL (FMRIB's Software Library), because they are widely used, well documented, multiplatform and sufficiently accurate and robust. They also support parallel computing, and are freely available.

For brain and non-brain tissue segmentation, SIENAX (120, 121) uses a deformable model (spherical tessellated surface) that evolves to fit the brain's surface by the application of a set of locally adaptive model forces, followed by intensity based tissue segmentation.

For analyzing voxel-wise differences in local gray matter volume/topography between populations, voxel-based morphometry (VBM) (43, 122) takes one step forward by registering the previous segmented images onto a standard space template image (MNI152, included in FSL). Tissue types are segmented, and finally, voxel-wise statistics are used to analyze the tissue probability according to the predefined model (e.g. patients vs. controls). This analysis requires no *a priori* information about the location of the possible differences.

For the segmentation of the subcortical gray matter structures, FIRST (123) utilizes the principles of the Active Shape and Appearance Models but places them within a Bayesian framework, allowing probabilistic relationships between shape and intensity to be fully exploited. The model is trained for 15 different subcortical structures using 336 manually labeled T1-weighted MR images (for details please see in sections *5.1* and *5.2*).

In our fourth study, we investigated partial brain volumes (atrophy) in Huntington's disease patients, using these approaches.

1.6.2. Diffusion tensor imaging

Diffusion-weighted imaging (DWI), which is based on Brownian motion of water molecules, has been in clinical use for more than two decades. It was originally focused on stroke imaging; however, the modality has evolved rapidly, gaining numerous clinical applications in neuroradiology and beyond. Diffusion-tensor imaging (DTI) is a recent application of diffusion imaging and is a non-invasive method for investigating the anatomical features of the white matter tracts.

Diffusion can be measured with a simple spin echo MRI sequence. Spins are flipped to the transversal plane and at half of the echo time another 180 degree refocusing pulse is applied that flip the direction of the precession. If spins precess with different speeds in a given voxel they gradually dephase, but if the refocusing pulse is applied at the echo time the spins are aligned again and the signal is maximal. However, if a spin is diffusing along a magnetic gradient (applied by gradient coils) during the diffusion experiment, the speed of precession will change and the signal will be submaximal at echo time. With this simple experiment, diffusion can be measured along the applied magnetic gradient. By repeating the experiment with different magnetic gradients, the diffusion ellipsoid can be mapped. Importantly, by selecting the diffusion time appropriately we can measure diffusion in a spatial range that approximates the distance of microscopic particles that hinder the diffusion. With this approach, even though the spatial resolution of the image is in the millimeter range, we gain information about the tissue microstructure.

The ellipsoid surface that describes the diffusion has a principal long axis and two small axes that describe its width and depth. All three of these are perpendicular to each other and cross at the center point of the ellipsoid. The directions and the lengths of the axes can be estimated with a simple mathematical algorithm (singular value decomposition). We call the axes in this setting eigenvectors and their lengths are the eigenvalues. The lengths are symbolized by the Greek letter λ. Since the diffusion is not hindered significantly along the axons, the longest vector is parallel with the main fiber direction (λ_1 – axial/parallel diffusivity or AD). The two smaller vectors, perpendicular to the longest, will have lengths λ_2 and λ_3 (radial or perpendicular diffusivities). The diffusivities in the two minor axes are often averaged to produce a measure of radial diffusivity ($\lambda_\perp$ or RD):

$$RD = \frac{\lambda_2 + \lambda_3}{2}$$

Mean diffusivity (MD) or apparent diffusion coefficient (ADC) – which summarizes the total diffusivity – is the average of the 3 main diffusion directions:

$$MD = \frac{\lambda_1 + \lambda_2 + \lambda_3}{3}$$

This measure is higher if water particles can diffuse in longer distances in every direction of the sphere (like diffusion in cortex compared to diffusion in cerebro-spinal fluid (CSF)). From the diffusion tensor, fractional anisotropy (FA) can be calculated, representing the local integrity of white matter:

$$FA = \sqrt{\frac{1}{2}} \frac{\sqrt{(\lambda_1 - \lambda_2)^2 + (\lambda_2 - \lambda_3)^2 + (\lambda_3 - \lambda_1)^2}}{\sqrt{\lambda_1^2 + \lambda_2^2 + \lambda_3^2}}$$

Fractional anisotropy (FA) is approximately 1 for anisotropic (ellipsoid, radial diffusivity relatively smaller than axial) and zero for isotropic (spherical, equal in all directions) diffusion. Diffusion-weighted and diffusion tensor imaging are based on the simplified premise of Gaussian distribution of water molecule diffusion in biological systems. In reality, the complex intra- and extracellular environment causes the diffusion of water molecules to deviate considerably from this pattern. The alteration of this normative pattern is called kurtosis. In diffusion kurtosis imaging this variation (non-Gaussian distribution in diffusion) is taken into account with more accurate models to describe tissue heterogeneity (124).

1.6.3. Probabilistic tractography

As described above, diffusion has direction in well-structured tissues, such as the white matter. Since membranes hinder diffusion, its magnitude is relatively small perpendicular to the main fiber direction, but unaltered parallel to it. With diffusion MRI the main direction of diffusion can be determined in each voxel as the largest diffusion that represents the main fiber direction. By tracing the vectors of the main diffusion direction, white matter tracts can be mapped. Tractography methods can reconstruct an entire white matter pathway (125, 126) based on the alignment of the dominant orientation of local water diffusion, which represents the mean orientation of white matter fibers from voxel to voxel (127).

There are various tractography algorithms, but probabilistic approaches are particularly attractive because they generate probabilistic maps of fiber connectivity between brain regions and can trace pathways into gray matter (128, 129). In case of probabilistic tractography the posterior probability distribution on the main diffusion direction is estimated at each voxel. The width in this distribution represents uncertainty in diffusion direction, which is due to factors such as the potential co-existence of many fiber directions within a voxel, image noise and subject motion in the scanner. The probabilistic tractography algorithm produces a likelihood map of the diffusion path between two ROIs (region-of-interest, seed/initial and target regions) by incorporating the uncertainty of the diffusion direction. Rather than delineate a single best path (like streamline tractography does), the likelihood map shows the probability that a particle diffusing between ROIs goes through each voxel. By tracing and superposing a tract between two points several thousand times one can infer the probability of the two points being connected and the probability of the path crossing a particular voxel in the brain.

An interesting application of probabilistic tractography is the connectivity-based segmentation of subcortical structures, which was first described Behrens and Johansen-Berg (115). In their approach, the probability of connection of every thalamic voxel to 10 cortical target regions was estimated. The connectivity pattern of the thalamus corresponded well with its known microscopic internal structure.

2. Objectives

The aim of this thesis was to investigate the effects of age, gender, normal hemispherical lateralization and inter-individual variability on the structural properties of the brain through our neuroimaging studies about healthy subjects (130) and patients with cluster headache (131), medication resistant tremor (132) and Huntington's disease (133). We also present retrospective identification of the target thalamic nuclei in four patients who underwent stereotactic *Vim* and *Vop* thalamotomy.

3. Participants

3.1. *Brain atrophy in presymptomatic Huntington's disease*

Seven presymptomatic HD mutation carriers (mean age at baseline: 36.43±10.29) and ten healthy control subjects (mean age: 37.1±9.23) were recruited. Data from six patients were available for the longitudinal analysis. MRI measurements were repeated three times:

baseline, 12 and 24 months. Patients had no motor symptoms (as measured with the motor section of the Unified Huntington's Disease Rating Scale) or cognitive disturbance over the period of the study (as measured by Mini Mental State Examination, Digit Span Test, Backward Digit Span, Listening Span Task, and Semantic Fluency Task). The controls had no neurological or psychiatric disorders.

Demographic and cognitive data are presented in **Table 1/a and b.**

	Huntington's patients	Healthy subjects
Age (mean years ± SD)	36.43 (±10.29)	37.1 (±9.23)
N (male)	7 (4)	10 (4)
CAG repeat number (range)	42.29 (37-50)	N.A.
UHDRS	0	N.A.

Table 1/a. Demographic and clinical data of subjects.

	1st year	2nd year	Difference (p<)
Digit Span	6.50 (±1.04)	6.83 (±1.69)	0.360
Corsi Block Tapping	5.33 (±1.36)	4.83 (±0.41)	0.450
Backward Digit Span	5.16 (±0.989)	5.00 (±1.41)	0.740
Listening Span	3.55 (±1.02)	3.49 (±0.69)	0.810
Letter fluency	13.75 (±4.29)	14.5 (±4.96)	0.650
Semantic fluency	24.42 (±4.68)	24.58 (±4.39)	0.900

Table 1/b. Cognitive performance of the patient population.

3.2. *Subcortical gray matter structures in healthy subjects*

3.2.1. Gender differences and Aging

Fifty-three healthy males (mean age: 31.08±10.03 years) and fifty age-matched healthy females (mean age: 33.00±11.34 years) with no history of any neurological or psychiatric disorder were included in the study.

Demographic data are presented in **Table 2.**

	Male	**Female**
N	53	50
Age (years, mean ± SD)	31.08±10.03	33.00±11.34
Left handed	6	7

Table 2. Demographic data of subjects.

3.2.2. Lateralization

Ninety-four healthy individuals (mean age: 32.59±10.43, male: 50) were included in the study. Inclusion criteria for the controls were: 18-80 years of age, no history of neurological (including primary headaches, other pain conditions) or psychiatric diseases. All the participants were right handed.

3.2.3. Inter-individual variability in the position of thalamic nuclei

Nine healthy individuals, with no history of neurological or psychiatric diseases were included in the study (mean age: 28.36±7.09, male: 3). Furthermore, four patients were also included, who underwent stereotactic thalamotomy (for results, see the case reports).

3.3. *Subcortical gray matter structures in cluster headache*

Inclusion criteria for the CH patients were: 18-80 years of age, primary CH according to The International Headache Society diagnostic criteria (80), no interval therapy for the CH, no accompanying neurological (including other primary headache disorders and pain conditions) or psychiatric disease, no regular neuro-psychiatric medication, negative routine MRI scan. Special attention was paid to the exclusion of depression, for which the Hamilton questionnaire was used (>16 points was the exclusion criterion) (134). There were 12 left-headache-sided (*LHS-CH*) and 10 right-headache-sided patients (*RHS-CH*) in the CH group. All the participants were right-handed.

Twenty-seven cluster headache (CH) patients were recruited into the study. Five patients were excluded due to comorbidity (depression, benign tumor), cessation of pain after tooth extraction (e.g. secondary cluster headache), and structural abnormality on the MRI scans. In the and, twenty-two patients were included (mean age: 38.10±11.33, male: 19).

Clinical variables, such as disease duration, time between bouts and average length of bouts were recorded for all patients. Furthermore, cumulative number of headache days – that is the total number of days the patient had experienced cluster headache over his/her entire life – was estimated for all the patients.

Control group was the same as the one used for the investigation of lateralization in subcortical gray matter structures.

Demographic data are presented in **Table 3.**

	Cluster headache patients		
	All	**LHS**	**RHS**
N (male)	22 (19)	12 (11)	10 (8)
Age (years, mean ± SD)	38.10 (±11.33)	36.96 (±11.64)	38.81 (±10.39)
Handedness (left)	0/22	-	-
Disease duration (years, mean ± SD)	7.41 (±6.20)	-	-
Lifetime attack number (days, range)	15-910	-	-

Table 3. Demographic and clinical data of subjects.

All studies were approved by the Ethics Committee of the University of Szeged (authority number: 87/2009), and all subjects provided their written informed consent.

4. Image acquisition

Imaging was carried out with a 1.5 T GE Signa Excite MRI scanner.

High-resolution axial T1-weighted images (*3D IR-FSPGR*: TR/TE/TI: 10.3/4.2/450 ms, flip angle: 15°, FOV: 25*25 cm, matrix: 256*256, slice thickness: 1 mm, ASSET: 2) and diffusion-weighted images (*DTI*: 60 direction diffusion-weighted images with 6 non-diffusion-weighted reference volumes. TR/TE: 13500/93.8 ms, flip angle: 90°, FOV: 23x23 cm, matrix: 96x96, in-plane resolution: 2.4x2.4 mm, which was resampled to a 0.89x0.89 mm by the scanner, slice thickness: 2.4 mm, b: $1000s/m^2$, NEX: 2, ASSET: 2) were acquired from all the participants.

In case of cluster headache patients, MR image acquisition took place at least one month after the end of the last headache bout.

In case of patients with tremor undergoing thalamotomy the preoperative scans were obtained using identical acquisition sequences to those used for control subjects. Postoperative scans were carried out three months after the surgery. High-resolution-T1 weighted images (with parameters identical to the preoperative ones) and sagittal 3D FLAIR images (*3D FLAIR*: TR/TE/TI: 6000/134.6/1839 ms, flip angle: 90°, FOV: 23*23 cm, matrix: 256*256, slice thickness: 2 mm) were acquired to localize the thalamotomy lesion.

5. Image processing

Tools from the FMRIB Software Library (FSL, version 5.0; Oxford Centre for Functional MRI of the Brain (FMRIB), UK; www.fmrib.ox.ac.uk/fsl) were used for data processing (135).

5.1. *Partial brain volumes*

Total intracranial volume, as well as the gray and white matter volumes, was estimated by SIENAX (120, 121). SIENAX starts by extracting brain and skull images from a single whole-head input data (136). The brain image is then affine-registered to MNI152 space (137, 138) (using the skull image to determine the registration scaling); this is primarily carried out in order to obtain the volumetric scaling factor (*v-scale*), to be used as normalization for head size. Next, tissue-type segmentation with partial volume calculation is carried out with FAST (139) in order to calculate the total volume of brain tissue (including separate estimates of volumes of gray matter, white matter, peripheral gray matter and ventricular CSF).

5.2. *Cortical thickness*

We employed an "optimized" VBM-style protocol (43, 122) using FSL (135). Non-brain parts were removed from all structural images (136), and tissue-type segmentation was carried out by FAST4 (139). The resulting GM partial volume images were registered to a standard space (MNI152) using linear transformation (138), followed by a non-linear registration. The resulting images were averaged to create a study-specific template, to which the native GM images were then nonlinearly re-registered. The registered partial volume images were then modulated (to correct for local expansion or contraction) dividing by the Jacobian of the warp field. The modulated segmented images were then smoothed with an

isotropic Gaussian kernel with a sigma of 2 mm in the case of group comparison. Finally, voxel-wise General Linear Model (GLM) was applied using permutation-based non-parametric testing. The model coded group membership to identify Huntington's disease related brain atrophy. Thresholding was carried out by a novel method called threshold-free cluster enhancement (TFCE) (140).

5.3. *Volumes of subcortical gray matter structures*

For comparisons of subcortical structure volumes between groups, FIRST analysis (123) was used. FIRST is a model-based segmentation/registration tool. This approach uses deformable surface meshes specific to subcortical structures (amygdala, caudate nucleus, hippocampus, pallidum, putamen and thalamus). Based on previously learned models, FIRST searches through linear combinations of shape modes of variation for the most probable shape instance given the observed intensities in a T1-weighted image. The nucleus accumbens was not investigated due to inappropriate segmentation.

5.4. *Diffusion parameters of subcortical gray matter structures*

In order to evaluate the internal microstructure of subcortical gray matter structures, diffusion parameters were estimated for each and compared between two groups. Initially, the raw diffusion data were corrected for eddy currents and motion artifacts with FDT (128) by 12 degrees-of-freedom affine linear registration to the first non-diffusion-weighted reference image (138). Diffusion tensors were fitted at each voxel. Fractional anisotropy (FA), mean diffusivity (MD), and diffusivity parallel (AD, axial) and perpendicular (RD, radial) to the principal diffusion direction were computed in every voxel of the brain. Each subjects' binary masks of subcortical structures segmented by FIRST were registered with FLIRT (138) to the subjects' own DWI images with 6 degrees-of-freedom (rotations and translations only). The transformed masks were thresholded at 0.5 and binarized again to avoid size increment due to registration. All registered images were then checked visually and corrected so as not to contain parts of ventricles or white matter tracts close to the subcortical structures. Average diffusion parameters were calculated under the masked areas.

5.5. *Probabilistic tractography*

The initial pre-processing steps for diffusion-weighted data are the same as described in section *5.3*. The images were then skull stripped using the BET (136) and the diffusion-

weighted images were registered to the high-resolution T1-weighted image with a 6 degree-of-freedom linear registration using FLIRT (138). Probability distributions of fiber orientation were estimated for each brain voxel in the acquired diffusion space using a multi-fiber extension (141) of the probabilistic tractography available in FDT (128).

Binary masks of the thalamus and the cortical targets were drawn manually for each subject. Probabilistic multi-fiber diffusion tractography was initiated 5000 times from every voxel inside the thalamic mask. Counters were increased every time an individual streamline reached the cortical target region. Hence, the values stored in thalamic voxels in one of the resulting images represent the probability of those voxels being connected to the particular target cortical mask assigned to that image (115). To investigate the inter-subject variability of the target nuclei, a specific distance reserving registration method was used: the high-resolution T1-weighted images were registered to the standard MNI brain with a 6 degree-of-freedom transformation that was based on landmark points in a way that kept the position of the anterior commissure fixed, while aligning the AC-PC line and the mid-sagittal plane between images. We also took further steps to exclude possible registration bias between the DTI and T1-weighted images that might originate from the EPI distortions. We manually compared the high-resolution T1-weighted image and the first volume of the diffusion data (no diffusion gradient applied) registered to the T1-weighted image for each subjects. The positions of the following landmarks were compared: AC, PC, the maximal width of the third ventricle at the level AC and the highest point of the corpus callosum in the midsagittal line.

In case of the patients going through thalamotomy, post-operative FLAIR images were registered and transformed to the preoperative T1-weighted structural image with 6 degrees-of-freedom linear registrations to overlay the lesion on the generated segmented thalamus to reveal correspondence between the location of the surgical lesion and the predicted *Vim* nucleus. As shown by the connectivity-based segmentation of the thalamus, regions connected with highest probability to the prefrontal, premotor, primary motor and sensory, parietal, occipital and temporal cortices were clearly delineated first. Ideally, the operative lesion of the thalamus, identified on the post-operative FLAIR images should have been situated in the region of the thalamus connecting to the premotor cortex with the highest probability (**Figure 1**).
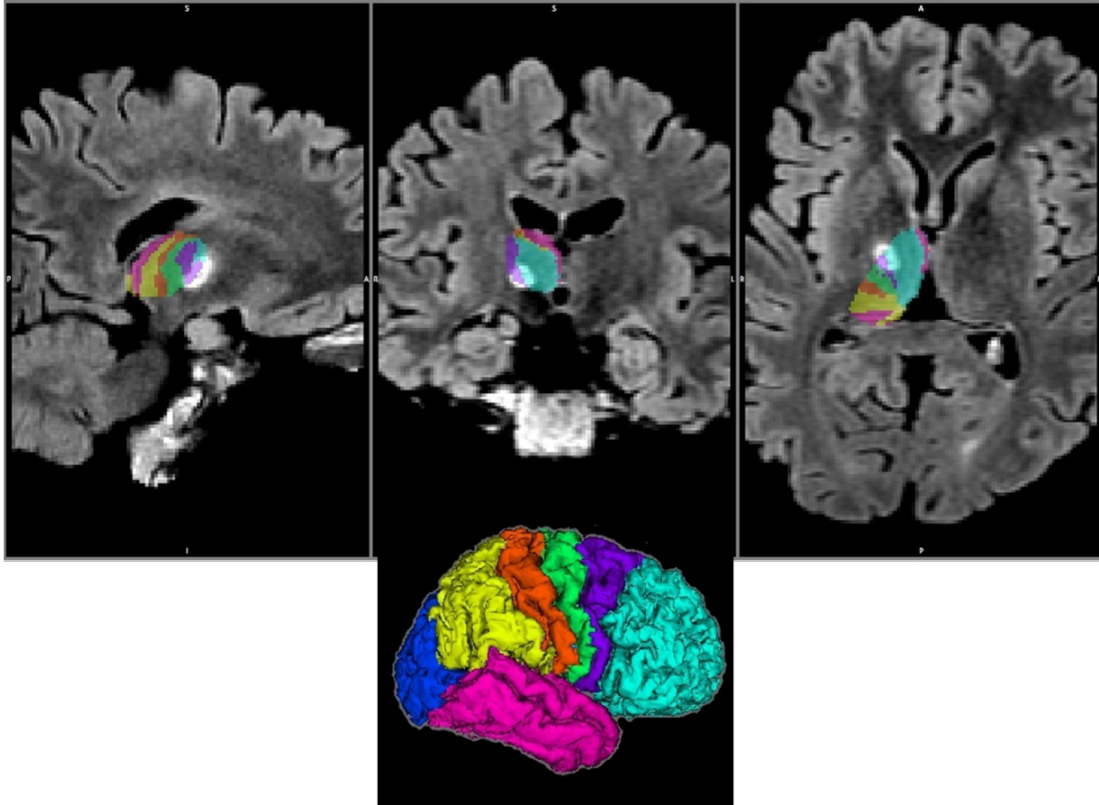
Figure 1. Connectivity-based segmentation of the right thalamus. Results are overlaid on the post-operative FLAIR images. The color in each thalamic voxel represents the color of the cortical area that has the highest connection probability to that voxel (light blue – frontal, purple – premotor, green – primary motor, orange – primary sensor, yellow – parietal, dark blue – occipital and dark-pink – temporal cortex).

6. Statistics

6.1. *Brain atrophy in presymptomatic Huntington's disease*

Voxel-wise General Linear Model (GLM) was applied using permutation-based non-parametric testing (5000 random permutations). The ANCOVA style GLM design used for VBM analysis coded for time point and gender. Thresholding was carried out by the method of threshold-free cluster enhancing technique (TFCE) (140). Results were corrected for multiple comparisons and p<0.05 was chosen as the significance threshold.

6.2. *Subcortical gray matter structures in healthy subjects*

6.2.1. *Gender differences and aging*

Raw volumes, volumes normalized to head size, and the diffusion parameters of subcortical structures were compared between groups. The output volumes of FIRST were multiplied by the *vscale* factor from SIENAX, obtaining normalized GM volumes of subcortical structures -

as if skull size was identical for all participants. Mean diffusion parameters were estimated for each segmented subcortical structure.

Multiple univariate analysis of variance with age as covariant (MANCOVA) was applied for statistical analysis (IBM SPSS Statistics 20).

Correlations between volumes of subcortical structures, gray/white matter ratio, partial brain volumes and age were calculated for both groups (IBM SPSS Statistics 20). The differences between groups in correlations with age were calculated with Fisher's r-to-z transformation. The results were Bonferroni-corrected (p_{corr}) and $p < 0.05$ was chosen as the significance threshold.

6.2.2. Lateralization

Left-right ratios of the size and diffusion parameters of the subcortical structures were estimated as the ratio of the left and right side parameters. A ratio above 1 indicates larger, while below 1 indicates smaller structures or diffusion parameters on the left. One sample t-test was used to test lateralization. The results were tested with a bootstrapping method described below in section 6.3.

6.2.3. Inter-individual variability in the position of thalamic nuclei

The Euclidean distance, given by the equation:

$$d(p,q) = \sqrt{\sum_{i=1}^{3}(q_i - p_i)^2}$$

was calculated for each subject between points representing the thalamic voxel with peak connection probability to the premotor cortex (for *Vop*), to the motor cortex (for *Vim*) and the standard space voxel with peak connectivity as indicated by the Oxford Thalamic Connectivity Map (116). The mean pair-wise distance was also calculated: the distance between the voxel with peak connection probability to the premotor (for *Vop*) and to the motor (for *Vim*) cortex was calculated between all possible pair of subjects and this inter-subject distance was averaged for *Vop* and *Vim* separately.

The connectivity images for the thalamus were thresholded at 10% of individual connectivity maximum and binarised in order to create masks of the thalamic regions connected to the premotor or motor cortex. To assess the similarity of positions the overlap between each pair

of masks (between subjects) were calculated according to the method proposed by Crum and colleagues (142). Overlap was measured by the Tanimoto Coefficient (TC), which is defined as the ratio of the number of voxels in the intersection of the two regions to the number of voxels in the union:

$$TC = \frac{N(A \cap B)}{N(A \cup B)}$$

### 6.3. *Subcortical gray matter structures in cluster headache*

The group differences (t_0, p_0) were evaluated by using a standard general linear model (GLM), where the model was encoding group membership. While our analysis in healthy controls found no gender or age effect in case of the diffusion parameters (see below), these two variables were included in the analysis to account for the theoretical effect. The solution of the regression model was estimated by ordinary least squares approach. Since the number of subjects in the control and patient groups differed significantly a bootstrap approach was used to confirm the stability of the findings (143). 5000 bootstrap samples were randomly drawn from each group by the size of the patient population ensuring that the size of the two compared groups are always the same. The parameter (t_B) of the GLM model was estimated for every bootstrap sample (t_{B1}-t_{B5000}), and then its mean was calculated ($\hat{t}$). The confidence interval for the bootstrapped t-values ($\hat{t}(CI)$) was used to perform an approximate two-sided test of the null hypothesis:

$$H_0: t_0 \in \hat{t}(CI).$$

The null hypothesis was to be rejected, and hence the original, non-bootstrapped parameter (t_0) was not from the bootstrapped distribution on the significance level of 0.05 if (t_0) laid outside the two-tailed ($1-\alpha$) confidence interval ($\hat{t}(CI)$). (**Figure 2.**)

A similar approach was used for the correlations between clinical variables, volumes and diffusion parameters (the correlation coefficient, *r* was used in the bootstrap resampling).
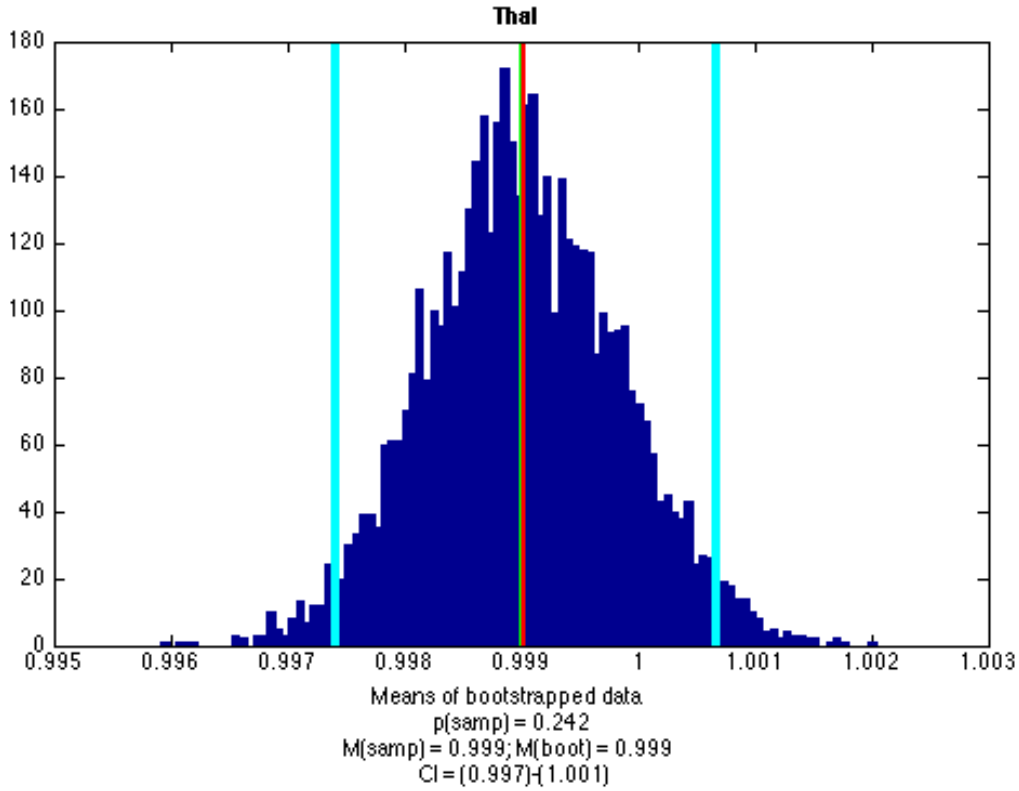
Figure 2. Bootstrapping. Color code: dark blue = 5000 bootstrap sample (t_{B1}-t_{B5000}), red - mean t-value for the original sample (t_0), green - mean of the bootstrapped distribution ($\hat{t}$), light blue - confidence interval of the bootstrapped distribution ($\hat{t}(CI)$).

7. Results

7.1. *Brain atrophy in presymptomatic Huntington's disease*

With VBM analysis, gradual gray matter atrophy was observed in the bilateral frontal regions, the temporal and insular cortices and in the anterior and posterior cingulate cortices during the two years of the investigation (**Figure 3**). With regards to the subcortical structures, the gray matter density of the head of the left caudate nucleus was reduced during the study period.
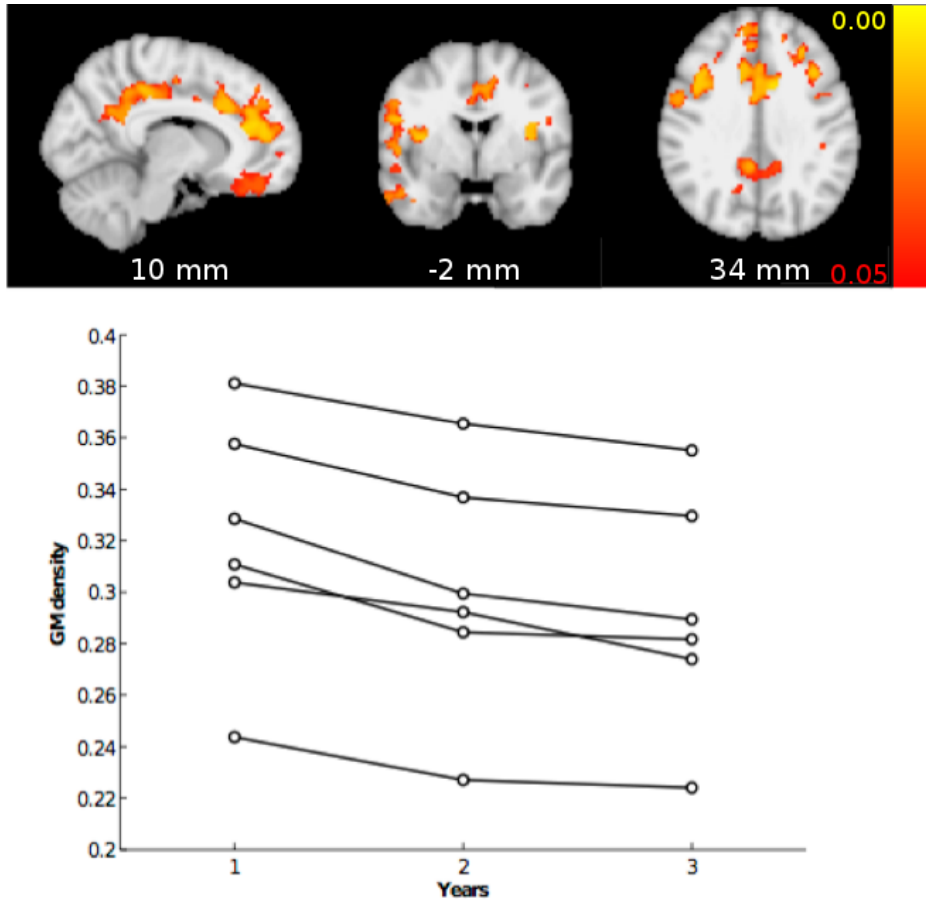
Figure 3. Gray matter atrophy in preclinical Huntington's disease during a two-year follow-up. Red-to-yellow colors indicate p-values (TFCE, corrected for multiple correlations). The graphs depict the voxel densities in each of the individual patients during the three consecutive years, at a frontal location of x = –28 mm, y = 20 mm, z = 4 mm.

7.2. *Subcortical gray matter structures in healthy subjects*

7.2.1. *Gender differences*

MANCOVA (mean age of comparison = 32.02 years) revealed that all subcortical structures (max. $p_{corr} < 0.002$) and all partial brain volumes (max. $p < 0.002$) without normalization for skull size were significantly larger in the male than in the female group (**Table 4 and Figure 4/a**). The gray/white matter ratio did not reveal a significant difference ($p < 0.077$).

No significant group difference was found between left/right volume ratios of the subcortical structures. However, it is noteworthy that volumes of the right caudate nucleus ($p_{corr} < 0.052$) and the left thalamus $p_{corr} < 0.049$) were larger than those of the corresponding contralateral structures in the male group only.

	Male	**Female**
Total intracranial	1192105.89 (±85334.42)	1064220.04 (±84530.88)
Total brain	1165217.63 (±83151.41)	1041990.31 (±82652.01)
Gray matter	642377.23 (±46905.62)	579578.16 (±42978.76)
White matter	522840.39 (±43260.20)	462412.14 (±44986.73)
Cortex	501307.86 (±37441.32)	451801.73 (±35256.74)
LEFT		
Amygdala	1340.62 (±213.64)	1215.80 (±143.41)
Caudate nucleus	3673.40 (±433.57)	3300.04 (±395.86)
Hippocampus	4102.41 (±407.65)	3812.38 (±364.76)
Globus pallidus	1862.35 (±141.06)	1651.94 (±162.64)
Putamen	5322.47 (±489.15)	4652.45 (±475.17)
Thalamus	8530.95 (±618.69)	7584.07 (±666.20)
RIGHT		
Amygdala	1314.54 (±236.11)	1185.43 (±153.42)
Caudate nucleus	3900.46 (±440.00)	3442.55 (±435.54)
Hippocampus	4067.21 (±483.68)	3780.09 (±349.15)
Globus pallidus	1903.79 (±143.87)	1672.84 (±154.89)
Putamen	5285.87 (±476.42)	4619.65 (±496.57)
Thalamus	8200.31 (±641.66)	7355.25 (±658.75)

Table 4. Volumes (mm^3, mean ± SD) of subcortical gray matter volumes separately for genders.
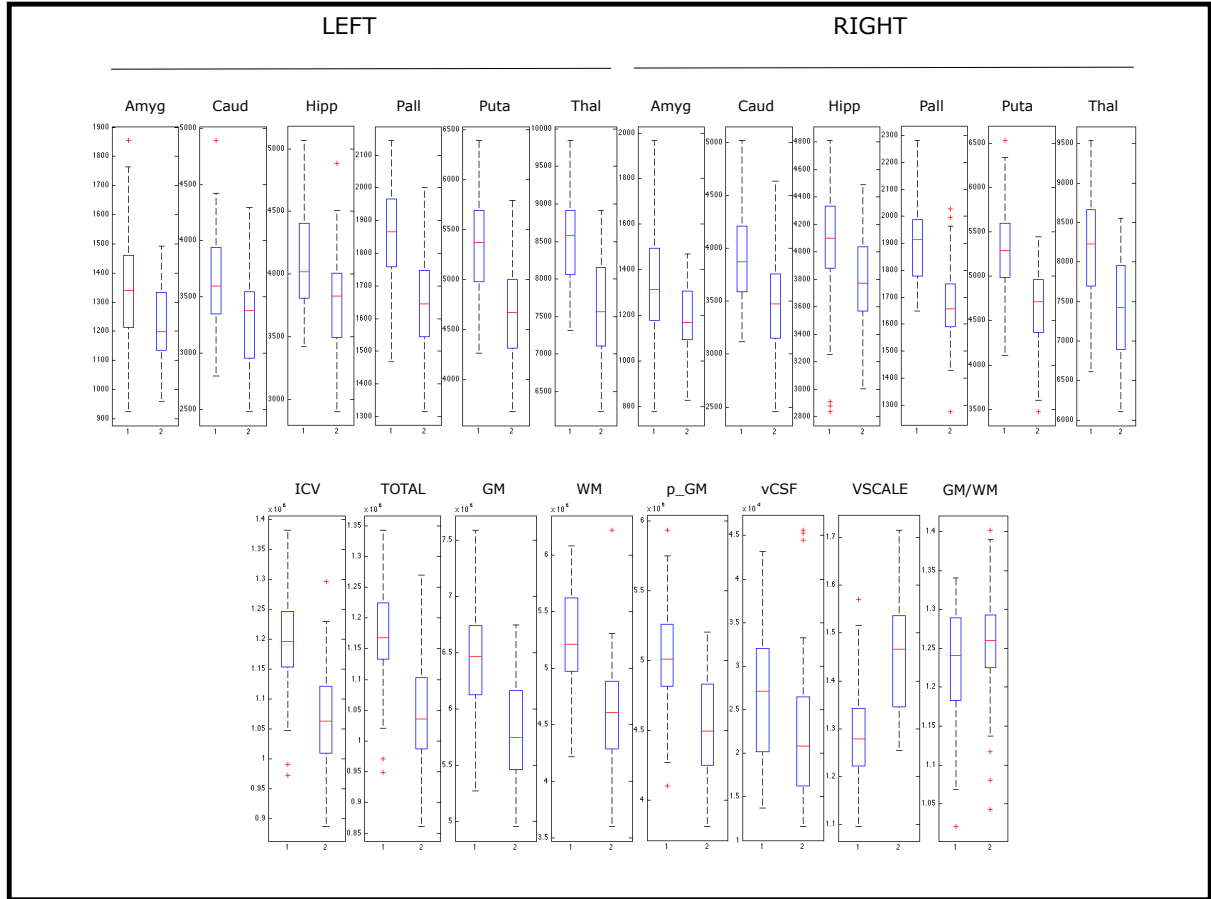
Figure 4/a. Gender differences in the raw subcortical structure and partial brain volumes. Red crosses indicate outliers.

After normalization for skull size, MANCOVA (mean age of comparison = 32.02 years) revealed significantly larger subcortical GM volumes for the left ($p_{corr} < 0.011$) and right hippocampus ($p_{corr} < 0.010$) in the female group. Strikingly, we found the total ($p < 0.003$) and the cortical GM to be larger in the female group as compared to males ($p < 0.009$) (**Figure 4/b**).

In the male group, the volumes of the right caudate nucleus ($p_{corr} < 0.047$) and the left thalamus ($p_{corr} < 0.015$) were found to remain significantly larger than the contralateral pair of these structures.

There were no differences in the diffusion parameters of the subcortical structures between groups. Also, there were no differences found in the left/right ratios of the diffusion parameters of the subcortical structures between groups.
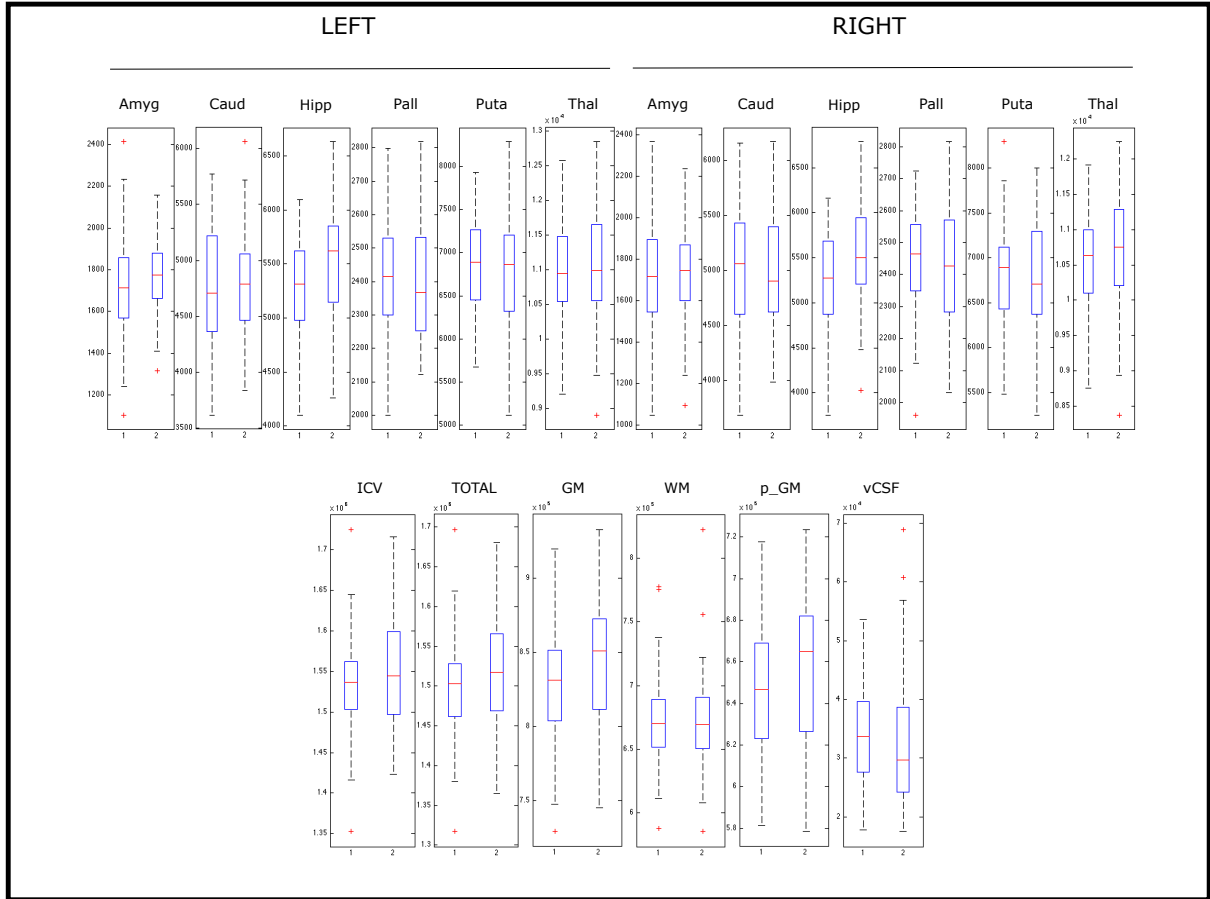
Figure 4/b. Gender differences in the head size normalized subcortical structure and partial brain volumes. Red crosses indicate outliers.

7.2.2. Aging (separately for genders, with and without normalization for skull size)

In the male group, total (R=-0.366, p<0.0071) and cortical GM volumes (R=-0.332, p<0.015), as well as the right thalamus (R=-0.365, p_{corr}<0.043) showed a significant negative correlation with age when corrected for multiple comparisons. As for the volume of the left thalamus a tendency to a significant negative correlation with age (R=-0.345, p_{corr}<0.069) was detected.

In the female group, volumes of total (R=-0.425, p<0.002) and cortical GM (R=-0.418, p<0.003), the right hippocampus (R=-0.411, p_{corr}<0.018), as well as the left (R=-0.373, p_{corr}<0.045) and the right thalamus (R=-0.439, p_{corr}<0.008) showed a significant negative correlation with age.

The gray/white matter ratio was found to correlate negatively with age for both males (R=-0.476, p<0.00032) and females (R=-0.397, p<0.004). However, the age-related gray/white matter ratio was found to be higher for females (p<0.016).

Interestingly, the left/right volume ratio of the hippocampus exhibited a significant positive correlation with age in the female group only (R=0.509, p_{corr}<0.00094).

In the male group, normalized total brain volume (R=-0.507, p<0.00011), total (R=-0.685, p<10^{-6}) and cortical GM (R=-0.616, p<10^{-6}), left (R=-0.393, p_{corr}<0.021) and right caudate nucleus volume (R=-0.376, p_{corr}<0.033), left (R=-0.384, p_{corr}<0.0274) and right putamen (R=-0.408, p_{corr}<0.014), as well as left (R=-0.489, p_{corr}<0.0012) and right thalamus volume (R=-0.508, p_{corr}<0.0006) showed a significant negative correlation with age.

In the female group a significant negative correlation with age was revealed for normalized total brain volume (R=-0.373, p<0.0076), total (R=-0.525, p<0.00009) and cortical GM (R=-0.516, p<0.00013), left (R=-0.399, p_{corr}<0.024) and right thalamus (R=-0.452, p_{corr}<0.006).

Interestingly, the decline with age in normalized GM volume occurred at a faster pace in the group of males than for females (z=2.21, p<0.0271).

The FA of the left putamen showed positive correlation with age only in the male group (R=0.366, p_{corr}<0.053). Otherwise, there was no correlation between age and the diffusion parameters of subcortical gray matter structures neither in the male nor the female group. Also, there were no differences in the correlation found between age and the left/right ratio of the diffusion parameters of subcortical gray matter structures between the male and female groups.

7.2.3. Lateralization

The laterality in the size and diffusion parameters of subcortical structures was investigated in 94 healthy control subjects.

Head size normalized volumes of the right caudate nucleus (p<0.001), left putamen (p<0.026) and left thalamus (p<0.001) were significantly higher than the contralateral pair of these structures.

The FA of the left amygdala (p<0.001), caudate nucleus (p<0.032), putamen (p<0.063) and right pallidum (p<0.001) was higher than the contralateral pair of these structures. AD and MD of all right side structures – except thalamus – were higher (p<0.001) than in the contralateral structures. RD of the right amygdala (p<0.001), caudate nucleus (p<0.001), pallidum (p<0.018), putamen (p<0.001) and the left hippocampus (p<0.001) were higher than in the contralateral structures (**Table 4**).

These results indicate that there is a significant lateralization of the size and diffusion parameters in healthy subjects.

	Left	Right	P_0	$Mean_0$	$Mean_{Boot}$	95% CI $(Mean_{Boot})$
Amygdala						
Volume	(+)	-	(0.068)	(1.032)	(1.032)	(0.997–1.065)
FA	+	-	<0.001	1.074	1.074	1.054–1.095
AD	-	+	<0.001	0.969	0.969	0.963–0.975
MD	-	+	<0.001	0.958	0.959	0.953–0.964
RD	-	+	<0.001	0.952	0.952	0.946–0.958
Caudatus						
Volume	-	+	<0.001	0.947	0.947	0.937–0.957
FA	+	-	0.032	1.014	1.014	1.001–1.026
AD	-	+	<0.001	0.978	0.978	0.974–0.982
MD	-	+	<0.001	0.979	0.979	0.976–0.982
RD	-	+	<0.001	0.980	0.980	0.976–0.983
Hippocampus						
Volume						
FA						
AD	-	+	<0.001	0.989	0.989	0.985–0.992
MD	-	+	<0.001	0.988	0.988	0.985–0.991
RD	+	-	<0.001	0.988	0.988	0.985–0.992
Pallidum						
Volume						
FA	-	+	<0.001	0.943	0.943	0.925–0.961
AD	-	+	<0.001	0.954	0.954	0.944–0.963
MD	-	+	<0.001	0.981	0.981	0.976–0.986
RD	-	+	0.018	1.016	1.016	1.003–1.029
Putamen						
Volume	+	-	0.026	1.013	1.013	1.001–1.024
FA	(+)	-	(0.063)	(1.012)	(1.012)	(0.999–1.025)
AD	-	+	<0.001	0.971	0.971	0.967–0.975
MD	-	+	<0.001	0.969	0.969	0.966–0.973
RD	-	+	<0.001	0.968	0.968	0.965–0.972
Thalamus						
Volume	+	-	<0.001	1.032	1.032	1.025–1.038
FA						
AD						
MD						
RD						

Table 4. Laterality in the volume and diffusion parameters of the subcortical gray matter structures in healthy subjects. *Italic* values and (+) highlights only close to be significant (0.05 < p < 0.1) results. p_0 = p-value with 1-sample T-test. $Mean_0$ = mean Left/Right ratio. $Mean_{Boot}$ = mean Left/Right ratio of the bootstrapped sample. 95% CI($Mean_{Boot}$) = two-tailed (1-alpha) confidence interval of the Left/Right ratio values from the bootstrapped sample.

7.2.4. *Inter-individual variability in the position of thalamic nuclei*

As found through manual comparison the shape and the position of the thalamus was not affected by EPI distortions. The largest misregistration was found along the anterior-posterior axis, but even that was minimal (for AC and PC 0.6±0.5mm). The width of the third ventricle

was not different, and the position of the highest point of the corpus callosum differed only in case of a single subject with 1 mm.

The premotor thalamus was consistently localized in all subjects, however, since the individual brain shapes differed, the exact location of the *Vop* and *Vim* nuclei varied substantially across subjects (**Figure 5**).
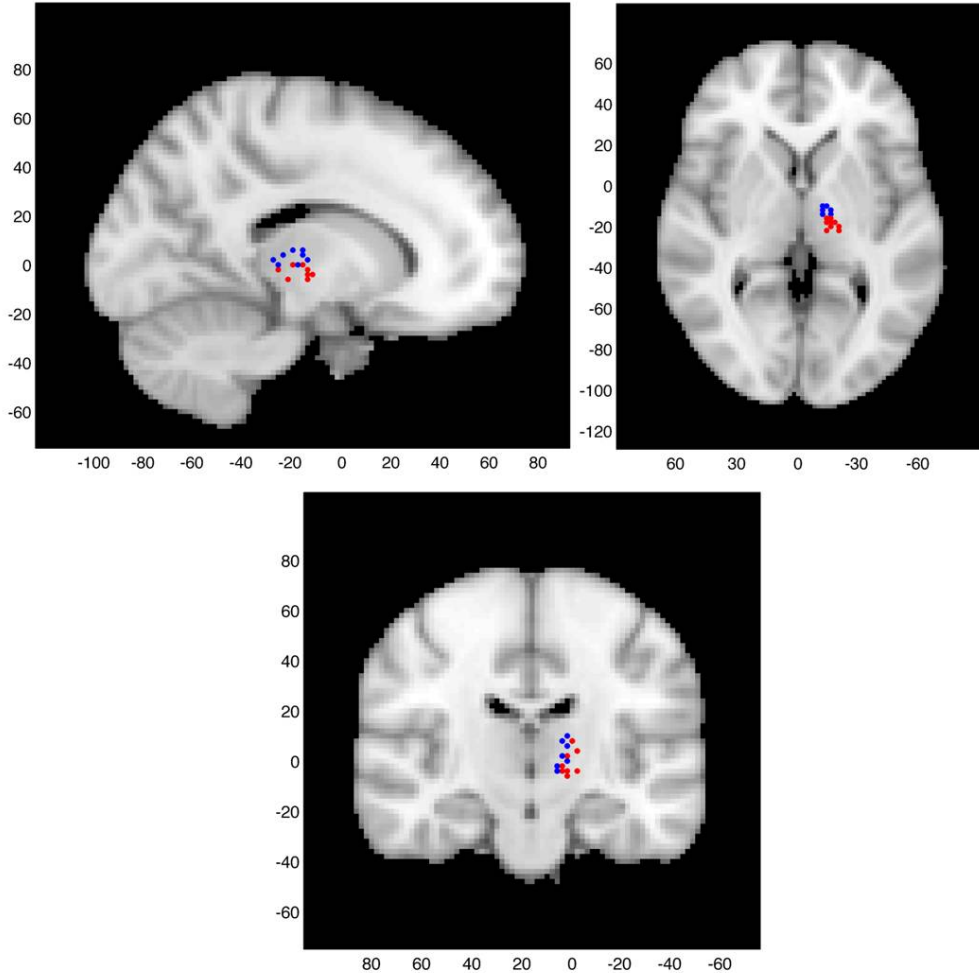
Figure 5. Spatial localization of registered peak *Vop* (blue – premotor cortex) and *Vim* (red – primary motor cortex) voxels as defined by probabilistic tractography. Orthogonal slices are shown.

The mean distance of the peak connection probability of *Vop* from the peak probability indicated by the Oxford Thalamic Connectivity map was 5.08 mm. The equivalent distance was 6.26 mm for the *Vim*. The mean pair-wise inter-subject distance of the peak connectivity voxel of *Vop* was 7.33±3.37 mm (range: 0–14.56 mm) and 7.42±3.35 mm (range: 2–14.28 mm) for *Vim*. The mean distances of the tractography defined *Vop* and *Vim* coordinates from the stereotactic target point defined by Hyam's method (114) were 7.19±4.36 mm (range: 2.45–14.89 mm) for *Vim* and 9.58±4.82 mm (range: 3.0–17.12 mm) for *Vop*. The mean pair-

wise overlap for *Vop* as calculated by the Tanimoto Coefficient was 40.2% (range: 15.5%–66.2%) and 31.8% (range: 3.2%–66.2%) for *Vim*.

7.3. *Subcortical gray matter structures in cluster headache*

7.3.1. *Volumes and diffusion parameters*

Since our analysis showed that there is a significant lateralization of the volumes and the diffusion parameters of subcortical structures in normal healthy subjects, we treated the left- and the right-sided headache patients as separate groups and did not pool patients by flipping their brain along the midsagittal axis. Because of the relatively smaller group sizes bootstrap statistics were used to test the stability of our findings.

The GLM analysis showed that the FA of the right amygdala was significantly higher in *CH* ($p<0.022$) and *LHS-CH* ($p<0.032$) patients than in healthy subjects. A similar tendency was found in case of the left amygdala in *RHS-CH* ($p<0.042$) patients. MD and RD of the right amygdala were higher in healthy subjects compared to the *CH* ($p<0.021$ and $p<0.012$) and *LHS-CH* ($p<0.048$ and $p<0.027$) patients. A similar tendency was found in *RHS-CH* ($p<0.062$ and $p<0.051$) patients.

AD of the right caudate nucleus was higher in *CH* ($p<0.006$), *RHS-CH* ($p<0.034$) and *LHS-CH* ($p<0.026$) patients as compared with healthy subjects. A similar tendency was found with MD and RD in *CH* ($p<0.026$ and $p<0.065$) and *LHS-CH* ($p<0.056$ and $p<0.092$) patients.

In case of the right pallidum FA was lower in *CH* ($p<0.048$) and *LHS-CH* ($p<0.049$) patients. RD of the right pallidum showed tendency to be higher in *CH* ($p<0.056$) and *LHS-CH* ($p<0.079$) patients than in healthy subjects. The head size normalized volume of the right pallidum was lower in *RHS-CH* ($p<0.013$) patients than in healthy subjects.

Total brain volume and gray and white matter volumes were not different between groups. Significance levels and bootstrap confidence intervals are presented in **Table 5**.

	CH (all)				RHS-CH				LHS-CH			
	P_0	T_0	t_{Boot}	95% CI (t_{Boot})	P_0	T_0	t_{Boot}	95% CI (t_{Boot})	P_0	T_0	t_{Boot}	95% CI (t_{Boot})
LEFT												
Amygdala												
Volume					0.042 •	1.744	0.877	(-1.324) - 3.328				
FA												
AD												
MD												
RD												
RIGHT												
Amygdala												
Volume												
FA	0.022 •	2.035	1.557	(-0.708) -4.291					0.032 •	1.875	1.238	(-1.267) - 3.962
AD	0.076	1.443	0.843	(-1.360) - 2.941								
MD	0.021	2.064	1.263	(-0.908) - 3.408	0.062	1.550	0.776	(-1.586) - 2.933	0.048	1.677	0.844	(-1.573) - 3.484
RD	0.012	2.301	1.417	(-0.742) - 3.567	0.051	1.647	0.892	(-1.371) - 3.041	0.027	1.944	1.007	(-1.318) - 3.599
Caudattus												
Volume					0.055	1.611	1.279	(-1.142) - 3.946				
FA												
AD	0.006 •	2.483	2.044	(-0.113) - 4.560	0.034 •	1.846	1.646	(-0.655) - 4.502	0.026 •	1.946	1.507	(-0.773) -4.469
MD	0.026 •	1.834	1.581	(-0.596) - 4.047					0.056 •	1.605	1.258	(-1.089) - 3.851
RD	0.065	1.527	1.378	(-0.761) - 3.523					0.092 •	1.337	1.001	(-1.296) - 3.456
Pallidum												
Volume					0.013	2.255	1.535	(-0.808) - 4.051				
FA	0.048	2.167	1.853	(-0.238) - 4.078					0.049	1.673	1.275	(-1.066) - 3.706
AD												
MD												
RD	0.056 •	1.597	1.275	(-0.948) - 3.592					0.079 •	1.419	1.185	(-1.266) - 3.838

Table 5. The volume and diffusion parameters of the subcortical gray matter structures compared to healthy controls. **Bold** values highlight significant and *italics* highlight close to be significant results. • = higher values in the CH group compared to healthy subjects. CH(all) = RHS-CH and RHS-CH patient together; RHS-CH = cluster headache patients with pain on the right side; LHS-CH = cluster headache patients with pain on the left side. p_0 = p-value from the original GLM. t_0 = t-value from the original GLM. t_{Boot} = mean t-value of the bootstrapped sample. 95% CI(t_{Boot}) = two-tailed (1-alpha) confidence interval of the t-values from the bootstrapped sample.

7.3.2. *Correlation with clinical parameters*

The head size normalized volume of the total brain and cortical gray matter showed positive correlation with the cumulative number of headache days in the *CH* patients. Similar correlation was found in the *LHS-CH* patients. The head size normalized volume of the total gray and white matter showed similar, but not significant tendency of correlation in the *CH* patients.

The head size normalized volume of the left (R=0.432, p<0.045) and right (R=0.431, p<0.045) hippocampus and right caudatus (R=0.562, p<0.007) showed positive, the AD of the left (R=-0.483, p<0.023) and right (R=-0.445, p<0.038) thalamus, the AD (R=-0.505, p<0.017), MD (R=-0.485, p<0.022) and RD (R=-0.439, p<0.041) of the left hippocampus showed negative correlation with the cumulative number of headache days in the *CH* patients. Head size normalized volume of the left pallidum (R=0.658, p<0.039), left (R=0.756, p<0.011) and right (R=0.717, p<0.020) thalamus showed positive, the AD of the left hippocampus (R=-0.667, p<0.035), the MD of the left pallidum (R=-0.835, p<0.003) showed negative correlation with the cumulative number of headache days in the *RHS-CH* patients.

The head size normalized volume of the left hippocampus (R=0.641, p<0.025) showed positive correlation with the cumulative number of headache days in the *LHS-CH* patients. Significance levels and bootstrap confidence intervals are presented in **Table 6**.

		CH (all)				RHS-CH				LHS-CH			
		P_0	R_0	R_{Boot}	95% CI (t_{Boot})	P_0	R_0	R_{Boot}	95% CI (t_{Boot})	P_0	R_0	R_{Boot}	95% CI (t_{Boot})
LEFT													
Hippocampus	Volume	**0.045**	0.432	0.398	(-0.076) - 0.725					**0.025**	0.641	0.592	(-0.088) - 0.90
	FA												
	AD	**0.017**	-0.505	-0.503	(-0692) – (-0.256)	**0.035**	-0.667	-0.684	(-0.921) - (-0.413)				
	MD	**0.022**	-0.485	-0.491	(-0.670) – (-0.249)	0.073	-0.589	-0.608	(-0.882) - (-0.236)				
	RD	**0.041**	-0.439	-0.445	(-0.649) - (-0.184)								
Pallidum	Volume					**0.039**	0.658	0.601	(-0.041) - 0.903				
	FA												
	AD												
	MD	0.083	-0.378	-0.356	(-0.687) - 0.056	**0.003**	-0.835	-0.837	(-0.992) - (-0.603)				
	RD												
Thalamus	Volume					**0.011**	0.756	0.752	0.382 - 0.947				
	FA												
	AD	**0.023**	-0.483	-0.453	(-0.776) - 0.022					0.073	-0.535	-0.427	(-0.902) - 0.711
	MD												
	RD												
RIGHT													
Caudatus	Volume	**0.007**	0.562	0.548	0.134 - 0.817	**0.041**	0.653	0.589	(-0.215) - 0.961	0.060	0.557	0.562	(-0.103) - 0.912
	FA												
	AD												
	MD												
	RD												
Hippocampus	Volume	**0.045**	0.431	0.449	0.111 - 0.752	0.091	0.562	0.560	0.179 - 0.853				
	FA												
	AD												
	MD												
	RD												
Thalamus	Volume					**0.020**	0.717	0.748	0.432 - 0.960				
	FA												
	AD	**0.038**	-0.445	-0.405	(-0.769) - 0.127								
	MD												
	RD												

Table 6. Correlation of the volume and diffusion parameters of the subcortical gray matter structures with lifetime attack number in Cluster Headache. **Bold** values highlight significant and *italics* highlight close to be significant results. CH(all) = RHS-CH and RHS-CH patient together; RHS-CH = cluster headache patients with pain on the right side; LHS-CH = cluster headache patients with pain on the left side. p_0 = p-value from the original GLM. R_0 = R-value from the original GLM. R_{Boot} = mean R-value of the bootstrapped sample. 95% CI(R_{Boot}) = two-tailed (1-alpha) confidence interval of the R-values from the bootstrapped sample.

7.4. *Case reports about thalamotomy results*

Case #1: Vop thalamotomy for posttraumatic tremor

A left-handed, 32-year-old male, after having a motorbike accident that caused brainstem bleeding (at the level of the red nucleus), developed a tremor with resting, postural and intention components, bradykinesia, rigidity and a slight paresis of the left arm.

Seven years after the accident, due to ineffective tremor control by various medication regimes, functional neurosurgery was considered. Because the patient did not accept deep brain stimulation implantation stereotactic thalamotomy was carried out on the right side in the region of *Vop/Vim* border with target coordinates according to Guiot's method (110, 144). During the standard surgical procedure the final position of the lesion along the selected trajectory was adjusted according to the tremor control driven by the intraoperative stimulation. After surgery the patient had an immediate relief from his left upper extremity tremor. Neither his muscle strength, nor the bradykinesia improved. At the three-month checkup, these findings had not changed for the left upper extremity, however a small amplitude flexion-extension tremor appeared in the left toes.

Probabilistic multi-fiber tractography initiated from the thalamic lesion showed connection to the medial premotor - prefrontal cortex and to the brain stem, particularly to the rubral/perirubral mesencephalic posthemorrhagic lesion and some fibers travelling further on to the cerebellum (**Figure 6**).
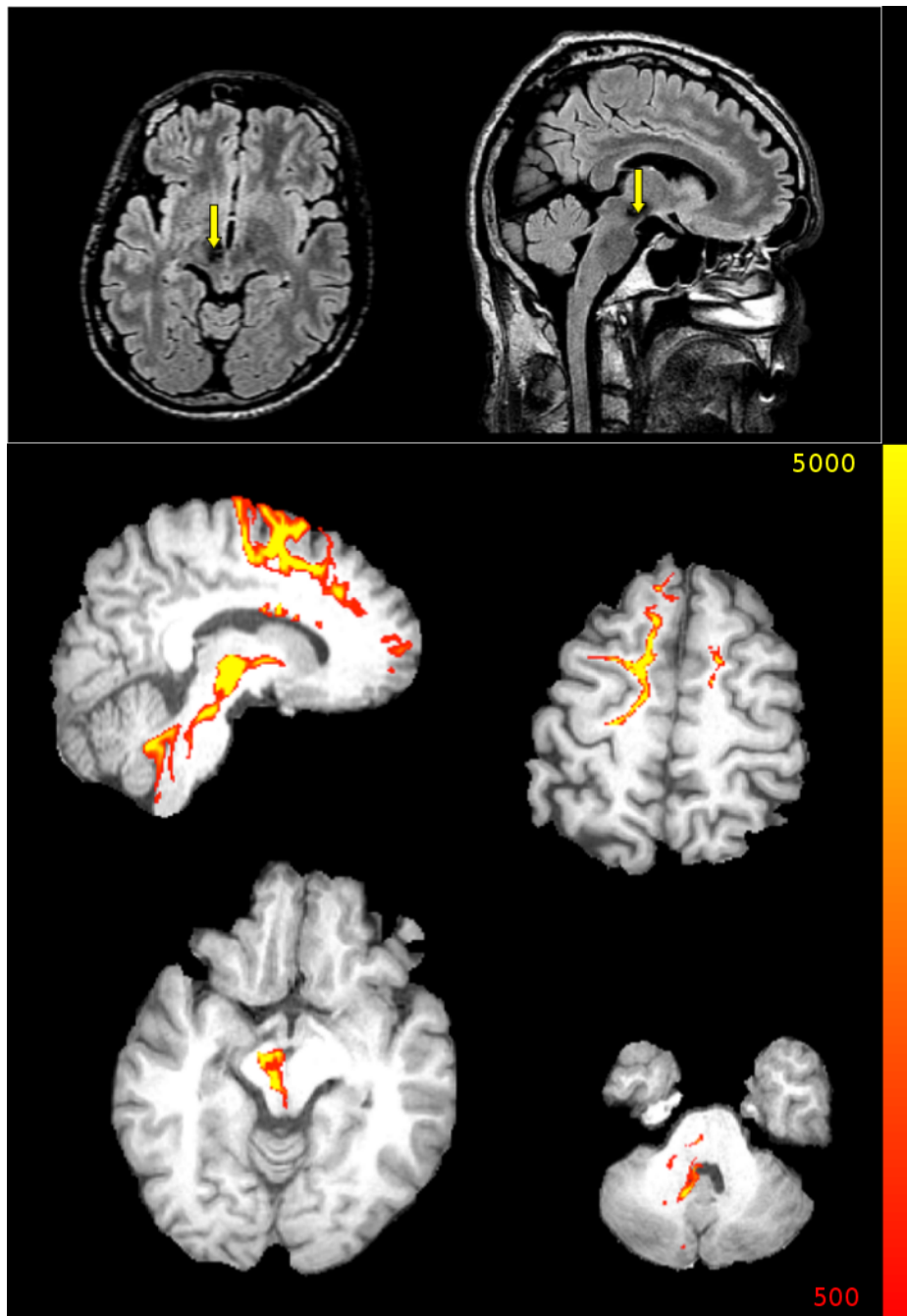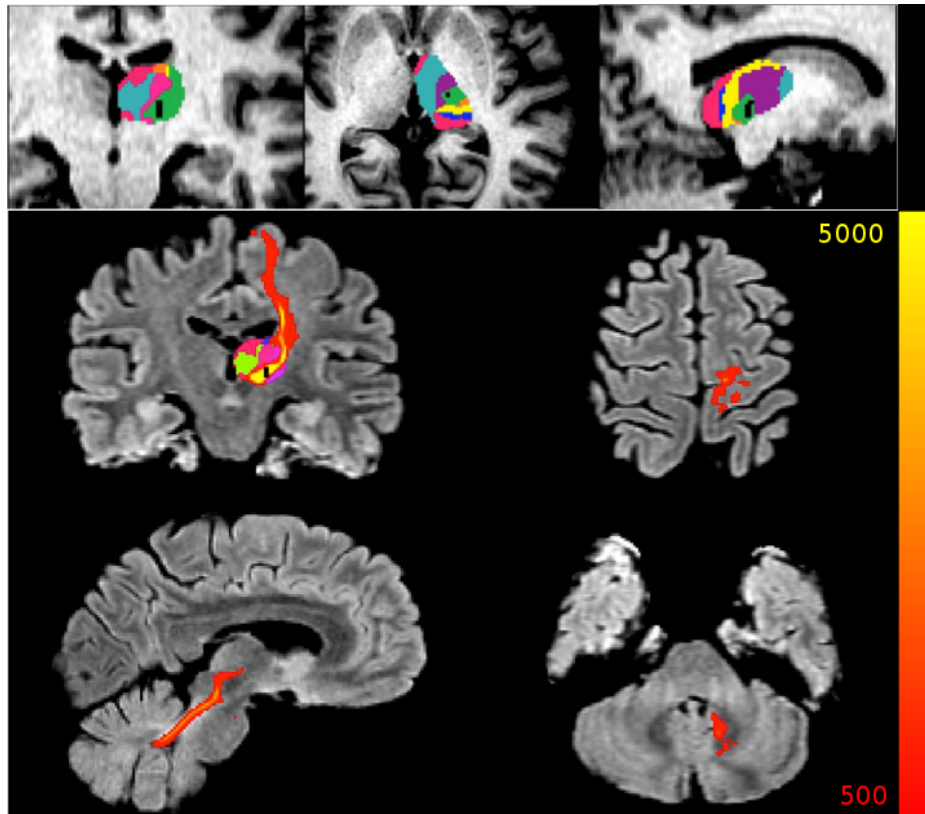
Figure 6. Preoperative FLAIR images show perirubral mesencephalic traumatic hemorrhage (dark area pointed by arrows). Probabilistic multi-fiber diffusion tractography, initiated from the thalamotomy lesion to the whole brain as a target, showed connections to the premotor cortex, nucleus ruber and the perirubral mesencephalon. Some tracts reach the ipsilateral cerebellar hemisphere too. Image is thresholded at 500 particles (10%).

Case #2: VIM thalamotomy for essential tremor

A right-handed, 50-year-old woman had developed tremor ten years earlier. The tremor was most prominent in the hands but also appeared in the head muscles with postural and action components, and was also present while walking. Her family history was unremarkable. Medication regimes that had been tried over the years were ineffective, and the tremor severely affected the quality of life of the patient. Stereotactic *Vim* thalamotomy was carried out with target coordinates according to Guiot (110, 144) that correspond well with the coordinates defined by Hyam's method (114). After surgery the tremor of the right hand improved significantly and on the three-month control examination this effect was found to be enduring (FMT score reduced from 17 to 11 points). No significant change was detected in the head-tremor or in the tremor of the left hand.

The postoperative T1-weighted image was registered to the preoperative T1-weighted image in order to identify the position of the lesion in relation to the diffusion–based connectivity results. The connectivity-based segmentation of the thalamus indicated that the surgical lesion was in the putative *Vim* nucleus, the region that showed the highest probability of connection to the primary motor cortex. Postoperative probabilistic tractography from the lesion showed that the lesioned thalamus was connected to the primary motor cortex, mainly to the medial structures, and downstream to the ipsilateral cerebellar hemisphere (**Figure 7**).
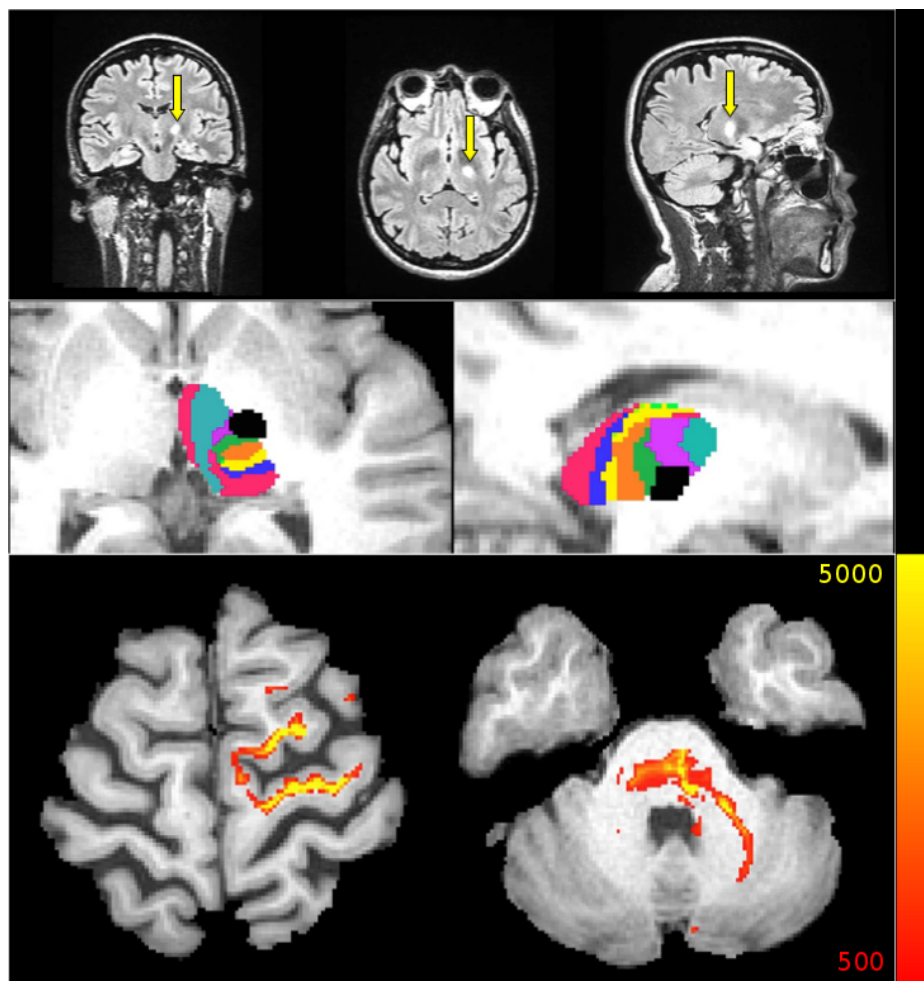
Figure 7. Connectivity-based segmentation results of the right thalamus are overlaid on the preoperative FLAIR images. The color in each thalamic voxel represents the color of the cortical area that has the highest connection probability to that voxel (*black spot – masked thalamotomy lesion;* light blue – frontal, purple – premotor, green – primary motor, orange – primary sensor, yellow – parietal, dark blue – occipital and dark-pink – temporal cortex). Probabilistic multi-fiber diffusion tractography, initiated from the thalamotomy lesion (black rectangle) to the whole brain as a target, showed connections to the left medial primary motor cortex and some tracts reach the ipsilateral cerebellar hemisphere too. Image is thresholded at 500 particles (10%).

Case #3: VIM thalamotomy for essential tremor

A right-handed, 36-year-old woman had developed tremor twelve years earlier. The coarse, resting and postural, flexion-extension like tremor was most prominent in the right hand but also appeared in the left leg to a lesser extent. Her symptoms have worsened lately, making her unable to use her right hand, so she had to write, eat and drink with her left hand. Because conventional medication regimes were ineffective, stereotactic left-side *Vim* thalamotomy was carried out with target coordinates according to Guiot (110, 145) that correspond well with the coordinates defined by Hyam's method (114). After surgery, tremor of the right hand ceased. On the three-month control patient complained of mild dysarthria, intermittent blurred vision, dizziness, fatigue, reduction in memory and bumping into things to her right side. Her post-operative status showed mild central facial paresis on right side, mild dysarthria and difficulties with articulation.

The thalamic lesion, identified on the postoperative FLAIR images (registered to the preoperative T1-weighted structural image with 6 degrees-of-freedom linear registration) was situated on the border of the thalamus and the internal capsule, with its majority in the region of the thalamus connecting to the premotor cortex with the highest probability, according to the connectivity-based segmentation. The probability tractography initiated from the thalamotomy lesion to the whole brain showed connection with the left medial premotor and primary motor cortex. Also, a downstream connection to the ipsilateral cerebellar hemisphere could be observed (**Figure 8**).

Figure 8. Thalamotomy lesion seen on post-operative FLAIR images (bright area pointed by). Connectivity-based segmentation results of the right thalamus are overlaid on the postoperative T1-weighted images. The color in each thalamic voxel represents the color of the cortical area that has the highest connection probability to that voxel (*black spot – masked thalamotomy lesion;* light blue – frontal, purple – premotor, green – primary motor, orange – primary sensor, yellow – parietal, dark blue – occipital and dark-pink – temporal cortex). Probabilistic multi-fiber diffusion tractography, initiated from the thalamotomy lesion to the whole brain as a target, showed connections to the left medial premotor and primary motor cortex. Some tracts reach the ipsilateral cerebellar hemisphere too. Image is thresholded at 500 particles (10%).

Case #4: VIM thalamotomy for Parkinson's disease

A right-handed, 73-year-old man had developed tremor 4.5 years earlier. Parkinson's disease was diagnosed. The tremor was resistant to various medication regimes. In his admission status, rigor, resting and postural, right-site dominant tremor – reduced but not ceased by movement – of both-site upper extremities, reduced synkinesis of right arm and mild flexed gait were seen. Deep-brain stimulation was offered to the patient who declined the possibility and opted for lesioning.

Stereotactic *Vim* thalamotomy by left frontal incision was carried out with target coordinates according to Guiot (110, 145) that correspond well with the coordinates defined by Hyam's method (114). After surgery, tremor of the right hand ceased.

At the two-month control examination, the patient complained of numbness in right side of the oral cavity and both sides of the tongue, significantly reduced taste sensation, appreciably slowed movements in his right hand and difficulty with speech.

The connectivity-based segmentation of the thalamus indicated that the surgical lesion was mainly in the putative Vim nucleus, the region that showed the highest probability of connection to the premotor and primary motor cortex. The probability tractography initiated from the thalamotomy lesion to the whole brain showed connection with the left medial premotor, primary motor cortex. Also, a downstream connection to the ipsilateral cerebellar hemisphere could be observed (**Figure 9**).
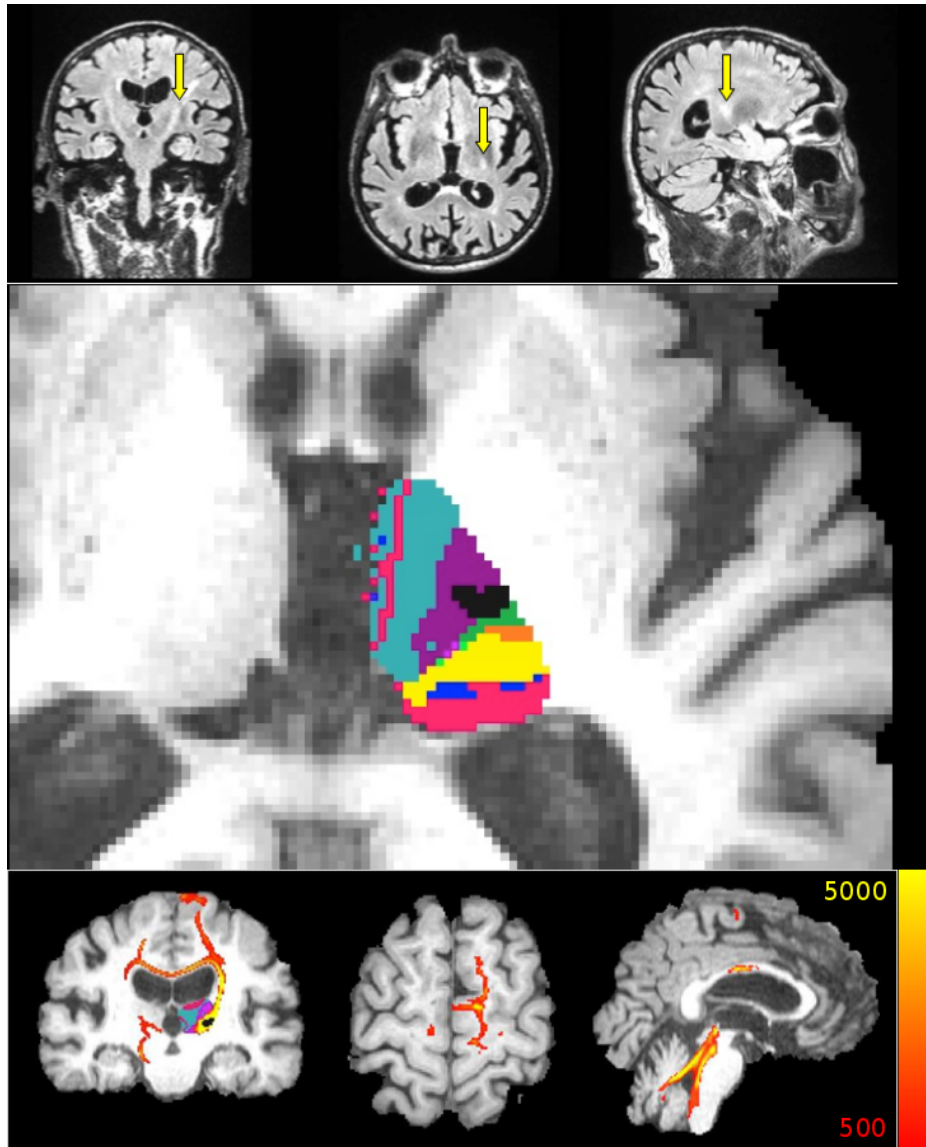
Figure 9. Thalamotomy lesion seen on post-operative FLAIR images (bright area pointed by arrow). Lower image: Connectivity-based segmentation of the right thalamus. Results are overlaid on the postoperative T1-weighted images. The color in each thalamic voxel represents the color of the cortical area that has the highest connection probability to that voxel (*black spot – masked thalamotomy lesion*; light blue – frontal, purple – premotor, green – primary motor, orange – primary sensor, yellow – parietal, dark blue – occipital and dark-pink – temporal cortex). Probabilistic multi-fiber diffusion tractography, initiated from the thalamotomy lesion to the whole brain as a target, showed connections mainly to the left medial premotor and partly to primary motor cortex. Some tracts reach the ipsilateral cerebellar hemisphere too. Image is thresholded at 500 particles (10%). Overlapped segmented thalamus can be seen with masked thalamotomy lesion (black spot).

8. Discussion

In our studies we aimed to identify effects of age, gender and lateralization on subcortical gray matter volumes and diffusion parameters, as well as to show the significance of inter-individual variability in the features of the human brain.

Hence, a complete set of analyses was run in three consecutive studies: A) automatized, deformable mesh based segmentation toolkit (FSL-FIRST) was used to extract subcortical structures, B) partial brain volumes were extracted with an intensity-based segmentation toolkit (FSL-SIENAX), C) cortical thickness was measured with voxel-based morphometry (VBM), D) diffusion tensor imaging (DTI, FSL-FDT) was used to get the diffusion parameters of the subcortical structures (which is defined by the internal microstructure), E) probabilistic tractography based segmentation of the thalamus (FSL-PROBTRACKX) was run to reveal inter-individual variability in the position of the thalamic nuclei *Vim* and *Vop*.

The most important results of our investigations can be summarized as follows:

(1) In general, male brains were found to be larger than females', with larger gray and white matter fractions, as well as subcortical structures. However, most of these differences disappeared after skull size was accounted for. Moreover, as a result of correction for total intracranial volume we found females to have larger cortical and subcortical GM volumes. Importantly, the volume of the hippocampus was found to be significantly larger in the female group as compared to males. We also detected a significant effect of hemisphere side in the male group only, with larger volumes of the right caudate and the left thalamus as compared to their contralateral structures.

(2) We found an age-dependent decrease in the volume of the subcortical gray matter. This remained significant in the caudate, putamen and thalamus bilaterally for males and the thalamus bilaterally for females after correction for skull size. Within the age range of 21 to 58 years we found a linear decrease in GM volume with age. Strikingly, this process proved to occur at a faster pace in males. Additionally, we found that FA values of the left putamen increased with age only in the male group.

(3) A significant lateralization of the size (caudate, putamen and thalamus) and diffusion parameters of the subcortical gray matter structures were found in healthy controls. By demonstrating this lateralization in a large cohort of healthy subjects, we showed that in

patients with unilateral symptoms, pooling of the data depending on the affected side to boost the number of observations is not recommended.

(4) We found that, compared to the size of the nucleus, the spatial variability of the position of thalamotomy target nuclei *Vim* and *Vop* is substantial. Our results call attention to the importance of defining such small targets individually for which our approach is suitable and is frequently used since the publication (146-148). We also showed that the lesion in four successful thalamotomy cases was in fact in the target nuclei as defined by tractography based segmentation.

(5) We showed that there is a progressive gray matter loss in Huntington patients even before the appearance of clinical symptoms. This gray matter atrophy represents the progressive neurodegeneration caused by the genetic alteration responsible for the disease.

We propose that the usefulness and importance of our current findings are two-fold: (i) they present methodological considerations for the investigation of subcortical structures and (ii) they raise potential functional implications related to gender and gray matter decline with age.

8.1. *Methodological considerations*

While there is converging research evidence for total brain and GM volumes to decline with age (34, 41, 47, 60, 149, 150), we propose that the inconsistency of findings about age and gender-related differences in subcortical GM volumes might arise from methodological differences and relatively small sample sizes (151). Most of the previous studies applied a VBM approach to identify gender differences in subcortical nuclei. While VBM is an excellent tool for the investigation of focal gray matter density differences, deformable surface model approaches such as FIRST are directly tuned for the volumetric analysis of subcortical structures. Further studies applied manual tracing of subcortical structures identifying an age-related volume decline in the thalamus (35), caudate and putamen (152). However, the investigation was limited to certain structures and the relationship with age was observed for both genders. Furthermore, in MRI studies, age, gender and head size (intracranial volume) are the most commonly included "nuisance" variables, though studies greatly vary as to which of the variables are included and which method is used for correction (63). Our results are consistent with a previous study reporting an age-related decline in the

caudate, putamen and nucleus accumbens and a marginal effect in the thalamus in a similar age-range (35-60 years) (153). However, the authors suggested that normalization to the cranium size accounted for the observed gender effect. Other studies included gender as a nuisance variable in the general linear model analysis and found a negative correlation between age and the volumes of the hippocampus, amygdala, caudate and putamen (149). Yet, other results were reported using Freesurfer, showing a disproportionate degeneration of the subcortical volumes with aging (154). Our current results regarding the hippocampus are in agreement with previous reports of larger relative hippocampal size in females with the use of FIRST, also confirmed by a VBM style analysis (2). Nevertheless, it is important to note the transformation approach and group intracranial volume considerations when reporting structural findings concerning the subcortical GM, since it might carry several implications for the interpretation of the results (155).

There are only a few studies about the diffusion parameters of subcortical deep gray matter structures. While Fabiano's findings are important and consistent with our findings, in their study the mean of diffusivity from only 3 directions were examined in a small cohort of healthy subjects and circular regions of interests were used in some of the structures (70). Wang and coworkers found age-dependent alteration in the diffusion parameters of the putamen and caudate nucleus, however, they used only 15 diffusion directions in case of DTI and manually delineated a 50 mm^2 area inside the structures (156). In the study of Abe and coworkers (157), gray matter volume and FA were negatively, whereas MD was positively correlated with age on a global scale. However, they used a VBM style analysis on DTI data with acquisition parameters of 5 mm slice thickness and 6 diffusion directions. Pfefferbaum et al (158), using an ROI based DTI analysis, found that both anisotropy and average diffusivity were higher in the caudate nucleus and putamen in the older group. They used 6 diffusion directions and recruited only 10 younger and10 older subjects. In our study we used a larger cohort of healthy subjects and found asymmetries in various diffusion parameters estimated from diffusion measurements using 60 different directions.

Despite the accurate stereotactic atlases (106, 159) that guide the standard methods for targeting, significant inter-subject variability still exists (106). The differences in gross thalamic morphology are already known: the medio-lateral aspect – as defined by the position of the internal capsule – and the height of the thalamus varies between subjects (106). The position of the pulvinar system varies between subjects even with the same AC-PC distance (106). Moreover, as emphasized by Morel, these variations are not homogenous even within

the thalamus, particularly along the medio-lateral axis (106). Our results, using a different modality, also indicate significant variability of the position of the *Vop* and *Vim* nuclei, especially when the size of the nucleus and the surgical lesion is considered. The distance between peak-probability *Vop* voxels was 7 mm on average and is similar for *Vim*, but in certain cases the distance was as much as 1.5 centimeters. The overlap between *Vop*-s on average was around only 40% and varies from 15% to 60%. Similar overlap values were found for *Vim*. It is also important to emphasize that in the current variability estimation only young, healthy individuals were included. Brain pathology may further increase the variability.

8.2. *(Patho)biological considerations*

8.2.1. *Brain atrophy in presymptomatic Huntington's disease*

In Huntington's disease, brain atrophy is more significant than during healthy aging. Although in our study we did not find correlation between cortical thickness and CAG repeat number, from previous studies we know that higher CAG repeat numbers are also associated with faster clinical progress (160) and earlier onset of symptoms (161). A previous neuropathological study described correlation between the CAG repeat number and cortical atrophy, but there was no association with the volume of the subcortical structures (162). In cross-sectional studies, striatal atrophy was found to correlate with CAG repeat numbers (163-166). Furthermore, frontal-, occipital-, parietal- and cerebellar atrophy was found to correlate with CAG repeat number in HD patients (167, 168). In a larger cohort of patients, a CAG repeat number increase of 1 resulted in the increment of brain atrophy rates by 0.12% per year (169). The association between CAG repeat numbers and gray matter atrophy might arise from the toxic function of the huntingtin protein caused by mutation in the IT15 gene and the polyglutamine expansion in the protein structure (170).

8.2.2. *Effect of age and gender on brain (micro) structure*

The aspect to be considered involves the underlying cellular, molecular and functional mechanisms of age and gender related differences of GM volume. Primarily, neuronal and synaptic pruning has been proposed to play a critical role (171). However, findings of post-mortem histological studies suggested, that it is rather the size than the number of the individual cells that explain age-related GM decline (172, 173). Recent results also imply the impact of aging on GM/WM diffusion changes, explaining some cognitive variability and even decline (174).

The background of the disproportionate GM volume changes in males and females has not yet been elucidated, but differences in hormone levels and the consequent sensitivity of the brain to hormonal effects are most certainly involved (175). Apart from structural differences, there is increasing evidence for the functional sexual dimorphism of subcortical structures. Amphetamine has been shown to cause a higher level of dopamine release in the male striatum, which correlates with the behavioral effect of the drug (176, 177). Hippocampus-related memory functions are differently affected by stress in males and females (178). Peripartum hormonal changes are known to modulate hippocampal function (179). In addition to gender effects, recent evidence supports the influence of brain hemisphere side showing lateralization of structure-function relationships, as well as more specific relationships between individual structures (e.g., left hippocampus) and functions relevant to particular aptitudes (e.g. vocabulary) (180). Our current results revealed a significant effect of hemisphere side in the male group only with larger volumes of the right caudate and the left thalamus as compared to their contralateral structures. It can be hypothesized that this difference relates to handedness, however, we did not find such a relationship. A recent study examining the deep gray matter of healthy adults by using magnetic susceptibility-weighted imaging did not reveal an association with handedness either (181).

In our study, similarly to previous studies (156-158, 182, 183), we found that FA increased in the putamen with advancing age. Although the study by Pfefferbaum et al (158) stated that high FA in the putamen is correlated with iron deposition, there are few interpretations for the age-related increase of FA.

The interpretation of age-related changes of DTI metrics in the basal ganglia might be different and more complicated than in the white matter. In contrast to the microstructure of the white matter, the basal ganglia consist predominantly of neurons and glia. Among the subcortical gray matter structures, the caudate nucleus and putamen have the same phylogenesis and the globus pallidus develops later. Neurons in the caudate nucleus and putamen have spherical dendritic arborization, which is covered densely with dendritic spines. These allow water to diffuse freely in these structures. In contrast, neuronal dendrites in the globus pallidus are long, smooth, and sparsely branched (184-186). The fibers in the globus pallidus are covered by myelin, and some fibers are arranged in bundles. The diffusion of water is, therefore, more restricted and more directed in the globus pallidus. Theoretically, the proportion of axial and radial diffusivity influences FA. Increased FA may result from increased AD, decreased RD, or both. Volume reduction with age due to the loss of neurons

in the striatum has already been reported (58, 187). The concurrent gliosis and tissue compaction hinder water diffusion. The cell membranes of the remaining atrophic neurons become less fluid and more rigid with aging, also the vessel wall shows some hyaline degeneration during aging, it becomes thicker and the water diffusion through the wall becomes more difficult. Also, the contribution of the extracellular and intracellular water fraction to the diffusion signal is not even. A combination of diffusion parameter changes could be explained by the change of the ratio of the extra and intracellular water fractions (e.g.: global shrinkage of the structure or intracellular edema) or for example protein deposits limiting water diffusion. These kinds of age-related changes add to the hindrance of water diffusion. Diffusivity in all directions could be affected, but in a previous study by Wang et al (156) RD presented decreasing change, while – in contrast to the high value in the white matter – AD in the basal ganglia was low. FA values were therefor easily influenced by changes in RD. Additionally, the body of the striatum, especially the putamen, is a region with an abundant blood supply compared to other regions in the brain. Hence, the pseudo diffusion effect caused by blood motion can be more significant here.

8.2.3. *Alteration of subcortical gray matter structures in cluster headache*

In our study we demonstrated that the microstructure of subcortical structures is altered in cluster headache (CH) interictally. Some of these microstructural changes were dependent on the lifetime disease burden.

Based on our results from healthy subjects we concluded that we couldn't pool data from the different hemispheres of CH patients. In our analysis we treated CH patients as one group regardless of the side of the headache, and only as a secondary test we compared the RHS-CH and LHS-CH patients to healthy subjects. Due to the small size of the groups, the results of these later comparisons have to be handled cautiously, even though the stability of the findings was evaluated by a bootstrap sampling.

Recent studies suggest that neurodegeneration could result in diffusion changes in related basal ganglia. In movement disorders involving the basal ganglia (Huntington's disease (188), Parkinson's disease (189), blepharospasm (190)), altered diffusivity parameters were detected. Macro- and microstructural alterations are well-known features of pain-related disorders (64, 191). As regarding CH, the seminal paper by May et al. (192) described increased gray matter volume in the inferior posterior hypothalamus in CH, but no other changes in gray matter density were found either in the cortex or in subcortical structures. In

contrast, another VBM analysis indicated a decreased gray matter volume in the right thalamus, in the head of the right caudate nucleus and in several cortical structures related to pain processing (73). Importantly, the decrease in gray matter volume did not depend on the side of the pain. While subcortical structures were found to be slightly smaller, no subcortical volume alteration was identified with our surface-based analysis approach (except the right pallidum that was smaller in *RHS-CH* than in healthy participants). However, a recent VBM style investigation proposed that cortical and subcortical volumetric alterations are dynamic in relation to the pain state (e.g. ictally, interictally and in chronic CH) (65).

With respect to the alterations in diffusion parameters of deep gray matter structures, increased fractional anisotropy has been reported in the thalamus contralateral to the affected body side in multiple sclerosis patients with extremity pain (193). In irritable bowel syndrome decreased FA was found in thalamic regions, while a reduced MD in the globus pallidus and higher MD in the thalamus were described (194). In migraineurs without aura, FA was reported to be higher and MD to be lower in the bilateral thalami as compared to controls in the interictal phase. Diffusivity parameters have also been found to be similar to those in controls in the ictal phase (195). In our study, we found increased FA of the bilateral amygdala. The amygdala is known for being an important center of emotional and affective aspects of pain. Also, it is an important hub in the processing of noxious stimuli and it was shown to have structural and functional connections to cortical and subcortical structures involved in pain processing (196, 197). It was shown by several studies that there is significant pain related plasticity in the amygdala in chronic pain conditions and amygdalar plasticity was suggested to be the key factor in the establishment of fear memory (198, 199). We propose that increased FA in CH patients might have a similar background. Interestingly, the pain related activation of amygdala is heavily lateralized to the right (200), but no such lateralization of diffusion parameters or size was found in our patients. While it is known that basal ganglia structures - such as the pallidum and caudate nucleus, which were found to have altered diffusion parameters in CH in our study – are activated in response to painful stimuli (76) and structural alterations are related to chronic pain conditions (71), the exact role of these structures in the processing of noxious stimuli is not fully understood yet.

8.2.4. Segmentation of the subcortical structures to guide functional neurosurgery

In this study we showed the inter-individual variability of the position of the thalamotomy target nuclei *Vim* and *Vop* as defined by probabilistic diffusion tractography. We found that,

compared to the size of these nuclei, the variability of their position is substantial. Despite the accurate stereotactic atlases (106, 201) that guide the standard methods for targeting, significant inter-subject variability still exists (106). Differences in gross thalamic morphology are already conspicuous: the medio-lateral aspect – as defined by the position of the internal capsule – and the height of the thalamus vary between subjects (106). The position of the pulvinar system even varies between subjects with the same AC-PC distance (106). Moreover, as emphasized by Morel, these variations are not homogenous even within the thalamus, particularly along the medio-lateral axis (106). Our results, using a different modality, also indicate significant variability of the position of the *Vop* and *Vim* nuclei, especially when the size of the nucleus and the surgical lesion is considered. The distance between peak-probability *Vop* voxels was 7 mm on average and is similar for *Vim*, but in certain cases the distance was as much as one and a half centimeters. The overlap between *Vop*-s on average was around only 40% and varies from 15% to 60%. Similar overlap values were found for *Vim*.

Instead of using the histology-based stereotactic atlas derived from a limited number of brains, a population based-probabilistic functional atlas was recently developed from data gathered from pre-, intra- and postoperative neuroimaging and electrophysiological investigations (107, 108). The advantage of this approach is the physiological control of lesion depth during awaken surgery by monitoring patient complains while trying different stimulation positions.

It follows from the discussion above that, ideally, individual anatomy should be taken into account when performing stereotactic thalamotomy. The approach used by Yamada and colleagues (202) incorporated tracking the cerebello-thalamo-cortical and spino-thalamic tracts that cross the thalamus, and the identification of anatomical landmarks on short tau inversion recovery (STIR) and fractional anisotropy images. Sedrak and co-workers (203) manually identified *Vim* as target for deep-brain-stimulation (DBS), then the connectivity of effective electrode location investigated by tractography showed connections to the sensory-motor cortex and to the cerebellum. Compared to these deterministic approaches, our method offers further advantages by utilizing probabilistic tractography (115, 128). This method is able to give statistical evaluation of connection probabilities to cortical targets for every thalamic voxel that – by appropriate selection of the cortical targets – are then able to delineate thalamic regions that correspond well to thalamic nuclei as defined by histology (115, 128, 204). This approach shows a high intra-subject reproducibility in terms of repeated

analysis as well as repeated data acquisitions (204).

9. Limitations

These analyses have some essential drawbacks. First of all, these are cross-sectional assessments of the focal shrinkage or alteration of diffusion parameters in subcortical gray matter structures. In order to acquire an in-depth understanding of the dynamics in brain atrophy and diffusion parameters longitudinal studies are needed, which are difficult to carry out in a timeframe, long enough to be useful in researching normal aging.

In case of cluster headache, we do not have exact information about the time elapsed from the last attack. A further drawback is the relatively low power of the secondary analyses (RHS-CH and LHS-CH) due to the limited number of patients. Given the central role of the hypothalamus in CH it would be crucial to investigate its size and microstructure. Unfortunately, segmenting the hypothalamus is limited by the low intensity contrast to the surrounding structures.

It has to be pointed out that in the reported thalamotomy cases we did not plan targeting with tractography based segmentation before the surgery. One possible caveat of our analysis that cannot be neglected is the misregistration when aligning the high resolution T1-weighted and diffusion weighted images. Diffusion-weighted images suffer significant distortions because of susceptibility artifacts; however, our analysis indicated that these distortions were minimal in the region of the thalamus. Extension of this study to compare the result of the stereotaxic neurosurgery with and without tractography based targeting is crucial. Further improvements might be expected if additional imaging modalities (e.g. relaxometry, fMRI) could also be utilized. It is also important to emphasize that in the current variability estimation only young, healthy individuals were included. Brain pathology may further increase the variability.

10. Acknowledgement

I would never have been able to finish my dissertation without the guidance of my committee members, help from friends, and support from my family.

I would like to thank Professor László Vécsei for giving an opportunity to work in the Department of Neurology and supporting my work.

I would like to express my deepest gratitude to my advisor, Zsigmond Tamás Kincses MD, for his excellent guidance, patience and care.

Many thanks to Nikoletta Szabó MD, Péter Faragó MD, Eszter Tóth MD, Bernadett Tuka, Gergő Csete MD, Krisztián Kocsis, Dániel Veréb MD, Bálint Kincses MD, Gábor Veres and Rita Török for their practical help and for providing me with an excellent atmosphere for doing research. My research would not have been possible without their help.

I would like to thank all colleagues at the Department of Neurology for their constant help and assistance.

I would also like to thank my family. They always supported and encouraged me with their best wishes. Finally, I would like to thank my friends. They were always there cheering me up and stood by me through the good times and the bad.

11. References

1.   Evans AC, Janke AL, Collins DL, Baillet S. Brain templates and atlases. NeuroImage. 2012 Aug 15;62(2):911-22. PubMed PMID: 22248580.

2.   Kauranen K, Vanharanta H. Influences of aging, gender, and handedness on motor performance of upper and lower extremities. Perceptual and motor skills. 1996 Apr;82(2):515-25. PubMed PMID: 8724924.

3.   Ruff RM, Parker SB. Gender- and age-specific changes in motor speed and eye-hand coordination in adults: normative values for the Finger Tapping and Grooved Pegboard Tests. Perceptual and motor skills. 1993 Jun;76(3 Pt 2):1219-30. PubMed PMID: 8337069.

4.   Cahill L. Sex-related influences on the neurobiology of emotionally influenced memory. Annals of the New York Academy of Sciences. 2003 Apr;985:163-73. PubMed PMID: 12724157.

5.   Bisagno V, Cadet JL. Stress, sex, and addiction: potential roles of corticotropin-releasing factor, oxytocin, and arginine-vasopressin. Behavioural pharmacology. 2014 Sep;25(5-6):445-57. PubMed PMID: 24949572. Pubmed Central PMCID: 4119500.

6.   Fattore L, Melis M, Fadda P, Fratta W. Sex differences in addictive disorders. Frontiers in neuroendocrinology. 2014 Aug;35(3):272-84. PubMed PMID: 24769267.

7.   Gershon J. A meta-analytic review of gender differences in ADHD. Journal of attention disorders. 2002 Jan;5(3):143-54. PubMed PMID: 11911007.

8.   Bourque M, Dluzen DE, Di Paolo T. Neuroprotective actions of sex steroids in Parkinson's disease. Frontiers in neuroendocrinology. 2009 Jul;30(2):142-57. PubMed PMID: 19410597.

9.   Geevarghese R, Lumsden DE, Hulse N, Samuel M, Ashkan K. Subcortical structure volumes and correlation to clinical variables in Parkinson's disease. Journal of neuroimaging : official journal of the American Society of Neuroimaging. 2015 Mar-Apr;25(2):275-80. PubMed PMID: 24593221.

10.   Gillies GE, Pienaar IS, Vohra S, Qamhawi Z. Sex differences in Parkinson's disease. Frontiers in neuroendocrinology. 2014 Mar 4. PubMed PMID: 24607323.

11.   Qian S, Zhang Z, Li B, Sun G. Functional-structural degeneration in dorsal and ventral attention systems for Alzheimer's disease, amnestic mild cognitive impairment. Brain imaging and behavior. 2014 Dec 2. PubMed PMID: 25452158.

12.   Macgregor EA, Rosenberg JD, Kurth T. Sex-related differences in epidemiological and clinic-based headache studies. Headache. 2011 Jun;51(6):843-59. PubMed PMID: 21631472.

13.   Greer JM, McCombe PA. Role of gender in multiple sclerosis: clinical effects and potential molecular mechanisms. Journal of neuroimmunology. 2011 May;234(1-2):7-18. PubMed PMID: 21474189.

14.   MacMaster FP, Carrey N, Langevin LM, Jaworska N, Crawford S. Disorder-specific volumetric brain difference in adolescent major depressive disorder and bipolar depression. Brain imaging and behavior. 2014 Mar;8(1):119-27. PubMed PMID: 24158718.

15.   Gifuni AJ, Ding Y, Olie E, Lawrence N, Cyprien F, Le Bars E, et al. Subcortical nuclei volumes in suicidal behavior: nucleus accumbens may modulate the lethality of acts. Brain imaging and behavior. 2015 Mar 12. PubMed PMID: 25759286.

16.   Gur RE, Gur RC. Sex differences in brain and behavior in adolescence: Findings from the Philadelphia Neurodevelopmental Cohort. Neuroscience and biobehavioral

reviews. 2016 Nov;70:159-70. PubMed PMID: 27498084. Pubmed Central PMCID: 5098398.

17.   Baron-Cohen S, Knickmeyer RC, Belmonte MK. Sex differences in the brain: implications for explaining autism. Science. 2005 Nov 4;310(5749):819-23. PubMed PMID: 16272115.

18.   Cahill L. Why sex matters for neuroscience. Nature reviews Neuroscience. 2006 Jun;7(6):477-84. PubMed PMID: 16688123.

19.   Cosgrove KP, Mazure CM, Staley JK. Evolving knowledge of sex differences in brain structure, function, and chemistry. Biological psychiatry. 2007 Oct 15;62(8):847-55. PubMed PMID: 17544382. Pubmed Central PMCID: 2711771.

20.   DeLacoste-Utamsing C, Holloway RL. Sexual dimorphism in the human corpus callosum. Science. 1982 Jun 25;216(4553):1431-2. PubMed PMID: 7089533.

21.   Goldstein JM, Seidman LJ, Horton NJ, Makris N, Kennedy DN, Caviness VS, Jr., et al. Normal sexual dimorphism of the adult human brain assessed by in vivo magnetic resonance imaging. Cerebral cortex. 2001 Jun;11(6):490-7. PubMed PMID: 11375910.

22.   Gur RC, Mozley PD, Resnick SM, Gottlieb GL, Kohn M, Zimmerman R, et al. Gender differences in age effect on brain atrophy measured by magnetic resonance imaging. Proceedings of the National Academy of Sciences of the United States of America. 1991 Apr 1;88(7):2845-9. PubMed PMID: 2011592. Pubmed Central PMCID: 51336.

23.   Sowell ER, Peterson BS, Kan E, Woods RP, Yoshii J, Bansal R, et al. Sex differences in cortical thickness mapped in 176 healthy individuals between 7 and 87 years of age. Cerebral cortex. 2007 Jul;17(7):1550-60. PubMed PMID: 16945978. Pubmed Central PMCID: 2329809.

24.   Scahill RI, Frost C, Jenkins R, Whitwell JL, Rossor MN, Fox NC. A longitudinal study of brain volume changes in normal aging using serial registered magnetic resonance imaging. Archives of neurology. 2003 Jul;60(7):989-94. PubMed PMID: 12873856.

25.   Giedd JN, Castellanos FX, Rajapakse JC, Vaituzis AC, Rapoport JL. Sexual dimorphism of the developing human brain. Progress in neuro-psychopharmacology & biological psychiatry. 1997 Nov;21(8):1185-201. PubMed PMID: 9460086.

26.   Ingalhalikar M, Smith A, Parker D, Satterthwaite TD, Elliott MA, Ruparel K, et al. Sex differences in the structural connectome of the human brain. Proceedings of the National Academy of Sciences of the United States of America. 2014 Jan 14;111(2):823-8. PubMed PMID: 24297904. Pubmed Central PMCID: 3896179.

27.   Luders E, Narr KL, Thompson PM, Rex DE, Woods RP, Deluca H, et al. Gender effects on cortical thickness and the influence of scaling. Human brain mapping. 2006 Apr;27(4):314-24. PubMed PMID: 16124013.

28.   Ahsan RL, Allom R, Gousias IS, Habib H, Turkheimer FE, Free S, et al. Volumes, spatial extents and a probabilistic atlas of the human basal ganglia and thalamus. NeuroImage. 2007 Nov 1;38(2):261-70. PubMed PMID: 17851093.

29.   Filipek PA, Richelme C, Kennedy DN, Caviness VS, Jr. The young adult human brain: an MRI-based morphometric analysis. Cerebral cortex. 1994 Jul-Aug;4(4):344-60. PubMed PMID: 7950308.

30.   Taber KH, Murphy DD, Blurton-Jones MM, Hurley RA. An update on estrogen: Higher cognitive function, receptor mapping, neurotrophic effects. J Neuropsych Clin N. 2001 Sum;13(3):313-7. PubMed PMID: WOS:000170433800001. English.

31.   Gray TS, Bingaman EW. The amygdala: Corticotropin-releasing factor, steroids, and stress. Crit Rev Neurobiol. 1996;10(2):155-68. PubMed PMID: WOS:A1996VZ29300002. English.

32.   Luders E, Gaser C, Narr KL, Toga AW. Why sex matters: brain size independent differences in gray matter distributions between men and women. The Journal of neuroscience : the official journal of the Society for Neuroscience. 2009 Nov 11;29(45):14265-70. PubMed PMID: 19906974. Pubmed Central PMCID: 3110817.

33.   Murphy DG, DeCarli C, McIntosh AR, Daly E, Mentis MJ, Pietrini P, et al. Sex differences in human brain morphometry and metabolism: an in vivo quantitative magnetic resonance imaging and positron emission tomography study on the effect of aging. Archives of general psychiatry. 1996 Jul;53(7):585-94. PubMed PMID: 8660125.

34.   Takahashi R, Ishii K, Kakigi T, Yokoyama K. Gender and age differences in normal adult human brain: voxel-based morphometric study. Human brain mapping. 2011 Jul;32(7):1050-8. PubMed PMID: 20607753.

35.   Sullivan EV, Rosenbloom M, Serventi KL, Pfefferbaum A. Effects of age and sex on volumes of the thalamus, pons, and cortex. Neurobiology of aging. 2004 Feb;25(2):185-92. PubMed PMID: 14749136.

36.   Rijpkema M, Everaerd D, van der Pol C, Franke B, Tendolkar I, Fernandez G. Normal sexual dimorphism in the human basal ganglia. Human brain mapping. 2012 May;33(5):1246-52. PubMed PMID: 21523857.

37.   Cheng Y, Chou KH, Decety J, Chen IY, Hung D, Tzeng OJ, et al. Sex differences in the neuroanatomy of human mirror-neuron system: a voxel-based morphometric investigation. Neuroscience. 2009 Jan 23;158(2):713-20. PubMed PMID: 19010397.

38.   Wilson RS, Rajan KB, Barnes LL, Hebert LE, Mendes de Leon CF, Evans DA. Cognitive aging and rate of hospitalization in an urban population of older people. The journals of gerontology Series A, Biological sciences and medical sciences. 2014 Apr;69(4):447-54. PubMed PMID: 24115773. Pubmed Central PMCID: 3968825.

39.   Mungas D, Reed BR, Jagust WJ, DeCarli C, Mack WJ, Kramer JH, et al. Volumetric MRI predicts rate of cognitive decline related to AD and cerebrovascular disease. Neurology. 2002 Sep 24;59(6):867-73. PubMed PMID: 12297568. Pubmed Central PMCID: 1820873.

40.   Rusinek H, De Santi S, Frid D, Tsui WH, Tarshish CY, Convit A, et al. Regional brain atrophy rate predicts future cognitive decline: 6-year longitudinal MR imaging study of normal aging. Radiology. 2003 Dec;229(3):691-6. PubMed PMID: 14657306.

41.   Courchesne E, Chisum HJ, Townsend J, Cowles A, Covington J, Egaas B, et al. Normal brain development and aging: quantitative analysis at in vivo MR imaging in healthy volunteers. Radiology. 2000 Sep;216(3):672-82. PubMed PMID: 10966694.

42.   Ge Y, Grossman RI, Babb JS, Rabin ML, Mannon LJ, Kolson DL. Age-related total gray matter and white matter changes in normal adult brain. Part I: volumetric MR imaging analysis. AJNR American journal of neuroradiology. 2002 Sep;23(8):1327-33. PubMed PMID: 12223373.

43.   Good CD, Johnsrude IS, Ashburner J, Henson RN, Friston KJ, Frackowiak RS. A voxel-based morphometric study of ageing in 465 normal adult human brains. NeuroImage. 2001 Jul;14(1 Pt 1):21-36. PubMed PMID: 11525331. Epub 2001/08/30. eng.

44.   Guttmann CR, Jolesz FA, Kikinis R, Killiany RJ, Moss MB, Sandor T, et al. White matter changes with normal aging. Neurology. 1998 Apr;50(4):972-8. PubMed PMID: 9566381.

45.   Pell GS, Briellmann RS, Chan CH, Pardoe H, Abbott DF, Jackson GD. Selection of the control group for VBM analysis: influence of covariates, matching and sample size. NeuroImage. 2008 Jul 15;41(4):1324-35. PubMed PMID: 18467131.

46.   Raz N, Gunning FM, Head D, Dupuis JH, McQuain J, Briggs SD, et al. Selective aging of the human cerebral cortex observed in vivo: differential vulnerability of the prefrontal gray matter. Cerebral cortex. 1997 Apr-May;7(3):268-82. PubMed PMID: 9143446.

47.   Smith CD, Chebrolu H, Wekstein DR, Schmitt FA, Markesbery WR. Age and gender effects on human brain anatomy: a voxel-based morphometric study in healthy elderly. Neurobiology of aging. 2007 Jul;28(7):1075-87. PubMed PMID: 16774798.

48.   Taki Y, Goto R, Evans A, Zijdenbos A, Neelin P, Lerch J, et al. Voxel-based morphometry of human brain with age and cerebrovascular risk factors. Neurobiology of aging. 2004 Apr;25(4):455-63. PubMed PMID: 15013566.

49.   Fotenos AF, Snyder AZ, Girton LE, Morris JC, Buckner RL. Normative estimates of cross-sectional and longitudinal brain volume decline in aging and AD. Neurology. 2005 Mar 22;64(6):1032-9. PubMed PMID: 15781822.

50.   Blatter DD, Bigler ED, Gale SD, Johnson SC, Anderson CV, Burnett BM, et al. Quantitative volumetric analysis of brain MR: normative database spanning 5 decades of life. AJNR American journal of neuroradiology. 1995 Feb;16(2):241-51. PubMed PMID: 7726068.

51.   Jernigan TL, Archibald SL, Fennema-Notestine C, Gamst AC, Stout JC, Bonner J, et al. Effects of age on tissues and regions of the cerebrum and cerebellum. Neurobiology of aging. 2001 Jul-Aug;22(4):581-94. PubMed PMID: 11445259.

52.   Pfefferbaum A, Mathalon DH, Sullivan EV, Rawles JM, Zipursky RB, Lim KO. A quantitative magnetic resonance imaging study of changes in brain morphology from infancy to late adulthood. Archives of neurology. 1994 Sep;51(9):874-87. PubMed PMID: 8080387.

53.   Raz N, Gunning-Dixon F, Head D, Rodrigue KM, Williamson A, Acker JD. Aging, sexual dimorphism, and hemispheric asymmetry of the cerebral cortex: replicability of regional differences in volume. Neurobiology of aging. 2004 Mar;25(3):377-96. PubMed PMID: 15123343.

54.   Walhovd KB, Westlye LT, Amlien I, Espeseth T, Reinvang I, Raz N, et al. Consistent neuroanatomical age-related volume differences across multiple samples. Neurobiology of aging. 2011 May;32(5):916-32. PubMed PMID: 19570593. Pubmed Central PMCID: 4040218.

55.   Pfefferbaum A, Rohlfing T, Rosenbloom MJ, Chu W, Colrain IM, Sullivan EV. Variation in longitudinal trajectories of regional brain volumes of healthy men and women (ages 10 to 85 years) measured with atlas-based parcellation of MRI. NeuroImage. 2013 Jan 15;65:176-93. PubMed PMID: 23063452. Pubmed Central PMCID: 3516371.

56.   Jack CR, Jr., Petersen RC, Xu Y, O'Brien PC, Smith GE, Ivnik RJ, et al. Rates of hippocampal atrophy correlate with change in clinical status in aging and AD. Neurology. 2000 Aug 22;55(4):484-89. PubMed PMID: 10953178. Pubmed Central PMCID: 2724764.

57.   Luft AR, Skalej M, Schulz JB, Welte D, Kolb R, Burk K, et al. Patterns of age-related shrinkage in cerebellum and brainstem observed in vivo using three-dimensional MRI volumetry. Cerebral cortex. 1999 Oct-Nov;9(7):712-21. PubMed PMID: 10554994.

58.   Raz N, Rodrigue KM, Kennedy KM, Head D, Gunning-Dixon F, Acker JD. Differential aging of the human striatum: longitudinal evidence. AJNR American journal of neuroradiology. 2003 Oct;24(9):1849-56. PubMed PMID: 14561615.

59.   Sullivan EV, Marsh L, Pfefferbaum A. Preservation of hippocampal volume throughout adulthood in healthy men and women. Neurobiology of aging. 2005 Jul;26(7):1093-8. PubMed PMID: 15748789.

60.   Lemaitre H, Crivello F, Grassiot B, Alperovitch A, Tzourio C, Mazoyer B. Age- and sex-related effects on the neuroanatomy of healthy elderly. NeuroImage. 2005 Jul 1;26(3):900-11. PubMed PMID: 15955500.

61.   Taki Y, Thyreau B, Kinomura S, Sato K, Goto R, Kawashima R, et al. Correlations among brain gray matter volumes, age, gender, and hemisphere in healthy individuals. PloS one. 2011;6(7):e22734. PubMed PMID: 21818377. Pubmed Central PMCID: 3144937.

62.   DeCarli C, Massaro J, Harvey D, Hald J, Tullberg M, Au R, et al. Measures of brain morphology and infarction in the framingham heart study: establishing what is normal. Neurobiology of aging. 2005 Apr;26(4):491-510. PubMed PMID: 15653178.

63.   Perlaki G, Orsi G, Plozer E, Altbacker A, Darnai G, Nagy SA, et al. Are there any gender differences in the hippocampus volume after head-size correction? A volumetric and voxel-based morphometric study. Neuroscience letters. 2014 Jun 6;570:119-23. PubMed PMID: 24746928.

64.   Szabo N, Kincses ZT, Pardutz A, Tajti J, Szok D, Tuka B, et al. White matter microstructural alterations in migraine: a diffusion-weighted MRI study. Pain. 2012 Mar;153(3):651-6. PubMed PMID: 22244439.

65.   Naegel S, Holle D, Desmarattes N, Theysohn N, Diener HC, Katsarava Z, et al. Cortical plasticity in episodic and chronic cluster headache. NeuroImage Clinical. 2014;6:415-23. PubMed PMID: 25379455. Pubmed Central PMCID: 4218933.

66.   Teepker M, Menzler K, Belke M, Heverhagen JT, Voelker M, Mylius V, et al. Diffusion tensor imaging in episodic cluster headache. Headache. 2012 Feb;52(2):274-82. PubMed PMID: 22082475.

67.   Takao H, Hayashi N, Ohtomo K. White matter asymmetry in healthy individuals: a diffusion tensor imaging study using tract-based spatial statistics. Neuroscience. 2011 Oct 13;193:291-9. PubMed PMID: 21824507.

68.   Buchel C, Raedler T, Sommer M, Sach M, Weiller C, Koch MA. White matter asymmetry in the human brain: a diffusion tensor MRI study. Cerebral cortex. 2004 Sep;14(9):945-51. PubMed PMID: 15115737.

69.   Gong G, Jiang T, Zhu C, Zang Y, He Y, Xie S, et al. Side and handedness effects on the cingulum from diffusion tensor imaging. Neuroreport. 2005 Oct 17;16(15):1701-5. PubMed PMID: 16189481.

70.   Fabiano AJ, Horsfield MA, Bakshi R. Interhemispheric asymmetry of brain diffusivity in normal individuals: a diffusion-weighted MR imaging study. AJNR American journal of neuroradiology. 2005 May;26(5):1089-94. PubMed PMID: 15891165.

71.   Schmidt-Wilcke T, Leinisch E, Ganssbauer S, Draganski B, Bogdahn U, Altmeppen J, et al. Affective components and intensity of pain correlate with structural differences in gray matter in chronic back pain patients. Pain. 2006 Nov;125(1-2):89-97. PubMed PMID: 16750298. Epub 2006/06/06. eng.

72.   Maleki N, Becerra L, Nutile L, Pendse G, Brawn J, Bigal M, et al. Migraine attacks the Basal Ganglia. Molecular pain. 2011;7:71. PubMed PMID: 21936901. Pubmed Central PMCID: 3192678. Epub 2011/09/23. eng.

73.   Absinta M, Rocca MA, Colombo B, Falini A, Comi G, Filippi M. Selective decreased grey matter volume of the pain-matrix network in cluster headache. Cephalalgia : an

international journal of headache. 2012 Jan;32(2):109-15. PubMed PMID: 22174349. Epub 2011/12/17. eng.

74. Borsook D, Upadhyay J, Chudler EH, Becerra L. A key role of the basal ganglia in pain and analgesia--insights gained through human functional imaging. Molecular pain. 2010;6:27. PubMed PMID: 20465845. Pubmed Central PMCID: 2883978.

75. Juri C, Rodriguez-Oroz M, Obeso JA. The pathophysiological basis of sensory disturbances in Parkinson's disease. Journal of the neurological sciences. 2010 Feb 15;289(1-2):60-5. PubMed PMID: 19758602.

76. Bingel U, Glascher J, Weiller C, Buchel C. Somatotopic representation of nociceptive information in the putamen: an event-related fMRI study. Cerebral cortex. 2004 Dec;14(12):1340-5. PubMed PMID: 15217895. Epub 2004/06/26. eng.

77. Chudler EH. Response properties of neurons in the caudate-putamen and globus pallidus to noxious and non-noxious thermal stimulation in anesthetized rats. Brain Res. 1998 Nov;812(1-2):283-8. PubMed PMID: 9813370. eng.

78. Hagelberg N, Jaaskelainen SK, Martikainen IK, Mansikka H, Forssell H, Scheinin H, et al. Striatal dopamine D2 receptors in modulation of pain in humans: a review. Eur J Pharmacol. 2004 Oct 1;500(1-3):187-92. PubMed PMID: 15464032. Epub 2004/10/07. eng.

79. Starr CJ, Sawaki L, Wittenberg GF, Burdette JH, Oshiro Y, Quevedo AS, et al. The contribution of the putamen to sensory aspects of pain: insights from structural connectivity and brain lesions. Brain. 2011 Jul;134(Pt 7):1987-2004. PubMed PMID: 21616963. Pubmed Central PMCID: PMC3122370. eng.

80. Headache Classification Subcommittee of the International Headache S. The International Classification of Headache Disorders: 2nd edition. Cephalalgia : an international journal of headache. 2004;24 Suppl 1:9-160. PubMed PMID: 14979299.

81. Russell MB. Epidemiology and genetics of cluster headache. Lancet neurology. 2004 May;3(5):279-83. PubMed PMID: 15099542.

82. Gardian G, Vecsei L. Huntington's disease: pathomechanism and therapeutic perspectives. Journal of neural transmission. 2004 Oct;111(10-11):1485-94. PubMed PMID: 15480847.

83. Peinemann A, Schuller S, Pohl C, Jahn T, Weindl A, Kassubek J. Executive dysfunction in early stages of Huntington's disease is associated with striatal and insular atrophy: a neuropsychological and voxel-based morphometric study. Journal of the neurological sciences. 2005 Dec 15;239(1):11-9. PubMed PMID: 16185716.

84. Kassubek J, Juengling FD, Ecker D, Landwehrmeyer GB. Thalamic atrophy in Huntington's disease co-varies with cognitive performance: a morphometric MRI analysis. Cerebral cortex. 2005 Jun;15(6):846-53. PubMed PMID: 15459079.

85. Antal A, Beniczky S, Kincses TZ, Jakab K, Benedek G, Vecsei L. Perceptual categorization is impaired in Huntington's disease: an electrophysiological study. Dementia and geriatric cognitive disorders. 2003;16(4):187-92. PubMed PMID: 14512712.

86. Nemeth D, Dye CD, Sefcsik T, Janacsek K, Turi Z, Londe Z, et al. Language deficits in pre-symptomatic Huntington's disease: evidence from Hungarian. Brain and language. 2012 Jun;121(3):248-53. PubMed PMID: 22538085. Pubmed Central PMCID: 3350800.

87. Papp KV, Kaplan RF, Snyder PJ. Biological markers of cognition in prodromal Huntington's disease: a review. Brain and cognition. 2011 Nov;77(2):280-91. PubMed PMID: 21889251.

88.   Quarrell OW, Rigby AS, Barron L, Crow Y, Dalton A, Dennis N, et al. Reduced penetrance alleles for Huntington's disease: a multi-centre direct observational study. Journal of medical genetics. 2007 Mar;44(3):e68. PubMed PMID: 17361007. Pubmed Central PMCID: 2598018.

89.   Vonsattel JP, Myers RH, Stevens TJ, Ferrante RJ, Bird ED, Richardson EP, Jr. Neuropathological classification of Huntington's disease. Journal of neuropathology and experimental neurology. 1985 Nov;44(6):559-77. PubMed PMID: 2932539.

90.   Thieben MJ, Duggins AJ, Good CD, Gomes L, Mahant N, Richards F, et al. The distribution of structural neuropathology in pre-clinical Huntington's disease. Brain. 2002 Aug;125(Pt 8):1815-28. PubMed PMID: 12135972.

91.   Andrew SE, Goldberg YP, Kremer B, Telenius H, Theilmann J, Adam S, et al. The relationship between trinucleotide (CAG) repeat length and clinical features of Huntington's disease. Nature genetics. 1993 Aug;4(4):398-403. PubMed PMID: 8401589.

92.   Aylward EH, Anderson NB, Bylsma FW, Wagster MV, Barta PE, Sherr M, et al. Frontal lobe volume in patients with Huntington's disease. Neurology. 1998 Jan;50(1):252-8. PubMed PMID: 9443488.

93.   Beglinger LJ, Nopoulos PC, Jorge RE, Langbehn DR, Mikos AE, Moser DJ, et al. White matter volume and cognitive dysfunction in early Huntington's disease. Cognitive and behavioral neurology : official journal of the Society for Behavioral and Cognitive Neurology. 2005 Jun;18(2):102-7. PubMed PMID: 15970729.

94.   Ciarmiello A, Cannella M, Lastoria S, Simonelli M, Frati L, Rubinsztein DC, et al. Brain white-matter volume loss and glucose hypometabolism precede the clinical symptoms of Huntington's disease. Journal of nuclear medicine : official publication, Society of Nuclear Medicine. 2006 Feb;47(2):215-22. PubMed PMID: 16455626.

95.   Fennema-Notestine C, Archibald SL, Jacobson MW, Corey-Bloom J, Paulsen JS, Peavy GM, et al. In vivo evidence of cerebellar atrophy and cerebral white matter loss in Huntington disease. Neurology. 2004 Sep 28;63(6):989-95. PubMed PMID: 15452288.

96.   Jernigan TL, Salmon DP, Butters N, Hesselink JR. Cerebral structure on MRI, Part II: Specific changes in Alzheimer's and Huntington's diseases. Biological psychiatry. 1991 Jan 1;29(1):68-81. PubMed PMID: 1825793.

97.   Muhlau M, Weindl A, Wohlschlager AM, Gaser C, Stadtler M, Valet M, et al. Voxel-based morphometry indicates relative preservation of the limbic prefrontal cortex in early Huntington disease. Journal of neural transmission. 2007 Mar;114(3):367-72. PubMed PMID: 17024326.

98.   Rosas HD, Koroshetz WJ, Chen YI, Skeuse C, Vangel M, Cudkowicz ME, et al. Evidence for more widespread cerebral pathology in early HD: an MRI-based morphometric analysis. Neurology. 2003 May 27;60(10):1615-20. PubMed PMID: 12771251.

99.   Paulsen JS, Hayden M, Stout JC, Langbehn DR, Aylward E, Ross CA, et al. Preparing for preventive clinical trials: the Predict-HD study. Archives of neurology. 2006 Jun;63(6):883-90. PubMed PMID: 16769871.

100.   Paulsen JS, Nopoulos PC, Aylward E, Ross CA, Johnson H, Magnotta VA, et al. Striatal and white matter predictors of estimated diagnosis for Huntington disease. Brain research bulletin. 2010 May 31;82(3-4):201-7. PubMed PMID: 20385209. Pubmed Central PMCID: 2892238.

101.   Rosas HD, Liu AK, Hersch S, Glessner M, Ferrante RJ, Salat DH, et al. Regional and progressive thinning of the cortical ribbon in Huntington's disease. Neurology. 2002 Mar 12;58(5):695-701. PubMed PMID: 11889230.

102.   Rosas HD, Hevelone ND, Zaleta AK, Greve DN, Salat DH, Fischl B. Regional cortical thinning in preclinical Huntington disease and its relationship to cognition. Neurology. 2005 Sep 13;65(5):745-7. PubMed PMID: 16157910.

103.   Tabrizi SJ, Langbehn DR, Leavitt BR, Roos RA, Durr A, Craufurd D, et al. Biological and clinical manifestations of Huntington's disease in the longitudinal TRACK-HD study: cross-sectional analysis of baseline data. Lancet neurology. 2009 Sep;8(9):791-801. PubMed PMID: 19646924. Pubmed Central PMCID: 3725974.

104.   Aylward EH, Nopoulos PC, Ross CA, Langbehn DR, Pierson RK, Mills JA, et al. Longitudinal change in regional brain volumes in prodromal Huntington disease. Journal of neurology, neurosurgery, and psychiatry. 2011 Apr;82(4):405-10. PubMed PMID: 20884680. Pubmed Central PMCID: 3105627.

105.   Tabrizi SJ, Scahill RI, Durr A, Roos RA, Leavitt BR, Jones R, et al. Biological and clinical changes in premanifest and early stage Huntington's disease in the TRACK-HD study: the 12-month longitudinal analysis. Lancet neurology. 2011 Jan;10(1):31-42. PubMed PMID: 21130037.

106.   Morel A, Magnin M, Jeanmonod D. Multiarchitectonic and stereotactic atlas of the human thalamus. The Journal of comparative neurology. 1997 Nov 3;387(4):588-630. PubMed PMID: 9373015.

107.   Nowinski WL, Belov D, Benabid AL. A community-centric internet portal for stereotactic and functional neurosurgery with a probabilistic functional atlas. Stereotactic and functional neurosurgery. 2002;79(1):1-12. PubMed PMID: 12677100.

108.   Nowinski WL, Belov D, Thirunavuukarasuu A, Benabid AL. A probabilistic functional atlas of the VIM nucleus constructed from pre-, intra- and postoperative electrophysiological and neuroimaging data acquired during the surgical treatment of Parkinson's disease patients. Stereotactic and functional neurosurgery. 2005;83(5-6):190-6. PubMed PMID: 16424683.

109.   Bittar RG, Hyam J, Nandi D, Wang S, Liu X, Joint C, et al. Thalamotomy versus thalamic stimulation for multiple sclerosis tremor. Journal of clinical neuroscience : official journal of the Neurosurgical Society of Australasia. 2005 Aug;12(6):638-42. PubMed PMID: 16098758.

110.   Dormont D, Cornu P, Pidoux B, Bonnet AM, Biondi A, Oppenheim C, et al. Chronic thalamic stimulation with three-dimensional MR stereotactic guidance. AJNR American journal of neuroradiology. 1997 Jun-Jul;18(6):1093-107. PubMed PMID: 9194437.

111.   Alusi SH, Aziz TZ, Glickman S, Jahanshahi M, Stein JF, Bain PG. Stereotactic lesional surgery for the treatment of tremor in multiple sclerosis: a prospective case-controlled study. Brain. 2001 Aug;124(Pt 8):1576-89. PubMed PMID: 11459749.

112.   Deoni SC, Josseau MJ, Rutt BK, Peters TM. Visualization of thalamic nuclei on high resolution, multi-averaged T1 and T2 maps acquired at 1.5 T. Human brain mapping. 2005 Jul;25(3):353-9. PubMed PMID: 15852386.

113.   Deoni SC, Rutt BK, Parrent AG, Peters TM. Segmentation of thalamic nuclei using a modified k-means clustering algorithm and high-resolution quantitative magnetic resonance imaging at 1.5 T. NeuroImage. 2007 Jan 1;34(1):117-26. PubMed PMID: 17070073.

114.   Hyam JA, Owen SL, Kringelbach ML, Jenkinson N, Stein JF, Green AL, et al. Contrasting connectivity of the ventralis intermedius and ventralis oralis posterior nuclei of the motor thalamus demonstrated by probabilistic tractography. Neurosurgery. 2012 Jan;70(1):162-9; discussion 9. PubMed PMID: 22158304.

115.   Behrens TE, Johansen-Berg H, Woolrich MW, Smith SM, Wheeler-Kingshott CA, Boulby PA, et al. Non-invasive mapping of connections between human thalamus and

cortex using diffusion imaging. Nature neuroscience. 2003 Jul;6(7):750-7. PubMed PMID: 12808459.

116. Johansen-Berg H, Behrens TE, Sillery E, Ciccarelli O, Thompson AJ, Smith SM, et al. Functional-anatomical validation and individual variation of diffusion tractography-based segmentation of the human thalamus. Cerebral cortex. 2005 Jan;15(1):31-9. PubMed PMID: 15238447.

117. Garcia-Finana M, Cruz-Orive LM, Mackay CE, Pakkenberg B, Roberts N. Comparison of MR imaging against physical sectioning to estimate the volume of human cerebral compartments. NeuroImage. 2003 Feb;18(2):505-16. PubMed PMID: 12595203.

118. Roberts N, Puddephat MJ, McNulty V. The benefit of stereology for quantitative radiology. The British journal of radiology. 2000 Jul;73(871):679-97. PubMed PMID: 11089458.

119. Geuze E, Vermetten E, Bremner JD. MR-based in vivo hippocampal volumetrics: 1. Review of methodologies currently employed. Molecular psychiatry. 2005 Feb;10(2):147-59. PubMed PMID: 15340353.

120. Smith SM, De Stefano N, Jenkinson M, Matthews PM. Normalized accurate measurement of longitudinal brain change. Journal of computer assisted tomography. 2001 May-Jun;25(3):466-75. PubMed PMID: 11351200.

121. Smith SM, Zhang Y, Jenkinson M, Chen J, Matthews PM, Federico A, et al. Accurate, robust, and automated longitudinal and cross-sectional brain change analysis. NeuroImage. 2002 Sep;17(1):479-89. PubMed PMID: 12482100.

122. Ashburner J, Friston KJ. Voxel-based morphometry--the methods. NeuroImage. 2000 Jun;11(6 Pt 1):805-21. PubMed PMID: 10860804.

123. Patenaude B, Smith SM, Kennedy DN, Jenkinson M. A Bayesian model of shape and appearance for subcortical brain segmentation. NeuroImage. 2011 Jun 1;56(3):907-22. PubMed PMID: 21352927. Pubmed Central PMCID: PMC3417233.

124. Jensen JH, Helpern JA, Ramani A, Lu H, Kaczynski K. Diffusional kurtosis imaging: the quantification of non-gaussian water diffusion by means of magnetic resonance imaging. Magnetic resonance in medicine. 2005 Jun;53(6):1432-40. PubMed PMID: 15906300.

125. Melhem ER, Mori S, Mukundan G, Kraut MA, Pomper MG, van Zijl PC. Diffusion tensor MR imaging of the brain and white matter tractography. AJR Am J Roentgenol. 2002 Jan;178(1):3-16. PubMed PMID: 11756078. Epub 2002/01/05. eng.

126. Mori S, van Zijl PC. Fiber tracking: principles and strategies - a technical review. NMR Biomed. 2002 Nov-Dec;15(7-8):468-80. PubMed PMID: 12489096. Epub 2002/12/19. eng.

127. Beaulieu C. The basis of anisotropic water diffusion in the nervous system - a technical review. NMR Biomed. 2002 Nov-Dec;15(7-8):435-55. PubMed PMID: 12489094. Epub 2002/12/19. eng.

128. Behrens TE, Woolrich MW, Jenkinson M, Johansen-Berg H, Nunes RG, Clare S, et al. Characterization and propagation of uncertainty in diffusion-weighted MR imaging. Magnetic resonance in medicine. 2003 Nov;50(5):1077-88. PubMed PMID: 14587019.

129. Parker GJ, Haroon HA, Wheeler-Kingshott CA. A framework for a streamline-based probabilistic index of connectivity (PICo) using a structural interpretation of MRI diffusion measurements. J Magn Reson Imaging. 2003;18:242-54.

130. Kiraly A, Szabo N, Toth E, Csete G, Farago P, Kocsis K, et al. Male brain ages faster: the age and gender dependence of subcortical volumes. Brain imaging and behavior. 2016 Sep;10(3):901-10. PubMed PMID: 26572143.

131. Kiraly A, Szabo N, Pardutz A, Toth E, Tajti J, Csete G, et al. Macro- and microstructural alterations of the subcortical structures in episodic cluster headache. Cephalalgia : an international journal of headache. 2017 Jan 1:333102417703762. PubMed PMID: 28425325.

132. Kincses ZT, Szabo N, Valalik I, Kopniczky Z, Dezsi L, Klivenyi P, et al. Target identification for stereotactic thalamotomy using diffusion tractography. PloS one. 2012;7(1):e29969. PubMed PMID: 22238685. Pubmed Central PMCID: 3251609.

133. Kiraly A, Kincses ZT, Szabo N, Toth E, Csete G, Farago P, et al. Gray matter atrophy in presymptomatic Huntington's patients. Ideggyogyaszati szemle. 2016 Jul 30;69(7-8):261-7. PubMed PMID: 29465891. A szurke allomany atrofiaja a preszimptomatikus huntingtonos betegekben.

134. Hamilton M. A rating scale for depression. Journal of neurology, neurosurgery, and psychiatry. 1960 Feb;23:56-62. PubMed PMID: 14399272. Pubmed Central PMCID: 495331.

135. Smith SM, Jenkinson M, Woolrich MW, Beckmann CF, Behrens TE, Johansen-Berg H, et al. Advances in functional and structural MR image analysis and implementation as FSL. NeuroImage. 2004;23 Suppl 1:S208-19. PubMed PMID: 15501092.

136. Smith SM. Fast robust automated brain extraction. Human brain mapping. 2002 Nov;17(3):143-55. PubMed PMID: 12391568.

137. Jenkinson M, Bannister P, Brady M, Smith S. Improved optimization for the robust and accurate linear registration and motion correction of brain images. NeuroImage. 2002 Oct;17(2):825-41. PubMed PMID: 12377157.

138. Jenkinson M, Smith S. A global optimisation method for robust affine registration of brain images. Medical image analysis. 2001 Jun;5(2):143-56. PubMed PMID: 11516708.

139. Zhang Y, Brady M, Smith S. Segmentation of brain MR images through a hidden Markov random field model and the expectation-maximization algorithm. IEEE transactions on medical imaging. 2001 Jan;20(1):45-57. PubMed PMID: 11293691.

140. Smith SM, Nichols TE. Threshold-free cluster enhancement: addressing problems of smoothing, threshold dependence and localisation in cluster inference. NeuroImage. 2009 Jan 1;44(1):83-98. PubMed PMID: 18501637.

141. Behrens TE, Berg HJ, Jbabdi S, Rushworth MF, Woolrich MW. Probabilistic diffusion tractography with multiple fibre orientations: What can we gain? NeuroImage. 2007 Jan 1;34(1):144-55. PubMed PMID: 17070705.

142. Crum WR, Camara O, Hill DL. Generalized overlap measures for evaluation and validation in medical image analysis. IEEE transactions on medical imaging. 2006 Nov;25(11):1451-61. PubMed PMID: 17117774.

143. Efron B. Missing Data, Imputation, and the Bootstrap. J Am Stat Assoc. 1994 Jun;89(426):463-75. PubMed PMID: WOS:A1994NN15500016. English.

144. Guiot G, Arfel G, Derome P, Kahn A. [Neurophysiologic control procedures for sterotaxic thalamotomy]. Neuro-Chirurgie. 1968 May;14(4):553-66. PubMed PMID: 4879813. Procedes de controle neurophysiologique pour la thalamotomie stereotaxique.

145. Guiot G, Derome P, Kahn A. [The ventral posterior nucleus: an electrophysiological reference point in stereotaxic thalamotomies]. Cesk Neurol. 1968 Mar;31(2):112-8. PubMed PMID: 4889923. Epub 1968/03/01. Le noyau ventral posterieur: repere electro-physiologique dans les thalamotomies stereotaxiques. fre.

146. Tian Q, Wintermark M, Jeffrey Elias W, Ghanouni P, Halpern CH, Henderson JM, et al. Diffusion MRI tractography for improved transcranial MRI-guided focused

ultrasound thalamotomy targeting for essential tremor. NeuroImage Clinical. 2018;19:572-80. PubMed PMID: 29984165. Pubmed Central PMCID: 6029558.

147. Munnich T, Klein J, Hattingen E, Noack A, Herrmann E, Seifert V, et al. Tractography Verified by Intraoperative Magnetic Resonance Imaging and Subcortical Stimulation During Tumor Resection Near the Corticospinal Tract. Operative neurosurgery. 2018 Apr 14. PubMed PMID: 29669002.

148. Middlebrooks EH, Tuna IS, Grewal SS, Almeida L, Heckman MG, Lesser ER, et al. Segmentation of the Globus Pallidus Internus Using Probabilistic Diffusion Tractography for Deep Brain Stimulation Targeting in Parkinson Disease. AJNR American journal of neuroradiology. 2018 Jun;39(6):1127-34. PubMed PMID: 29700048.

149. Barnes J, Ridgway GR, Bartlett J, Henley SM, Lehmann M, Hobbs N, et al. Head size, age and gender adjustment in MRI studies: a necessary nuisance? NeuroImage. 2010 Dec;53(4):1244-55. PubMed PMID: 20600995.

150. Ge Y, Grossman RI, Babb JS, Rabin ML, Mannon LJ, Kolson DL. Age-related total gray matter and white matter changes in normal adult brain. Part II: quantitative magnetization transfer ratio histogram analysis. AJNR American journal of neuroradiology. 2002 Sep;23(8):1334-41. PubMed PMID: 12223374.

151. Callaert DV, Ribbens A, Maes F, Swinnen SP, Wenderoth N. Assessing age-related gray matter decline with voxel-based morphometry depends significantly on segmentation and normalization procedures. Frontiers in aging neuroscience. 2014;6:124. PubMed PMID: 25002845. Pubmed Central PMCID: 4066859.

152. Abedelahi A, Hasanzadeh H, Hadizadeh H, Joghataie MT. Morphometric and volumetric study of caudate and putamen nuclei in normal individuals by MRI: Effect of normal aging, gender and hemispheric differences. Polish journal of radiology / Polish Medical Society of Radiology. 2013 Jul;78(3):7-14. PubMed PMID: 24115954. Pubmed Central PMCID: 3789937.

153. Goodro M, Sameti M, Patenaude B, Fein G. Age effect on subcortical structures in healthy adults. Psychiatry research. 2012 Jul 30;203(1):38-45. PubMed PMID: 22863654. Pubmed Central PMCID: 3444666.

154. Li W, van Tol MJ, Li M, Miao W, Jiao Y, Heinze HJ, et al. Regional specificity of sex effects on subcortical volumes across the lifespan in healthy aging. Human brain mapping. 2014 Jan;35(1):238-47. PubMed PMID: 22996803.

155. Schwab NA, Tanner JJ, Nguyen PT, Schmalfuss IM, Bowers D, Okun M, et al. Proof of principle: Transformation approach alters caudate nucleus volume and structure-function associations. Brain imaging and behavior. 2014 Nov 21. PubMed PMID: 25413122. Pubmed Central PMCID: 4440856.

156. Wang Q, Xu X, Zhang M. Normal aging in the basal ganglia evaluated by eigenvalues of diffusion tensor imaging. AJNR American journal of neuroradiology. 2010 Mar;31(3):516-20. PubMed PMID: 19892817.

157. Abe O, Yamasue H, Aoki S, Suga M, Yamada H, Kasai K, et al. Aging in the CNS: comparison of gray/white matter volume and diffusion tensor data. Neurobiology of aging. 2008 Jan;29(1):102-16. PubMed PMID: 17023094.

158. Pfefferbaum A, Adalsteinsson E, Rohlfing T, Sullivan EV. Diffusion tensor imaging of deep gray matter brain structures: effects of age and iron concentration. Neurobiology of aging. 2010 Mar;31(3):482-93. PubMed PMID: 18513834. Pubmed Central PMCID: 2815127.

159. Macchi G, Jones EG. Toward an agreement on terminology of nuclear and subnuclear divisions of the motor thalamus. J Neurosurg. 1997 Apr;86(4):670-85. PubMed PMID: 9120632.

160.   Rosenblatt A, Liang KY, Zhou H, Abbott MH, Gourley LM, Margolis RL, et al. The association of CAG repeat length with clinical progression in Huntington disease. Neurology. 2006 Apr 11;66(7):1016-20. PubMed PMID: 16606912.

161.   Aziz NA, Jurgens CK, Landwehrmeyer GB, Group ERS, van Roon-Mom WM, van Ommen GJ, et al. Normal and mutant HTT interact to affect clinical severity and progression in Huntington disease. Neurology. 2009 Oct 20;73(16):1280-5. PubMed PMID: 19776381.

162.   Halliday GM, McRitchie DA, Macdonald V, Double KL, Trent RJ, McCusker E. Regional specificity of brain atrophy in Huntington's disease. Exp Neurol. 1998 Dec;154(2):663-72. PubMed PMID: 9878201.

163.   Rosas HD, Goodman J, Chen YI, Jenkins BG, Kennedy DN, Makris N, et al. Striatal volume loss in HD as measured by MRI and the influence of CAG repeat. Neurology. 2001 Sep 25;57(6):1025-8. PubMed PMID: 11571328.

164.   Aylward E, Mills J, Liu D, Nopoulos P, Ross CA, Pierson R, et al. Association between Age and Striatal Volume Stratified by CAG Repeat Length in Prodromal Huntington Disease. PLoS currents. 2011;3:RRN1235. PubMed PMID: 21593963. Pubmed Central PMCID: 3092625.

165.   Henley SM, Wild EJ, Hobbs NZ, Scahill RI, Ridgway GR, Macmanus DG, et al. Relationship between CAG repeat length and brain volume in premanifest and early Huntington's disease. Journal of neurology. 2009 Feb;256(2):203-12. PubMed PMID: 19266143.

166.   Aylward EH, Li Q, Stine OC, Ranen N, Sherr M, Barta PE, et al. Longitudinal change in basal ganglia volume in patients with Huntington's disease. Neurology. 1997 Feb;48(2):394-9. PubMed PMID: 9040728.

167.   Ruocco HH, Bonilha L, Li LM, Lopes-Cendes I, Cendes F. Longitudinal analysis of regional grey matter loss in Huntington disease: effects of the length of the expanded CAG repeat. J Neurol Neurosurg Psychiatry. 2008 Feb;79(2):130-5. PubMed PMID: 17615168.

168.   Gomez-Anson B, Alegret M, Munoz E, Monte GC, Alayrach E, Sanchez A, et al. Prefrontal cortex volume reduction on MRI in preclinical Huntington's disease relates to visuomotor performance and CAG number. Parkinsonism Relat D. 2009 Mar;15(3):213-9. PubMed PMID: WOS:000264584700007. English.

169.   Henley SMD, Wild EJ, Hobbs NZ, Frost C, MacManus DG, Barker RA, et al. Whole-Brain Atrophy as a Measure of Progression in Premanifest and Early Huntington's Disease. Movement Disord. 2009 Apr 30;24(6):932-6. PubMed PMID: WOS:000265587900022. English.

170.   Gardian G, Vecsei L. Huntington's disease: pathomechanism and therapeutic perspectives. J Neural Transm. 2004 Oct;111(10-11):1485-94. PubMed PMID: 15480847. Epub 2004/10/14. eng.

171.   Webb SJ, Monk CS, Nelson CA. Mechanisms of postnatal neurobiological development: implications for human development. Developmental neuropsychology. 2001;19(2):147-71. PubMed PMID: 11530973.

172.   Terry RD, DeTeresa R, Hansen LA. Neocortical cell counts in normal human adult aging. Annals of neurology. 1987 Jun;21(6):530-9. PubMed PMID: 3606042.

173.   Peters A, Morrison JH, Rosene DL, Hyman BT. Feature article: are neurons lost from the primate cerebral cortex during normal aging? Cerebral cortex. 1998 Jun;8(4):295-300. PubMed PMID: 9651126.

174.   Salminen LE, Conturo TE, Laidlaw DH, Cabeen RP, Akbudak E, Lane EM, et al. Regional age differences in gray matter diffusivity among healthy older adults. Brain imaging and behavior. 2015 Apr 12. PubMed PMID: 25864197.

175.   Barron AM, Pike CJ. Sex hormones, aging, and Alzheimer's disease. Frontiers in bioscience. 2012;4:976-97. PubMed PMID: 22201929. Pubmed Central PMCID: 3511049.

176.   Riccardi P, Park S, Anderson S, Doop M, Ansari MS, Schmidt D, et al. Sex differences in the relationship of regional dopamine release to affect and cognitive function in striatal and extrastriatal regions using positron emission tomography and [(1)(8)F]fallypride. Synapse. 2011 Feb;65(2):99-102. PubMed PMID: 20506565. Pubmed Central PMCID: 2965297.

177.   Munro CA, McCaul ME, Wong DF, Oswald LM, Zhou Y, Brasic J, et al. Sex differences in striatal dopamine release in healthy adults. Biological psychiatry. 2006 May 15;59(10):966-74. PubMed PMID: 16616726.

178.   Guenzel FM, Wolf OT, Schwabe L. Sex differences in stress effects on response and spatial memory formation. Neurobiology of learning and memory. 2014 Mar;109:46-55. PubMed PMID: 24315929.

179.   Galea LA, Leuner B, Slattery DA. Hippocampal plasticity during the peripartum period: Influence of sex steroids, stress and ageing. Journal of neuroendocrinology. 2014 Jul 15. PubMed PMID: 25039797.

180.   Jung RE, Ryman SG, Vakhtin AA, Carrasco J, Wertz C, Flores RA. Subcortical correlates of individual differences in aptitude. PloS one. 2014;9(2):e89425. PubMed PMID: 24586770. Pubmed Central PMCID: 3934897.

181.   Liu Y, Wang G, Zhao L, Geng M, Wang L, Bai X, et al. SWI phase asymmetries in deep gray matter of healthy adults: is there an association with handedness? Brain imaging and behavior. 2013 Jun;7(2):220-6. PubMed PMID: 23329356.

182.   Zhang YT, Zhang CY, Zhang J, Li W. Age-related changes of normal adult brain structure: analysed with diffusion tensor imaging. Chinese medical journal. 2005 Jul 5;118(13):1059-65. PubMed PMID: 16098256.

183.   Bhagat YA, Beaulieu C. Diffusion anisotropy in subcortical white matter and cortical gray matter: changes with aging and the role of CSF-suppression. Journal of magnetic resonance imaging : JMRI. 2004 Aug;20(2):216-27. PubMed PMID: 15269946.

184.   Yelnik J. Functional anatomy of the basal ganglia. Movement disorders : official journal of the Movement Disorder Society. 2002;17 Suppl 3:S15-21. PubMed PMID: 11948751.

185.   Mukherjee P, Miller JH, Shimony JS, Philip JV, Nehra D, Snyder AZ, et al. Diffusion-tensor MR imaging of gray and white matter development during normal human brain maturation. AJNR American journal of neuroradiology. 2002 Oct;23(9):1445-56. PubMed PMID: 12372731.

186.   Yelnik J, Francois C, Percheron G, Tande D. Morphological taxonomy of the neurons of the primate striatum. The Journal of comparative neurology. 1991 Nov 8;313(2):273-94. PubMed PMID: 1722488.

187.   Walhovd KB, Fjell AM, Reinvang I, Lundervold A, Dale AM, Eilertsen DE, et al. Effects of age on volumes of cortex, white matter and subcortical structures. Neurobiology of aging. 2005 Oct;26(9):1261-70; discussion 75-8. PubMed PMID: 16005549.

188.   Syka M, Keller J, Klempir J, Rulseh AM, Roth J, Jech R, et al. Correlation between Relaxometry and Diffusion Tensor Imaging in the Globus Pallidus of Huntington's Disease Patients. PloS one. 2015;10(3):e0118907. PubMed PMID: 25781024.

189. Kim HJ, Kim SJ, Kim HS, Choi CG, Kim N, Han S, et al. Alterations of mean diffusivity in brain white matter and deep gray matter in Parkinson's disease. Neuroscience letters. 2013 Aug 29;550:64-8. PubMed PMID: 23831353.

190. Blood AJ, Tuch DS, Makris N, Makhlouf ML, Sudarsky LR, Sharma N. White matter abnormalities in dystonia normalize after botulinum toxin treatment. Neuroreport. 2006 Aug 21;17(12):1251-5. PubMed PMID: 16951564. Pubmed Central PMCID: 3039124.

191. Szabo N, Kincses ZT, Pardutz A, Toth E, Szok D, Csete G, et al. White matter disintegration in cluster headache. The journal of headache and pain. 2013 Dec;14(1):64. PubMed PMID: 23883140. Pubmed Central PMCID: 3728007.

192. May A, Goadsby PJ. Hypothalamic involvement and activation in cluster headache. Current pain and headache reports. 2001 Feb;5(1):60-6. PubMed PMID: 11252139.

193. Deppe M, Muller D, Kugel H, Ruck T, Wiendl H, Meuth SG. DTI detects water diffusion abnormalities in the thalamus that correlate with an extremity pain episode in a patient with multiple sclerosis. NeuroImage : clinical. 2013;2:258-62. PubMed PMID: 24179780.

194. Ellingson BM, Mayer E, Harris RJ, Ashe-McNally C, Naliboff BD, Labus JS, et al. Diffusion tensor imaging detects microstructural reorganization in the brain associated with chronic irritable bowel syndrome. Pain. 2013 Sep;154(9):1528-41. PubMed PMID: 23721972. Pubmed Central PMCID: 3758125.

195. Coppola G, Tinelli E, Lepre C, Iacovelli E, Di Lorenzo C, Di Lorenzo G, et al. Dynamic changes in thalamic microstructure of migraine without aura patients: a diffusion tensor magnetic resonance imaging study. European journal of neurology : the official journal of the European Federation of Neurological Societies. 2014 Feb;21(2):287-e13. PubMed PMID: 24200371.

196. Bach DR, Behrens TE, Garrido L, Weiskopf N, Dolan RJ. Deep and superficial amygdala nuclei projections revealed in vivo by probabilistic tractography. The Journal of neuroscience : the official journal of the Society for Neuroscience. 2011 Jan 12;31(2):618-23. PubMed PMID: 21228170. Pubmed Central PMCID: PMC3059574.

197. Mishra A, Rogers BP, Chen LM, Gore JC. Functional connectivity-based parcellation of amygdala using self-organized mapping: a data driven approach. Human brain mapping. 2014 Apr;35(4):1247-60. PubMed PMID: 23418140. Pubmed Central PMCID: PMC3919874.

198. Ji G, Neugebauer V. Differential effects of CRF1 and CRF2 receptor antagonists on pain-related sensitization of neurons in the central nucleus of the amygdala. J Neurophysiol. 2007 Jun;97(6):3893-904. PubMed PMID: 17392412.

199. Tsvetkov E, Carlezon WA, Benes FM, Kandel ER, Bolshakov VY. Fear conditioning occludes LTP-induced presynaptic enhancement of synaptic transmission in the cortical pathway to the lateral amygdala. Neuron. 2002 Apr 11;34(2):289-300. PubMed PMID: 11970870.

200. Ji G, Neugebauer V. Hemispheric lateralization of pain processing by amygdala neurons. J Neurophysiol. 2009 Oct;102(4):2253-64. PubMed PMID: 19625541. Pubmed Central PMCID: PMC2776996.

201. Gallay MN, Jeanmonod D, Liu J, Morel A. Human pallidothalamic and cerebellothalamic tracts: anatomical basis for functional stereotactic neurosurgery. Brain structure & function. 2008 Aug;212(6):443-63. PubMed PMID: 18193279. Pubmed Central PMCID: 2494572.

202.   Yamada K, Akazawa K, Yuen S, Goto M, Matsushima S, Takahata A, et al. MR imaging of ventral thalamic nuclei. AJNR American journal of neuroradiology. 2010 Apr;31(4):732-5. PubMed PMID: 19926703.

203.   Sedrak M, Gorgulho A, Frew A, Behnke E, DeSalles A, Pouratian N. Diffusion tensor imaging and colored fractional anisotropy mapping of the ventralis intermedius nucleus of the thalamus. Neurosurgery. 2011 Nov;69(5):1124-9; discussion 9-30. PubMed PMID: 21697755.

204.   Traynor C, Heckemann RA, Hammers A, O'Muircheartaigh J, Crum WR, Barker GJ, et al. Reproducibility of thalamic segmentation based on probabilistic tractography. NeuroImage. 2010 Aug 1;52(1):69-85. PubMed PMID: 20398772.

I.

CrossMark

ORIGINAL RESEARCH

Male brain ages faster: the age and gender dependence of subcortical volumes

András Király[1] · Nikoletta Szabó[1,2] · Eszter Tóth[1] · Gergő Csete[1] · Péter Faragó[1] ·
Krisztián Kocsis[1] · Anita Must[1] · László Vécsei[1,3] · Zsigmond Tamás Kincses[1,2]

Abstract Effects of gender on grey matter (GM) volume differences in subcortical structures of the human brain have consistently been reported. Recent research evidence suggests that both gender and brain size influences volume distribution in subcortical areas independently. The goal of this study was to determine the effects of the interplay between brain size, gender and age contributing to volume differences of subcortical GM in the human brain. High-resolution T1-weighted images were acquired from 53 healthy males and 50 age-matched healthy females. Total GM volume was determined using voxel-based morphometry. We used model-based subcortical segmentation analysis to measure the volume of subcortical nuclei. Main effects of gender, brain volume and aging on subcortical structures were examined using multivariate analysis of variance. No significant difference was found in total brain volume between the two genders after correcting for total intracranial volume. Our analysis revealed significantly larger hippocampus volume for females. Additionally, GM volumes of the caudate nucleus, putamen and thalamus displayed a significant age-related decrease in males as compared to females. In contrast to this only the thalamic volume loss proved significant for females. Strikingly, GM volume decreases faster in males than in females emphasizing the interplay between aging and gender on subcortical structures. These findings might have important implications for the interpretation of the effects of unalterable factors (i.e. gender and age) in cross-sectional structural MRI studies. Furthermore, the volume distribution and changes of subcortical structures have been consistently related to several neuropsychiatric disorders (e.g. Parkinson's disease, attention deficit hyperactivity disorder, etc.). Understanding these changes might yield further insight in the course and prognosis of these disorders.

Keywords Subcortical structures · Brain volume · Gender · Aging · MRI

✉ Zsigmond Tamás Kincses
kincses.zsigmond.tamas@med.u-szeged.hu; http://www.nepsy.
szote.u-szeged.hu/~kincsesz

1   Department of Neurology, Albert Szent-Györgyi Clinical Center,
     University of Szeged, Semmelweis u. 6, Szeged H-6725, Hungary

2   International Clinical Research Center, St. Anne's University
     Hospital Brno, Brno, Czech Republic

3   MTA-SZTE Neuroscience Research Group, Szeged, Hungary

Introduction

Gender differences in behavioral aspects of addiction (Bisagno and Cadet 2014; Fattore et al. 2014), motor control (Kauranen and Vanharanta 1996; Ruff and Parker 1993), emotional memory (Cahill 2003) and several major neuropsychiatric disorders, including attention deficit hyperactivity disorder (ADHD) (Gershon 2002) and Parkinson's disease (Bourque et al. 2009) have been recently reported. Accordingly, the sexual dimorphism of the human brain anatomy has gained attention with neuroimaging methods being widely used to detect these differences (Cahill 2006; Cosgrove et al. 2007; DeLacoste-Utamsing and Holloway 1982; Goldstein et al. 2001). Whereas males convergingly exhibit larger cerebral volumes (Gur et al. 1991; Sowell et al. 2007) and head sizes (Scahill et al. 2003), females generally have a thicker cortex in several regions of the brain (Luders et al. 2006; Sowell et al. 2007).

Springer

There is much less evidence on the sexual dimorphism of subcortical grey matter (GM) structures including the amygdala, caudate nucleus, accumbens, hippocampus, amygdala, pallidum, putamen and thalamus (Ahsan et al. 2007; Filipek et al. 1994). Considering that the basal ganglia nuclei possess a high density of sex steroid receptors (for reviews, see: (Taber et al. 2001), (Gray and Bingaman 1996)), the effect of gender on the volume of these structures might be crucial. Nevertheless, results are somewhat contradictory with several studies reporting larger volumes of the caudate nuclei (Luders et al. 2009), hippocampus (Murphy et al. 1996) and thalamus in females (Murphy et al. 1996; Takahashi et al. 2011), and some with opposing results (Sullivan et al. 2004; Rijpkema et al. 2012). The amygdala (Cheng et al. 2009), pallidum and the putamen (Rijpkema et al. 2012) have been consistently found to be larger in males.

Research evidence confirms aging to be associated with decrease in whole-brain volume (Courchesne et al. 2000; Gur et al. 1991; Scahill et al. 2003), grey matter volume (Courchesne et al. 2000; Ge et al. 2002a; Good et al. 2001; Guttmann et al. 1998; Pell et al. 2008; Raz et al. 1997; C. D. Smith et al. 2007; Taki et al. 2004), cortical thickness (Sowell et al. 2007), as well as temporal lobe volume (Scahill et al. 2003) and the hippocampal and thalamic volumes (Good et al. 2001). Studies on effects of aging on white matter (WM) volume decrease are inconsistent: some studies did not find a significant effect of aging on WM changes (Good et al. 2001; Taki et al. 2004), while others reported an increase in volume until middle adulthood, followed by a decline (Courchesne et al. 2000; Ge et al. 2002a) and yet others concluded that there was a steady decline with progressing aging (Guttmann et al. 1998; Lemaitre et al. 2005; Taki et al. 2011). Two studies using voxel-based techniques that reported no overall significant effect of aging on WM volume did reveal a decline with age in some areas (Good et al. 2001; Taki et al. 2004). The combined effects of age and gender on the human brain have been assessed suggesting a more profound decline in GM volume in males (Ge et al. 2002a; Raz et al. 1997; Taki et al. 2004). However, research evidence is inconsistent on one hand (Lemaitre et al. 2005) and sparse on the other, especially considering the subcortical GM structures. Most of the studies focusing on subcortical nuclei applied a voxel-based morphometric approach to identify gender differences. The deformable surface model based segmentation approach what we used in the current analysis offers advantages over intensity based procedures especially in regions with low tissue contrast. While age, gender and head size (intracranial volume) are the most commonly included "nuisance" variables when performing neuroimaging analysis, studies vary as to which of these variables are included and which method is used for correction (Perlaki et al. 2014). These factors might widely account for the great variability in the results.

In the present study an automatized, deformable mesh based segmentation toolkit (FSL-FIRST) was used to extract subcortical structures from the brain. Partial brain volumes were extracted with an intensity-based segmentation toolkit (FSL-SIENAX). Multivariate analysis of covariance and correlation analysis were run to evaluate the following: (1) gender effects on subcortical GM volumes with and without normalization for skull size; (2) interactions between aging and gender affecting volume changes.

Methods and materials

Participants

Fifty-three healthy males (mean age: 31.08 ± 10.03 years) and fifty age-matched healthy females (mean age: 33.00 ± 11.34 years) with no history of any neurological or psychiatric disorder were included in the study (Table 1).

The study was approved by the Ethics Committee of University of Szeged (authority number: 87/2009). All enrolled participants provided their written informed consent.

Image acquisition

Imaging was carried out with a 1.5 T GE Signa Excite MRI scanner. High-resolution T1-weighted images (3D IR-FSPGR: TR/TE/TI: 10.3/4.2/450 ms, flip angle: 15°, ASSET: 2, FOV: 25*25 cm, matrix: 256*256, slice thickness: 1 mm) were acquired.

Image processing

Tools from the FMRIB Software Library (FSL, version 5.0; Oxford Centre for Functional MRI of the Brain (FMRIB), UK; www.fmrib.ox.ac.uk/fsl) were used for data processing.

Comparison of basal ganglia and partial brain volumes

We used FIRST, a model-based segmentation/registration tool for volume comparison of the subcortical structures of males and females (Patenaude et al. 2011). This approach uses deformable surface meshes specific to subcortical structures, namely the amygdala, caudate nucleus, hippocampus, pallidum, putamen and thalamus. Given the observed intensities in a T1-weighted image, FIRST searches through linear combinations of shape modes of variation for the most probable shape instance based on learned models. We decided not

Table 1 Demographic data on the participant subjects

	Male			Female		
	mean	±SD	range	mean	±SD	range
N	53	–	–	50	–	–
Age (years)	31.08	10.03	21–58	33.00	11.34	21–57
Handedness (left)	6	–	–	7	–	–
Volumes						
Total intracranial (mm^3)	1,192,105.89	85,334.42	972,761.85–1,381,750.59	1,064,220.04	84,530.88	887,409.06–1,296,592.68
Total brain (mm^3)	1,165,217.63	83,151.41	948,950.34–1,342,429.91	1,041,990.31	82,652.01	861,476.12–1,270,109.32
Gray matter (mm^3)	642,377.23	46,905.62	527,133.52–758,544.08	579,578.16	42,978.76	495,802.20–674,384.25
White matter (mm^3)	522,840.39	43,260.20	421,816.82–608,111.83	462,412.14	44,986.73	360,447.47–621,760.47
Cortex (mm^3)	501,307.86	37,441.32	410,306.09–593,261.73	451,801.73	35,256.74	381,160.13–520,349.99

to include the nucleus accumbens due to inappropriate segmentation.

Specific entities of brain volume (total brain volume, total GM, white matter, cortical GM and ventricular cerebrospinal fluid) were compared between the two groups with and without normalization for total intracranial volume. Total intracranial volume as well as grey and white matter volumes were estimated using SIENAX (S. M. Smith et al. 2001; S. M. Smith et al. 2002), an approach included in the FSL (S. M. Smith et al. 2004). SIENAX starts by extracting brain and skull images from the single whole-head input data (S. M. Smith 2002). The brain image is then affine-registered to MNI152 space (Jenkinson et al. 2002; Jenkinson and Smith 2001) using the skull image to determine the registration scaling, primarily to obtain the volumetric scaling factor (*vscale*), which is then used as normalization for head size. Subsequently, tissue-type segmentation with partial volume calculation is carried out (Zhang et al. 2001) in order to calculate the total volume of brain tissue, including separate estimates of grey and white matter partial volumes.

The raw and the normalised volumes of the subcortical structures were compared between the groups. For normalisation, the FIRST output volumes were multiplied by the *vscale* factor, obtaining normalised GM volumes of subcortical structures - as if skull size would have been identical for all participants.

Additionally, left/right volume ratios of subcortical structures were compared between groups. A ratio larger than 1 indicates larger structures on the left, while smaller than 1 larger structures on the right.

Multiple univariate analysis of variance with age as covariant (MANCOVA) was applied for statistical analysis (IBM SPSS Statistics 20). Correlations between volumes of subcortical structures, grey/white matter ratio, partial brain volumes and age were calculated for both groups (IBM SPSS Statistics 20). The results were Bonferroni-corrected (p_{corr}) and $p < 0.05$ was chosen as the significance threshold.

For voxel-based morphometric analysis of the cortical gray matter, please see: Supplementary material.

Results

Gender differences of partial brain volumes and subcortical structures – raw data

MANCOVA (mean age of comparison = 32.02 years) revealed that all subcortical structures (max. $P_{corr} < 0.002$) and all partial brain volumes (max. $p < 0.002$) without normalization for skull size were significantly larger in the male than in the female group (Fig. 1). The grey/white matter ratio did not reveal a significant difference ($p < 0.077$).

No significant group difference was found between left/right volume ratios of subcortical structures. However, it is noteworthy that volumes of the right caudate nucleus ($p_{corr} < 0.052$) and the left thalamus $p_{corr} < 0.049$) were significantly larger than those of the corresponding contralateral structures in the male group only..

Gender differences of partial brain volumes and subcortical structures – skull size normalised data

After normalization for skull size, MANCOVA (mean age of comparison = 32.02 years) revealed significantly larger subcortical GM volumes for the left ($p_{corr} < 0.011$) and right hippocampus ($p_{corr} < 0.010$) in the female group. Strikingly, the total ($p < 0.003$) and the cortical GM were also found to be relatively more extended in the female group as compared to males ($p < 0.009$) (Fig. 2).

In the male group, the volumes of the right caudate nucleus ($p_{corr} < 0.047$) and the left thalamus ($p_{corr} < 0.015$) were found to remain significantly larger than the contralateral pair of these structures.

LEFT   RIGHT
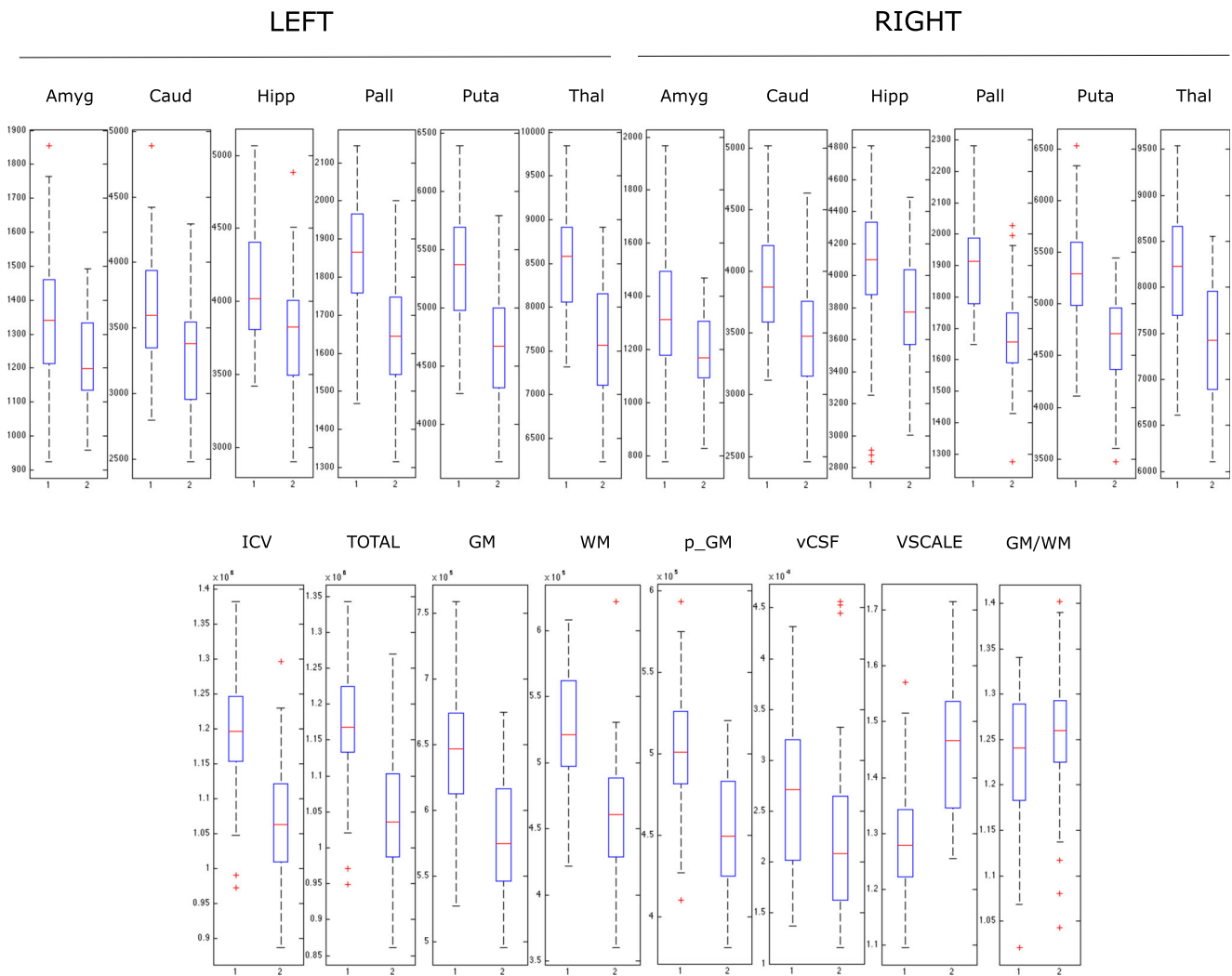
Fig. 1 Gender differences in the raw volumes

Correlation of total, partial and subcortical GM volumes with age – raw data

In the male group, total GM volumes (R = −0.366, $p < 0.0071$), cortical GM volumes (R = −0.332, $p < 0.015$) and the right thalamus (R = −0.365, $p_{corr} < 0.043$) showed a significant negative correlation with age when corrected for multiple comparisons. As for the volume of the left thalamus a tendency to a significant negative correlation with age (R = −0.345, $p_{corr} < 0.069$) was detected.

In the female group, volumes of total GM (R = −0.425, $p < 0.002$), cortical GM (R = −0.418, $p < 0.003$), the right hippocampus (R = −0.411, $p_{corr} < 0.018$) as well as the left (R = −0.373, $p_{corr} < 0.045$) and the right thalamus (R = −0.439, $p_{corr} < 0.008$) showed a significant negative correlation with age.

The grey/white matter ratio was found to correlate negatively with age for both males (R = −0.476, $p < 0.00032$) and females (R = −0.397, $p < 0.004$). However, the age-related

grey/white matter ratio was found to be higher for females ($p < 0.016$).

Interestingly, the left/right volume ratio of the hippocampus exhibited a significant positive correlation with age in the female group only (R = 0.509, $p_{corr} < 0.00094$).

Correlation of total, partial and subcortical GM volumes with age – skull size normalised data

In the male group, total brain volume (R = −0.507, $p < 0.00011$), total (R = −0.685, $p < 10^{-6}$) and cortical GM (R = −0.616, $p < 10^{-6}$), left (R = −0.393, $p_{corr} < 0.021$) and right caudate nucleus volume (R = −0.376, $p_{corr} < 0.033$), left (R = −0.384, $p_{corr} < 0.0274$) and right putamen (R = −0.408, $p_{corr} < 0.014$) as well as left (R = −0.489, $p_{corr} < 0.0012$) and right thalamus volume (R = −0.508, $p_{corr} < 0.0006$) showed a significant negative correlation with age (Figs. 3 and 4).

In the female group a significant negative correlation with age was revealed for total brain volume (R = −0.373,
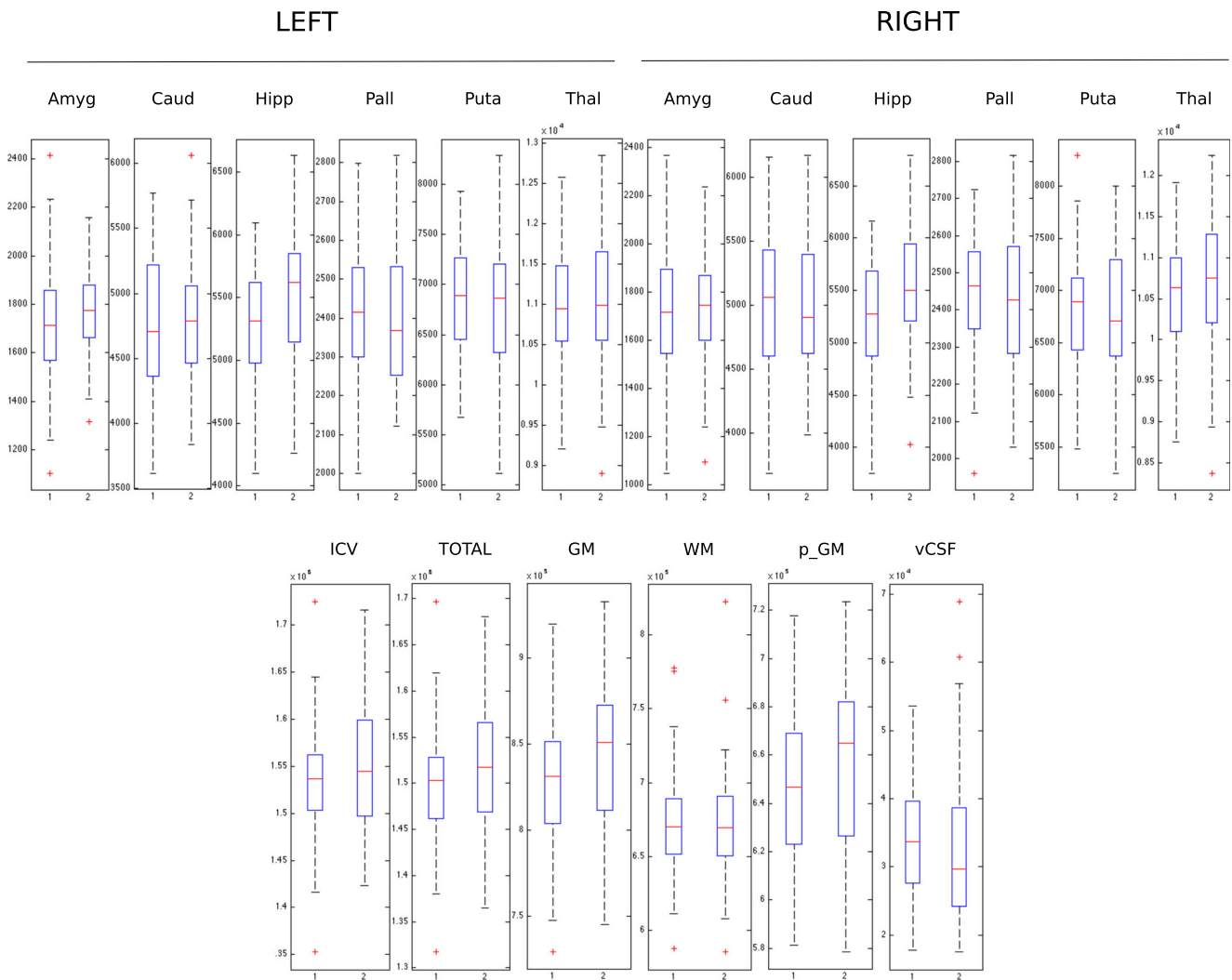
Fig. 2 Gender differences in the normalised volumes

$p < 0.0076$), total (R = −0.525, $p < 0.00009$) and cortical GM (R = −0.516, $p < 0.00013$), left (R = −0.399, $p_{corr} < 0.024$) and right thalamus (R = −0.452, $p_{corr} < 0.006$) (Figs. 3 and 4).

Interestingly, the decline with age in normalized GM volume occurred at a faster pace in the group of males than for females (z = 2.21, $p < 0.0271$) (Fig. 3).

Discussion

In the current study we aimed to identify gender effects on subcortical GM volumes as well as interactions between aging and gender affecting volume changes in the human brain.

To our best knowledge, this study is the first to report the effect of interplay between gender and aging accounting for differences in head size on subcortical structures using a model-based segmentation tool. The main strength of our study consists in the large size of our cohort with homogeneous acquisition and analyses procedures.

In general, male brains were found to be larger than females', with larger grey and white matter as well as subcortical structures. However, most of these differences disappear when skull size is accounted for. As a result of correction for total intracranial volume we found females to have larger cortical and subcortical GM volume. Noteworthy, the volume of the hippocampus was found significantly larger in the female group as compared to males. We also detected a significant effect of hemisphere in the male group only, with larger volmes of the right caudate and the left thalamus as compared to their contralateral structures.

More importantly, we found an age dependent decrease in the the volume of cortical as well as subcortical grey matter. Latter remained significant after correction for skull size in the caudate, putamen and thalamus bilaterally for males and the thalamus bilaterally for females. Within the age-range of 21 to 58 years we found a linear decrease in GM volume with aging. Strikingly, this process proved to occur at a faster pace in males.
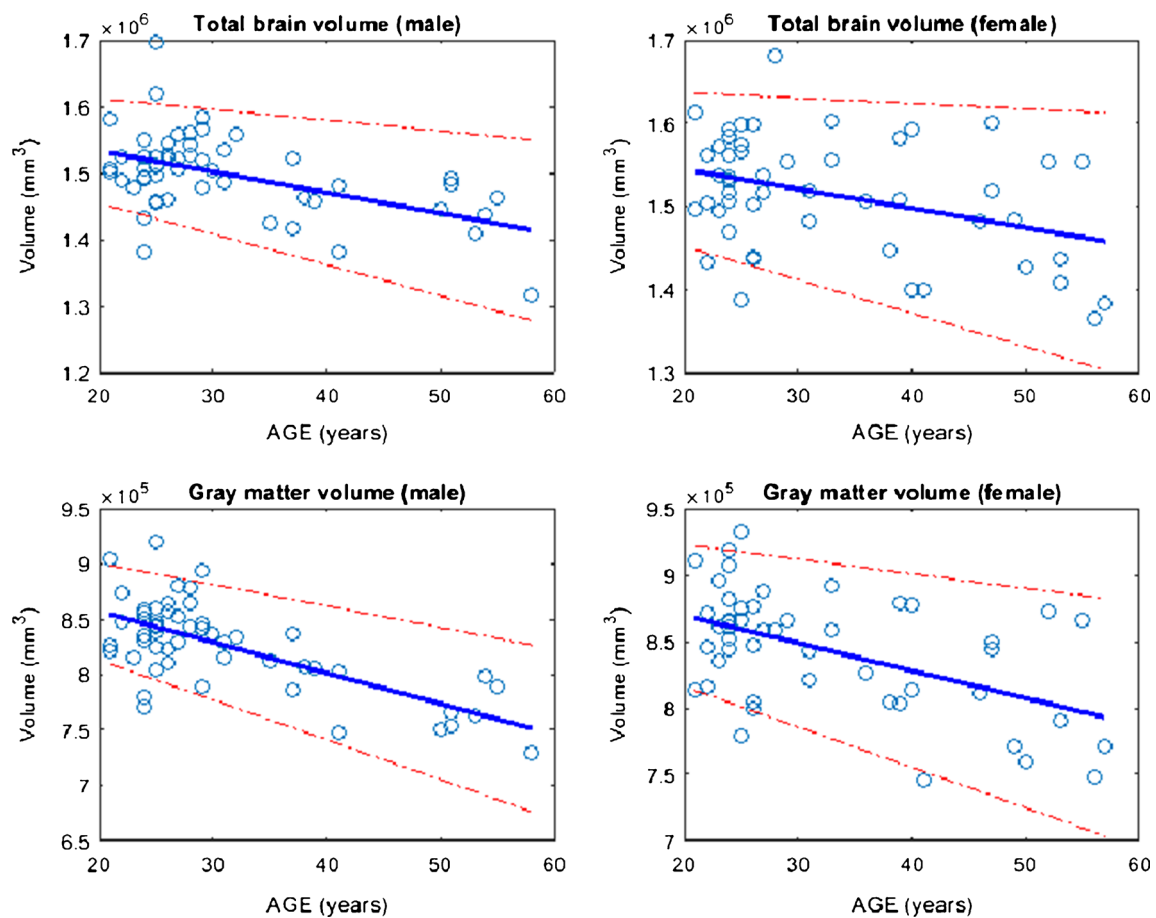
Fig. 3 Age-related decline in the normalized brain volumes in males and females

We propose the use and importance of our current findings to be two-fold: (1) methodological considerations of the investigation of subcortical structures and (2) potential functional implications related to gender and GM decline with age.

(1) While there is converging research evidence for total brain and GM volume to decline with age (Barnes et al. 2010; Courchesne et al. 2000; Ge et al. 2002b; C. D. Smith et al. 2007; Lemaitre et al. 2005; Takahashi et al. 2011), analysis approaches are typically different (Callaert et al. 2014). Volumes of the insular, medial frontal, posterior-parietal, occipital and temporal regions were shown to correlate negatively with age in an elderly population (C. D. Smith et al. 2007). Furthermore, a VBM study revelaed that cortical volume loss is not homogeneous (Takahashi et al. 2011).

Research evidence becomes much more sparse when focusing on the subcortical structures. Pevious VBM style analyses indicated a decline with age in the caudate and thalamic volumes (Callaert et al. 2014; C. D. Smith et al. 2007). However, the enlargement of the third and fourth ventricles might be a confounding variable in VBM analysis (C. D. Smith et al. 2007). Further studies applied manual tracing of subcortical structures identifying an age-related volume decline in the thalamus (Sullivan et al. 2004), the caudate and the putamen (Abedelahi et al. 2013). However, investigation was limited to

certain structures and the relationship with age was observed for both genders. A recent study found significant brain size effects in the right amygdala and the bilateral caudate nucleus and significant gender effects in the bilateral putamen but no interactions between brain size and gender (Tang et al. 2013).

Our results echoed a previous study reporting an age-related decline in the caudate, putamen and nucleus accumbens and a marginal effect in the thalamus in a similar age-range (35–60 years) (Goodro et al. 2012). However, the authors suggested that normalization to the cranium size accounted for the observed gender effect. Other studies have included gender as a nuisance variable in the general linear model analysis and found a negative correlation between age and the volumes of the hippocampus, amygdala, caudate and putamen (Barnes et al. 2010). Yet, other results were reported using Freesurfer, with a disproportionate degeneration of the subcortical volumes with aging (Li et al. 2014). Our current results regarding the hippocampus are in agreement with previous reports of larger relative hippocampal size in females with the use of FIRST, also confirmed by a VBM style analysis (Kauranen and Vanharanta 1996).

We propose that the inconsistency of findings about gender and age-related differences in subcortical GM volumes might stem from methodological differences and relatively small
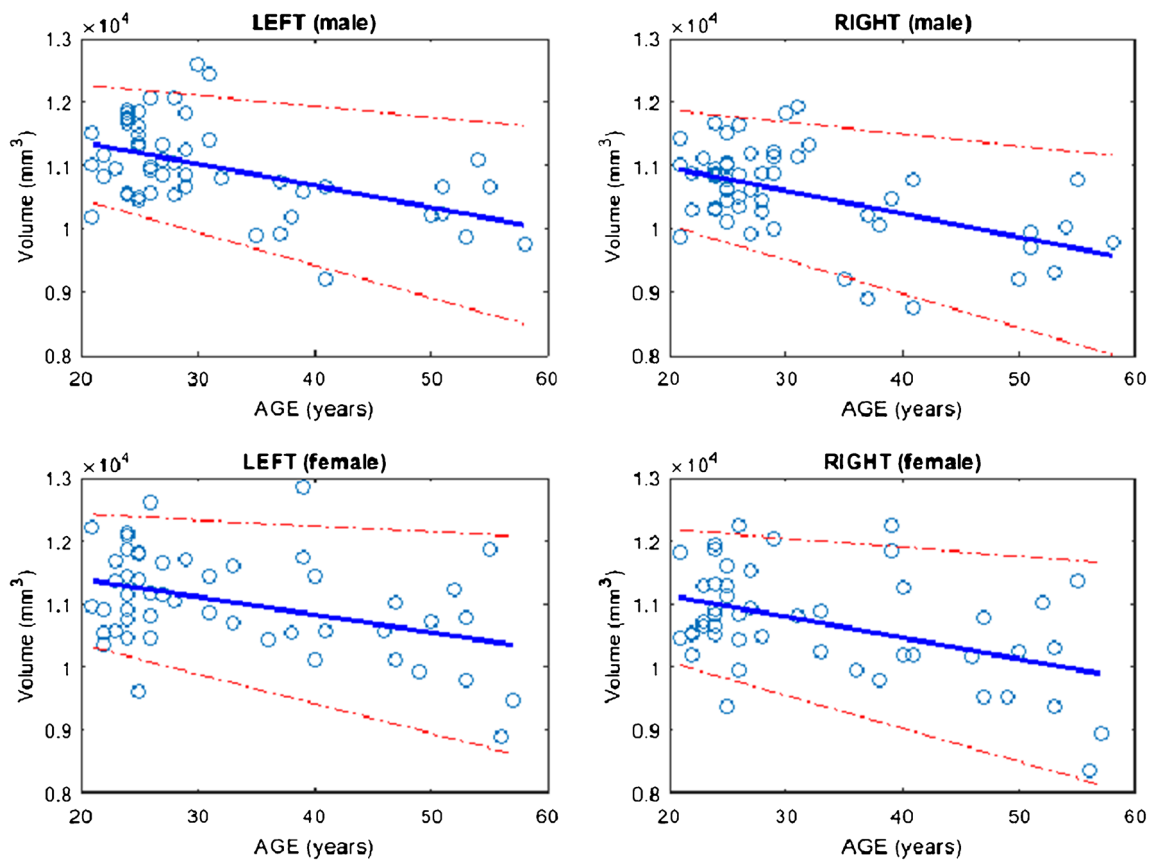
Fig. 4 Age-related decline in the normalized thalamic volumes in males and females

sample sizes. Most of the studies applied a VBM approach to identify gender differences in subcortical nuclei. While VBM is an excellent tool for the investigation of focal grey matter density differences, deformable surface model approaches such as FIRST are directly tuned for the volumetric analysis of the subcortical structures. Furthermore, in MRI studies, age, gender and head size (intracranial volume) are the most commonly included "nuisance" variables, though studies greatly vary as to which of the variables are included and which method is used for correction (Perlaki et al. 2014). Nevertheless, it is important to communicate transformation approach and group intracranial volume considerations when reporting structural findings of subcortical GM since it might carry several implications for interpretation of the results (Schwab et al. 2014).

In contrast with FIRST, the VBM analysis in our study did not detected any effects of age or gender on the subcortical structures (supplementary material). While the VBM approach is based on tissue-type/locally-averaged GM segmentation, FIRST utilises shape and intensity information jointly (Patenaude et al. 2011).

(2) The second aspect involves the underlying cellular, molecular and functional mechanisms of the age and gender related decline of GM volume. Primarily, neuronal and synaptic pruning has been proposed to play a critical role (Webb et al.

2001). However, findings of post-mortem histological studies suggested, that it is rather the size than the number of the individual cells explaining the age-related decline of GM (Terry et al. 1987; Peters et al. 1998). At the molecular level the expression of NoGo-A, a myelin-associated neurite growth inhibitor protein decreases with age (Kumari and Thakur 2014). Recent results also imply the impact of aging on GM/WM diffusion changes, explaining some cognitive variability and even decline (Salminen et al. 2015).

The background of the disproportionate GM volume changes in males and females has not yet been elucidated, but the changes in hormone levels and the consequent sensitivity of the brain to hormonal effects are most certainly involved (Barron and Pike 2012). Above the structural differences, there is increasing evidence for the functional sexual dimorphism of subcortical structures. Amphetamine has been shown to cause a higher level of dopamine release in the male striatum, which correlates with the behavioural effect of the drug (Riccardi et al. 2011; Munro et al. 2006). Hippocampus-related memory functions are differently affected by stress in males and females (Guenzel et al. 2014). Peripartum hormonal changes are known to modulate the hippocampal function (Galea et al. 2014). In addition to gender effects, recent evidence supports the influence of brain hemisphere showing lateralization of structure-function relationships, as well as

more specific relationships between individual structures (e.g., left hippocampus) and functions relevant to particular aptitudes (e.g. vocabulary) (Jung et al. 2014). Our current results revealed a significant effect of hemisphere in the male group only, with larger volmes of the right caudate and the left thalamus as compared to their contralateral structures. It might be hypothesized that this difference relates to handedness, however, we did not find such a relationship. A recent study examining the deep GM of healthy adults by using magnetic susceptibility-weighted imaging did not reveal an association with handedness (Liu et al. 2013).

Considering that the volume of subcortical GM critically impacts the size of neurons, glia cells and number of synapses it entails, we might hypothesis that this also affects the function and performance of these structures. It is clear that deducing motor, cognitive and affective functional activity of subcortical GM solely from their structural characteristics would be inadmissibly simplified. Furthermore, observing changes in volume of subcortical GM influenced by gender and aging might yield better insight and with furhter investigations, even explain some clinically significant differences in males and females in several neurological and psychiatric conditions, e.g. Alzheimer's dementia (Qian et al. 2014), Parkinson's disorder (Gillies et al. 2014; Geevarghese et al. 2015), headache disorders (Macgregor et al. 2011), multiple sclerosis (Greer and McCombe 2011), major depression and bipolar disorder (MacMaster et al. 2014). Strikingly, some recent findings suggest that the volume of certain subcortical nuclei is even associated with crucial psychiatric conditions such as suicidal behavior (Gifuni et al. 2015). Further investigation of functional and behavioral correlates of accurately identified subcortical structures might have crucial implications for preventive measures and treatment of related disorders.

References

Abedelahi, A., Hasanzadeh, H., Hadizadeh, H., & Joghataie, M. T. (2013). Morphometric and volumetric study of caudate and putamen nuclei in normal individuals by MRI: Effect of normal aging, gender and hemispheric differences. *Pol J Radiol, 78*(3), 7–14. doi:10.12659/PJR.889364.

Ahsan, R. L., Allom, R., Gousias, I. S., Habib, H., Turkheimer, F. E., Free, S., et al. (2007). Volumes, spatial extents and a probabilistic atlas of the human basal ganglia and thalamus. *NeuroImage, 38*(2), 261–270. doi:10.1016/j.neuroimage.2007.06.004.

Andersson, J. L. R., Jenkinson, M., & Smith, S. (2007). Non-linear optimisation. FMRIB technical report. *Oxford*.

Ashburner, J., & Friston, K. J. (2000). Voxel-based morphometry–the methods. *NeuroImage, 11*(6 Pt 1), 805–821. doi:10.1006/nimg.2000.0582.

Barnes, J., Ridgway, G. R., Bartlett, J., Henley, S. M., Lehmann, M., Hobbs, N., et al. (2010). Head size, age and gender adjustment in MRI studies: a necessary nuisance? *NeuroImage, 53*(4), 1244–1255. doi:10.1016/j.neuroimage.2010.06.025.

Barron, A. M., & Pike, C. J. (2012). Sex hormones, aging, and alzheimer's disease. *Frontiers in Bioscience (Elite Edition), 4*, 976–997.

Bisagno, V., & Cadet, J. L. (2014). Stress, sex, and addiction: potential roles of corticotropin-releasing factor, oxytocin, and arginine-vasopressin. *Behavioural Pharmacology, 25*(5–6), 445–457. doi:10.1097/FBP.0000000000000049.

Bourque, M., Dluzen, D. E., & Di Paolo, T. (2009). Neuroprotective actions of sex steroids in parkinson's disease. *Frontiers in Neuroendocrinology, 30*(2), 142–157. doi:10.1016/j.yfrne.2009.04.014.

Cahill, L. (2003). Sex-related influences on the neurobiology of emotionally influenced memory. *Annals of the New York Academy of Sciences, 985*, 163–173.

Cahill, L. (2006). Why sex matters for neuroscience. *Nature Reviews. Neuroscience, 7*(6), 477–484. doi:10.1038/nrn1909.

Callaert, D. V., Ribbens, A., Maes, F., Swinnen, S. P., & Wenderoth, N. (2014). Assessing age-related gray matter decline with voxel-based morphometry depends significantly on segmentation and normalization procedures. *Frontiers in Aging Neuroscience, 6*, 124. doi:10.3389/fnagi.2014.00124.

Cheng, Y., Chou, K. H., Decety, J., Chen, I. Y., Hung, D., Tzeng, O. J., et al. (2009). Sex differences in the neuroanatomy of human mirror-neuron system: a voxel-based morphometric investigation. *Neuroscience, 158*(2), 713–720. doi:10.1016/j.neuroscience.2008.10.026.

Cosgrove, K. P., Mazure, C. M., & Staley, J. K. (2007). Evolving knowledge of sex differences in brain structure, function, and chemistry. *Biological Psychiatry, 62*(8), 847–855. doi:10.1016/j.biopsych.2007.03.001.

Courchesne, E., Chisum, H. J., Townsend, J., Cowles, A., Covington, J., Egaas, B., et al. (2000). Normal brain development and aging: quantitative analysis at in vivo MR imaging in healthy volunteers. *Radiology, 216*(3), 672–682. doi:10.1148/radiology.216.3.r00au37672.

DeLacoste-Utamsing, C., & Holloway, R. L. (1982). Sexual dimorphism in the human corpus callosum. *Science, 216*(4553), 1431–1432.

Fattore, L., Melis, M., Fadda, P., & Fratta, W. (2014). Sex differences in addictive disorders. *Frontiers in Neuroendocrinology, 35*(3), 272–284. doi:10.1016/j.yfrne.2014.04.003.

Filipek, P. A., Richelme, C., Kennedy, D. N., & Caviness Jr., V. S. (1994). The young adult human brain: an MRI-based morphometric analysis. *Cerebral Cortex, 4*(4), 344–360.

Galea, L. A., Leuner, B., & Slattery, D. A. (2014). Hippocampal plasticity during the peripartum period: influence of sex steroids, stress and ageing. *Journal of Neuroendocrinology.* doi:10.1111/jne.12177.

Ge, Y., Grossman, R. I., Babb, J. S., Rabin, M. L., Mannon, L. J., & Kolson, D. L. (2002a). Age-related total gray matter and white matter changes in normal adult brain. Part I: volumetric MR imaging analysis. *AJNR. American Journal of Neuroradiology, 23*(8), 1327–1333.

Ge, Y., Grossman, R. I., Babb, J. S., Rabin, M. L., Mannon, L. J., & Kolson, D. L. (2002b). Age-related total gray matter and white matter changes in normal adult brain. Part II: quantitative magnetization transfer ratio histogram analysis. *AJNR. American Journal of Neuroradiology, 23*(8), 1334–1341.

Geevarghese, R., Lumsden, D. E., Hulse, N., Samuel, M., & Ashkan, K. (2015). Subcortical structure volumes and correlation to clinical

variables in parkinson's disease. *Journal of Neuroimaging*, 25(2), 275–280. doi:10.1111/jon.12095.

Gershon, J. (2002). A meta-analytic review of gender differences in ADHD. *Journal of Attention Disorders*, 5(3), 143–154.

Gifuni, A. J., Ding, Y., Olie, E., Lawrence, N., Cyprien, F., Le Bars, E., et al. (2015). Subcortical nuclei volumes in suicidal behavior: nucleus accumbens may modulate the lethality of acts. *Brain Imaging and Behavior*. doi:10.1007/s11682-015-9369-5.

Gillies, G. E., Pienaar, I. S., Vohra, S., & Qamhawi, Z. (2014). Sex differences in parkinson's disease. *Frontiers in Neuroendocrinology*. doi:10.1016/j.yfrne.2014.02.002.

Goldstein, J. M., Seidman, L. J., Horton, N. J., Makris, N., Kennedy, D. N., Caviness Jr., V. S., et al. (2001). Normal sexual dimorphism of the adult human brain assessed by in vivo magnetic resonance imaging. *Cerebral Cortex*, 11(6), 490–497.

Good, C. D., Johnsrude, I. S., Ashburner, J., Henson, R. N., Friston, K. J., & Frackowiak, R. S. (2001). A voxel-based morphometric study of ageing in 465 normal adult human brains. *NeuroImage*, 14(1 Pt 1), 21–36. doi:10.1006/nimg.2001.0786.

Goodro, M., Sameti, M., Patenaude, B., & Fein, G. (2012). Age effect on subcortical structures in healthy adults. *Psychiatry Research*, 203(1), 38–45. doi:10.1016/j.pscychresns.2011.09.014.

Gray, T. S., & Bingaman, E. W. (1996). The amygdala: corticotropin-releasing factor, steroids, and stress. *Critical Reviews in Neurobiology*, 10(2), 155–168.

Greer, J. M., & McCombe, P. A. (2011). Role of gender in multiple sclerosis: clinical effects and potential molecular mechanisms. *Journal of Neuroimmunology*, 234(1–2), 7–18. doi:10.1016/j.jneuroim.2011.03.003.

Guenzel, F. M., Wolf, O. T., & Schwabe, L. (2014). Sex differences in stress effects on response and spatial memory formation. *Neurobiology of Learning and Memory*, 109, 46–55. doi:10.1016/j.nlm.2013.11.020.

Gur, R. C., Mozley, P. D., Resnick, S. M., Gottlieb, G. L., Kohn, M., Zimmerman, R., et al. (1991). Gender differences in age effect on brain atrophy measured by magnetic resonance imaging. *Proceedings of the National Academy of Sciences of the United States of America*, 88(7), 2845–2849.

Guttmann, C. R., Jolesz, F. A., Kikinis, R., Killiany, R. J., Moss, M. B., Sandor, T., et al. (1998). White matter changes with normal aging. *Neurology*, 50(4), 972–978.

Jenkinson, M., Bannister, P., Brady, M., & Smith, S. (2002). Improved optimization for the robust and accurate linear registration and motion correction of brain images. *NeuroImage*, 17(2), 825–841.

Jenkinson, M., & Smith, S. (2001). A global optimisation method for robust affine registration of brain images. *Medical Image Analysis*, 5(2), 143–156. doi: 10.1016/S1361-8415(01)00036-6

Jung, R. E., Ryman, S. G., Vakhtin, A. A., Carrasco, J., Wertz, C., & Flores, R. A. (2014). Subcortical correlates of individual differences in aptitude. *PloS One*, 9(2), e89425. doi:10.1371/journal.pone.0089425.

Kauranen, K., & Vanharanta, H. (1996). Influences of aging, gender, and handedness on motor performance of upper and lower extremities. *Perceptual and Motor Skills*, 82(2), 515–525. doi:10.2466/pms.1996.82.2.515.

Kumari, A., & Thakur, M. K. (2014). Age-dependent decline of nogo-a protein in the mouse cerebrum. *Cellular and Molecular Neurobiology*. doi:10.1007/s10571-014-0088-z.

Lemaitre, H., Crivello, F., Grassiot, B., Alperovitch, A., Tzourio, C., & Mazoyer, B. (2005). Age- and sex-related effects on the neuroanatomy of healthy elderly. *NeuroImage*, 26(3), 900–911. doi:10.1016/j.neuroimage.2005.02.042.

Li, W., van Tol, M. J., Li, M., Miao, W., Jiao, Y., Heinze, H. J., et al. (2014). Regional specificity of sex effects on subcortical volumes across the lifespan in healthy aging. *Human Brain Mapping*, 35(1), 238–247. doi:10.1002/hbm.22168.

Liu, Y., Wang, G., Zhao, L., Geng, M., Wang, L., Bai, X., et al. (2013). SWI phase asymmetries in deep gray matter of healthy adults: is there an association with handedness? *Brain Imaging and Behavior*, 7(2), 220–226. doi:10.1007/s11682-012-9217-9.

Luders, E., Gaser, C., Narr, K. L., & Toga, A. W. (2009). Why sex matters: brain size independent differences in gray matter distributions between men and women. *The Journal of Neuroscience*, 29(45), 14265–14270. doi:10.1523/JNEUROSCI.2261-09.2009.

Luders, E., Narr, K. L., Thompson, P. M., Rex, D. E., Woods, R. P., Deluca, H., et al. (2006). Gender effects on cortical thickness and the influence of scaling. *Human Brain Mapping*, 27(4), 314–324. doi:10.1002/hbm.20187.

Macgregor, E. A., Rosenberg, J. D., & Kurth, T. (2011). Sex-related differences in epidemiological and clinic-based headache studies. *Headache*, 51(6), 843–859. doi:10.1111/j.1526-4610.2011.01904.x.

MacMaster, F. P., Carrey, N., Langevin, L. M., Jaworska, N., & Crawford, S. (2014). Disorder-specific volumetric brain difference in adolescent major depressive disorder and bipolar depression. *Brain Imaging and Behavior*, 8(1), 119–127. doi:10.1007/s11682-013-9264-x.

Munro, C. A., McCaul, M. E., Wong, D. F., Oswald, L. M., Zhou, Y., Brasic, J., et al. (2006). Sex differences in striatal dopamine release in healthy adults. *Biological Psychiatry*, 59(10), 966–974. doi:10.1016/j.biopsych.2006.01.008.

Murphy, D. G., DeCarli, C., McIntosh, A. R., Daly, E., Mentis, M. J., Pietrini, P., et al. (1996). Sex differences in human brain morphometry and metabolism: an in vivo quantitative magnetic resonance imaging and positron emission tomography study on the effect of aging. *Archives of General Psychiatry*, 53(7), 585–594.

Patenaude, B., Smith, S. M., Kennedy, D. N., & Jenkinson, M. (2011). A bayesian model of shape and appearance for subcortical brain segmentation. *NeuroImage*, 56(3), 907–922. doi:10.1016/j.neuroimage.2011.02.046.

Pell, G. S., Briellmann, R. S., Chan, C. H., Pardoe, H., Abbott, D. F., & Jackson, G. D. (2008). Selection of the control group for VBM analysis: influence of covariates, matching and sample size. *NeuroImage*, 41(4), 1324–1335. doi:10.1016/j.neuroimage.2008.02.050.

Perlaki, G., Orsi, G., Plozer, E., Altbacker, A., Darnai, G., Nagy, S. A., et al. (2014). Are there any gender differences in the hippocampus volume after head-size correction? A volumetric and voxel-based morphometric study. *Neuroscience Letters*, 570, 119–123. doi:10.1016/j.neulet.2014.04.013.

Peters, A., Morrison, J. H., Rosene, D. L., & Hyman, B. T. (1998). Feature article: are neurons lost from the primate cerebral cortex during normal aging? *Cerebral Cortex*, 8(4), 295–300.

Qian, S., Zhang, Z., Li, B., & Sun, G. (2014). Functional-structural degeneration in dorsal and ventral attention systems for alzheimer's disease, amnestic mild cognitive impairment. *Brain Imaging and Behavior*. doi:10.1007/s11682-014-9336-6.

Raz, N., Gunning, F. M., Head, D., Dupuis, J. H., McQuain, J., Briggs, S. D., et al. (1997). Selective aging of the human cerebral cortex observed in vivo: differential vulnerability of the prefrontal gray matter. *Cerebral Cortex*, 7(3), 268–282.

Riccardi, P., Park, S., Anderson, S., Doop, M., Ansari, M. S., Schmidt, D., et al. (2011). Sex differences in the relationship of regional dopamine release to affect and cognitive function in striatal and extrastriatal regions using positron emission tomography and [(1)(8)F]fallypride. *Synapse*, 65(2), 99–102. doi:10.1002/syn.20822.

Rijpkema, M., Everaerd, D., van der Pol, C., Franke, B., Tendolkar, I., & Fernandez, G. (2012). Normal sexual dimorphism in the human basal ganglia. *Human Brain Mapping*, 33(5), 1246–1252. doi:10.1002/hbm.21283.

Ruff, R. M., & Parker, S. B. (1993). Gender- and age-specific changes in motor speed and eye-hand coordination in adults: normative values

for the finger tapping and grooved pegboard tests. *Perceptual and Motor Skills*, *76*(3 Pt 2), 1219–1230. doi:10.2466/pms.1993.76.3c.1219.

Salminen, L. E., Conturo, T. E., Laidlaw, D. H., Cabeen, R. P., Akbudak, E., Lane, E. M., et al. (2015). Regional age differences in gray matter diffusivity among healthy older adults. *Brain Imaging and Behavior*. doi:10.1007/s11682-015-9383-7.

Scahill, R. I., Frost, C., Jenkins, R., Whitwell, J. L., Rossor, M. N., & Fox, N. C. (2003). A longitudinal study of brain volume changes in normal aging using serial registered magnetic resonance imaging. *Archives of Neurology*, *60*(7), 989–994. doi:10.1001/archneur.60.7.989.

Schwab, N. A., Tanner, J. J., Nguyen, P. T., Schmalfuss, I. M., Bowers, D., Okun, M., et al. (2014). Proof of principle: transformation approach alters caudate nucleus volume and structure-function associations. *Brain Imaging and Behavior*. doi:10.1007/s11682-014-9332-x.

Smith, C. D., Chebrolu, H., Wekstein, D. R., Schmitt, F. A., & Markesbery, W. R. (2007). Age and gender effects on human brain anatomy: a voxel-based morphometric study in healthy elderly. *Neurobiology of Aging*, *28*(7), 1075–1087. doi:10.1016/j.neurobiolaging.2006.05.018.

Smith, S. M. (2002). Fast robust automated brain extraction. *Human Brain Mapping*, *17*(3), 143–155. doi:10.1002/hbm.10062.

Smith, S. M., De Stefano, N., Jenkinson, M., & Matthews, P. M. (2001). Normalized accurate measurement of longitudinal brain change. *Journal of Computer Assisted Tomography*, *25*(3), 466–475.

Smith, S. M., Jenkinson, M., Woolrich, M. W., Beckmann, C. F., Behrens, T. E., Johansen-Berg, H., et al. (2004). Advances in functional and structural MR image analysis and implementation as FSL. *NeuroImage*, *23*(Suppl 1), S208–S219. doi:10.1016/j.neuroimage.2004.07.051.

Smith, S. M., & Nichols, T. E. (2009). Threshold-free cluster enhancement: addressing problems of smoothing, threshold dependence and localisation in cluster inference. *NeuroImage*, *44*(1), 83–98. doi:10.1016/j.neuroimage.2008.03.061.

Smith, S. M., Zhang, Y., Jenkinson, M., Chen, J., Matthews, P. M., Federico, A., et al. (2002). Accurate, robust, and automated longitudinal and cross-sectional brain change analysis. *NeuroImage*, *17*(1), 479–489. doi:10.1006/nimg.2002.1040.

Sowell, E. R., Peterson, B. S., Kan, E., Woods, R. P., Yoshii, J., Bansal, R., et al. (2007). Sex differences in cortical thickness mapped in 176 healthy individuals between 7 and 87 years of age. *Cerebral Cortex*, *17*(7), 1550–1560. doi:10.1093/cercor/bhl066.

Sullivan, E. V., Rosenbloom, M., Serventi, K. L., & Pfefferbaum, A. (2004). Effects of age and sex on volumes of the thalamus, pons, and cortex. *Neurobiology of Aging*, *25*(2), 185–192.

Taber, K. H., Murphy, D. D., Blurton-Jones, M. M., & Hurley, R. A. (2001). An update on estrogen: higher cognitive function, receptor mapping, neurotrophic effects. *Journal of Neuropsychiatry and Clinical Neurosciences*, *13*(3), 313–317. doi:10.1176/Appi.Neuropsych.13.3.313.

Takahashi, R., Ishii, K., Kakigi, T., & Yokoyama, K. (2011). Gender and age differences in normal adult human brain: voxel-based morphometric study. *Human Brain Mapping*, *32*(7), 1050–1058. doi:10.1002/hbm.21088.

Taki, Y., Goto, R., Evans, A., Zijdenbos, A., Neelin, P., Lerch, J., et al. (2004). Voxel-based morphometry of human brain with age and cerebrovascular risk factors. *Neurobiology of Aging*, *25*(4), 455–463. doi:10.1016/j.neurobiolaging.2003.09.002.

Taki, Y., Thyreau, B., Kinomura, S., Sato, K., Goto, R., Kawashima, R., et al. (2011). Correlations among brain gray matter volumes, age, gender, and hemisphere in healthy individuals. *PloS One*, *6*(7), e22734. doi:10.1371/journal.pone.0022734.

Tang, T., Jiao, Y., Wang, X., & Lu, Z. (2013). Gender versus brain size effects on subcortical gray matter volumes in the human brain. *Neuroscience Letters*, *556*, 79–83. doi:10.1016/j.neulet.2013.09.060.

Terry, R. D., DeTeresa, R., & Hansen, L. A. (1987). Neocortical cell counts in normal human adult aging. *Annals of Neurology*, *21*(6), 530–539. doi:10.1002/ana.410210603.

Webb, S. J., Monk, C. S., & Nelson, C. A. (2001). Mechanisms of postnatal neurobiological development: implications for human development. *Developmental Neuropsychology*, *19*(2), 147–171. doi:10.1207/S15326942DN1902_2.

Zhang, Y., Brady, M., & Smith, S. (2001). Segmentation of brain MR images through a hidden markov random field model and the expectation-maximization algorithm. *IEEE Transactions on Medical Imaging*, *20*(1), 45–57. doi:10.1109/42.906424.

II.

Original Article

Macro- and microstructural alterations of the subcortical structures in episodic cluster headache

András Király[1], Nikoletta Szabó[1,2], Árpád Párdutz[1],
Eszter Tóth[1], János Tajti[1], Gergő Csete[1], Péter Faragó[1],
Péter Bodnár[3], Délia Szok[1], Bernadett Tuka[1,4], Éva Pálinkás[5],
Csaba Ertsey[6], László Vécsei[1,4] and Zsigmond Tamás Kincses[1,2]

Abstract

Background: Previous functional and structural imaging studies have revealed that subcortical structures play a key a role in pain processing. The recurring painful episodes might trigger maladaptive plasticity or alternatively degenerative processes that might be detected by MRI as changes in size or microstructure. In the current investigation, we aimed to identify the macro- and microstructural alterations of the subcortical structures in episodic cluster headache.

Methods: High-resolution T1-weighted and diffusion-weighted MRI images with 60 gradient directions were acquired from 22 patients with cluster headache and 94 healthy controls. Surface-based segmentation analysis was used to measure the volume of the subcortical nuclei, and mean diffusion parameters (fractional anisotropy, mean, radial and axial diffusivity) were determined for these structures. In order to understand whether the size and diffusion parameters could be investigated in a headache lateralised manner, first the asymmetry of the size and diffusion parameters of the subcortical structures was analysed. Volumes and diffusion parameters were compared between groups and correlated with the cumulative number of headache days. To account for the different size of the patient and control group, a bootstrap approach was used to investigate the stability of the findings.

Results: A significant lateralisation of the size (caudate, putamen and thalamus) and the diffusion parameters of the subcortical structures were found in normal controls. In cluster headache patients, the mean fractional anisotropy of the right amygdalae, the mean axial and mean diffusivity of the right caudate nucleus and the radial diffusivity of the right pallidum were higher. The mean anisotropy of the right pallidum was lower in patients.

Conclusion: The analysis of the pathology in the subcortical structures in episodic cluster headache reveals important features of the disease, which might allow a deeper insight into the pathomechanism of the pain processing in this headache condition.

[1]Department of Neurology, Albert Szent-Györgyi Clinical Center, University of Szeged, Szeged, Hungary
[2]International Clinical Research Center, St. Anne's University Hospital Brno, Brno, Czech Republic
[3]Department of Image Processing and Computer Graphics, Faculty of Science and Informatics, Szeged, Hungary
[4]MTA-SZTE Neuroscience Research Group, Szeged, Hungary
[5]Bacs-Kiskun County Hospital, Kecskemét, Hungary
[6]Department of Neurology, Semmelweis University, Budapest, Hungary

Corresponding author:
Zsigmond Tamás Kincses, Neuroimaging Research Group, Department of Neurology, Albert Szent-Györgyi Clinical Center, University of Szeged, Semmelweis u. 6, H-6725 Szeged, Hungary.
Email: kincses.zsigmond.tamas@med.u-szeged.hu

Introduction

Episodic cluster headache (CH) is a primary headache disorder with the prominent feature of extremely severe unilateral, periorbital headache attacks accompanied by ipsilateral autonomic symptoms, and occurs in clusters usually lasting some weeks, followed by much longer headache-free periods (1,2).

The basal ganglia and generally the subcortical structures were recently proposed to have a central role in nociception. The facts that they receive input

directly from the spinal cord and also via the thalamus, and exhibit connections with various cortical regions involved in pain processing, suggest that this system is ideal for the integration of various aspects of pain-related information (for an in-depth review, see (3) and (4)). Furthermore, it has been shown that basal ganglia structures are activated during painful stimuli (5), and putaminal and pallidal neurons are able to encode the intensity of noxious thermal stimuli (6). There are opioid receptors in the striatum, and nociceptive neurones have also been found (7). The nociceptive neurones of the spinal cord project directly to the globus pallidus, amygdala and hypothalamus (8). Moreover, the activation of the striatum correlates with the variability in pain sensation (9). Putaminal lesions have been shown to alter nociceptive information processing (10). Neuroimaging studies have demonstrated structural alterations in the striatum in chronic pain syndromes (11). In migraine, a larger caudate nucleus was observed in patients who displayed a high attack frequency (12). Imaging studies have also indicated the involvement of the subcortical structures in CH. Atrophy of the thalamus and caudate nucleus has been reported in CH (13).

Disease related structural alterations could possibly be captured at the macrostructural level as size changes, and the highly organized microstructure of the subcortical nuclei makes them readily available to study with diffusion weighted MRI. The two features might show parallel alterations, but since the histological background of the diffusion alterations in the grey matter is not well understood, the micro- and macrostructural alterations may also occur independently.

In the current study, we set out to investigate volumetric changes in CH by an approach highly tuned to the detection of subcortical volume changes (FIRST (14)). Furthermore, we made use of the highly organized microstructure of subcortical nuclei to investigate diffusion in the segmented nuclei. We also hypothesised that the disease did not affect all subcortical structures at the same rate, and we also wanted to analyse the co-occurrence of the micro- and macrostructural alterations in CH.

We expected two possible outcomes: (i) Repetitive painful attacks might induce maladaptive plasticity in pain related cortical and subcortical structures, and these changes might present in a volume augmentation and possibly in a more organized microstructure, as detected by diffusion tensor imaging. (ii) Alternatively, the recurrent severe pain and concurrent pathological processes might induce degenerative changes, which might present in the form of microstructural disintegration and atrophy.

Investigating the brain structures by pooling data as being contralateral or ipsilateral to the headache side is a frequently used approach in the headache literature to boost the number of observations. However, this approach can only be used if no lateralisation exists in healthy subjects. The lateralisation in healthy subjects was investigated by processing the MRIs of a large group of volunteers, measured with the same parameters as those of the CH patients. The same large control group was used in all further comparisons, since any selection of a subgroup could cause a statistical bias. In order to account for the different size of the groups compared, a bootstrap approach was used to confirm stability of the findings (15). The bootstrap approach takes random samples from each subgroup, of the same size. By repeating the random sampling with replacement a large number of times, the bootstrap approach not only gives a statistical estimator of the model, but the stability of that estimator can also be evaluated.

Methods

Participants

Twenty-seven patients were recruited into the study. Five patients were excluded due to comorbidity (depression, benign tumour), cessation of pain after tooth extraction (e.g. secondary cluster headache), and structural abnormality on the MRI scans. Finally, 22 patients were included (mean age: 38.10 ± 11.33, male: 19). Inclusion criteria for the CH patients were: 18–80 years of age, primary CH according to The International Headache Society diagnostic criteria (1), no interval therapy for the CH, no accompanying neurological (including other primary headache disorders and pain conditions) or psychiatric disease, no regular neuro-psychiatric medication, negative routine MRI scan. Special attention was paid to the exclusion of depression, for which the Hamilton questionnaire was used (>16 points was the exclusion criterion) (16). The MRI acquisitions were carried out in the interictal period (at least one month after the last headache episode). There were 12 left-headache-sided (*LHS-CH*) and 10 right-headache-sided patients (*RHS-CH*) in the CH group. All the participants were right handed. Clinical variables, such as disease duration, time between bouts and average length of bouts were recorded for all patients. Furthermore, the cumulative number of headache days – that is, the total number of days the patient had experienced cluster headache over his/her entire life – was estimated for all the patients.

In all, 94 healthy individuals (mean age: 32.59 ± 10.43, male: 50) were included in the study. Inclusion criteria for the controls were: 18–80 years of age, no history of neurological (including primary headaches, other pain conditions) or psychiatric diseases. All the participants were right handed. Demographic data and the corresponding *p* values are presented in Table 1(a) and 1(b).

The study was approved by the Ethics Committee of the University of Szeged (authority number: 87/2009), and all the subjects provided their written informed consent.

Image acquisition

MR image acquisition took place at least one month after the end of the last headache bout. Imaging was carried out with a 1.5 T GE Signa Excite MRI scanner. High-resolution T1-weighted images (3D IR-FSPGR: TR/TE/TI: 10.3/4.2/450 ms, flip angle: 15°, ASSET: 2, FOV: 25×25 cm, matrix: 256×256, slice thickness: 1 mm) and 60 direction diffusion-weighted images with six non-diffusion-weighted reference volumes (TE: 93.8 ms, TR: 13500 ms, matrix: 96×96, FOV: 23×23 cm, flip angle: 90°, in-plane resolution: 2.4×2.4 mm, which was resampled to 0.89×0.89 mm by the scanner, slice thickness: 2.4 mm, b: $1000 \, s/m^2$, NEX: 2, ASSET) were recorded.

Table 1(a). Demographic data of the participants.

	Age			
	Control	CH (all)	LHS-CH	RHS-CH
Gender				
Control		0.038*	0.177	0.081
CH (all)	**0.004**			
LHS-CH	0.105			0.724
RHS-CH	**0.011**		0.427	

*Not significant while bootstrapping.
Bold value highlights only significant (p < 0.05) results.
CH (all): RHS-CH and RHS-CH patient together. RHS-CH: cluster headache patients with pain on the right side. LHS-CH: cluster headache patients with pain on the left side.

Table 1(b). Statistics (p-values) of the demographic data.

	CH (all)		
	LHS-CH	RHS-CH	Control
N (male)	22 (19)		94 (50)
	12 (11)	10 (8)	
Age (SD)	38.10 (11.33)		32.59 (10.43)
	36.96 (11.64)	38.81 (10.39)	
Handedness (L/R)	0/22		0/94
Side of headache (L/R)	12/10		–
Disease duration (years (SD))	7.41 (6.20)		–
Lifetime attack number (days)	15–910		–

CH (all): RHS-CH and RHS-CH patient together. RHS-CH: cluster headache patients with pain on the right side. LHS-CH: cluster headache patients with pain on the left side.

Image processing

Data were processed by means of the tools from the FMRIB Software Library (FSL, version 5.0; Oxford Centre for Functional MRI of the Brain (FMRIB), UK; www.fmrib.ox.ac.uk/fsl).

Partial brain volumes of the brain and subcortical structures

For comparisons of the volumes of the subcortical structures between the groups, FIRST analysis was used (14). FIRST is a model-based segmentation/registration tool. It uses deformable surface meshes specific to subcortical structures (the amygdala, caudate nucleus, hippocampus, pallidum, putamen and thalamus). Based on learned models, FIRST searches through linear combinations of shape modes of variation for the most probable shape instance given the observed intensities in a T1-weighted image. The nucleus accumbens was not investigated because of the inappropriate segmentation.

Partial brain volumes (total brain volume, total grey matter, white matter, peripheral grey matter [cortex] and ventricular cerebrospinal fluid), with and without normalization for the intracranial volume, were compared between the two groups. The intracranial volume and the grey and white matter volumes were estimated by SIENAX (17,18), part of FSL (19). SIENAX starts by extracting brain and skull images from the single whole-head input data (20). The brain image is then affine-registered to MNI152 space (21,22) (using the skull image to determine the registration scaling); this is primarily carried out in order to obtain the volumetric scaling factor (*vscale*) to be used as normalization for the head size. Next, tissue-type segmentation with partial volume calculation is carried out (23) in order to calculate the total volume of brain tissue (including separate estimates of the volumes of the grey and white matter), and the grey and white matter partial volumes.

Diffusion parameters of the basal ganglia

In order to evaluate the internal microstructure of the subcortical structures, diffusion parameters were estimated for each of the segmented subcortical structures and compared between the two groups. The diffusion data were corrected for eddy currents and movement artefacts by 12 degrees of freedom affine linear registration to the first non-diffusion-weighted reference image (22). Diffusion tensors at each voxel were fitted by the algorithm included in the Diffusion Toolbox (FDT) of the FMRIB's Software Library (FSL v. 4.0, www.fmrib.ox.ac.uk/fsl; (19)). Fractional anisotropy (FA), mean diffusivity (MD), and diffusivity parallel (AD, axial) and perpendicular (RD, radial) to

the principal diffusion direction were computed for the whole brain. The binary masks of subcortical structures segmented by FIRST analysis of each subject were registered (FLIRT) to the subjects' own DWI images with 6 degrees of freedom. The transformed masks were thresholded at 0.5 and binarised again. All registered images were then checked visually and corrected so they did not contain parts of ventricles or white matter tracts close to the subcortical structures. Mean diffusion parameters were calculated under the masked areas.

Furthermore, the trigeminal nerves were identified in the axial plane using colour orientation maps created by overlaying the principal eigenvector image (V1) over the FA map. Then, 15 voxel sized ROIs were manually drawn on the root entry zone of the trigeminal nerves. The maximum and the mean of the diffusion parameters were estimated.

Statistical analysis

Lateralisation in healthy subjects. The left-right ratio of the size and diffusion parameters of the subcortical structures was estimated as the ratio of the left and right side parameters (1 meaning no lateralisation, numbers higher than 1 indicating higher parameters on the left and numbers lower than 1 indicating higher parameters on the right). One sample t-test was used to test lateralisation.

Alteration of the size and diffusion parameters of the subcortical structures in CH. The group differences (t_0, p_0) were evaluated by using a standard general linear model, where the model was encoding group membership. While our analysis in healthy controls found no gender or age effect, these two variables were included in the analysis to account for the theoretical effect. The solution of the regression model was estimated by the ordinary least squares approach. Since the number of subjects in the control and patient groups differed significantly a bootstrap approach was used to confirm the stability of the findings (15). Five thousand bootstrap samples were randomly drawn from each group by the size of the patient population ($N = 22$), ensuring that the size of the two compared groups was always the same. The parameters (t_B) of the GLM model were estimated for every bootstrap sample ($t_{B1} - t_{B5000}$), then the mean of it was calculated ($\hat{t}$). The confidence interval for the bootstrapped t-values ($\hat{t}(CI)$) was used to perform an approximate two-sided test of a null hypothesis of the form:

$$H_0 : t_0 \in \hat{t}(CI)$$

The null hypothesis was to be rejected, and hence the original, non-bootstrapped parameter (t_0) was not from the bootstrapped distribution at the significance level of 0.05, if t_0 lay outside the two-tailed ($1\text{-}\alpha$) confidence interval $\hat{t}(CI)$.

A similar approach was used for the correlations between clinical variables, volumes and diffusion parameters (the correlation coefficient r was used in the bootstrap resampling).

Results

Asymmetry of the size and diffusion parameters of the subcortical structures in healthy subjects

The laterality of the size and the diffusion parameters of the subcortical structures were investigated in 94 healthy control subjects.

Head size normalized volumes of the right caudate nucleus, left putamen and left thalamus were significantly higher than the contralateral pair of these structures.

The FA of the left amygdala, caudate nucleus, putamen and right pallidum was higher than the contralateral pair of these structures. The AD and MD of all right side structures – except the thalamus – were higher than in the contralateral structures. The RD of the right amygdala, caudate nucleus, pallidum, putamen and the left hippocampus were higher than in the contralateral structures (Table 2).

These results indicate that there is a significant lateralisation of the size and diffusion parameters in healthy subjects. Consequently, pooled parameters according to the headache side cannot be used in the group comparisons.

Alteration of the size and diffusion parameters of the subcortical structures in CH

The GLM analysis showed that the FA of the right amygdala was significantly higher in CH and LHS-CH patients than in healthy subjects. A similar tendency was found in case of the left amygdala in RHS-CH patients. The MD and RD of the right amygdala were higher in healthy subjects compared to the CH and LHS-CH patients. A similar tendency was found in RHS-CH patients.

The AD of the right caudate nucleus was higher in CH, RHS-CH and LHS-CH patients compared with healthy subjects. A similar tendency was found with MD and RD in CH and LHS-CH patients.

In the case of the right pallidum, FA was lower in CH and LHS-CH patients. The RD of the right pallidum showed a tendency to be higher in CH and LHS-CH patients than in healthy subjects. The head size normalized volume of the right pallidum was lower in RHS-CH patients than in healthy subjects.

Table 2. Laterality in healthy subjects: The volume and diffusion parameters of the subcortical gray matter structures.

	Left	Right	p_0	$Mean_0$	$Mean_{Boot}$	95% CI ($Mean_{Boot}$)
Amygdala						
Volume	(+)	−	(0.068)	(1.032)	(1.032)	(0.997–1.065)
FA	+	−	<0.001	1.074	1.074	1.054–1.095
AD	−	+	<0.001	0.969	0.969	0.963–0.975
MD	−	+	<0.001	0.958	0.959	0.953–0.964
RD	−	+	<0.001	0.952	0.952	0.946–0.958
Caudatus						
Volume	−	+	<0.001	0.947	0.947	0.937–0.957
FA	+	−	0.032	1.014	1.014	1.001–1.026
AD	−	+	<0.001	0.978	0.978	0.974–0.982
MD	−	+	<0.001	0.979	0.979	0.976–0.982
RD	−	+	<0.001	0.980	0.980	0.976–0.983
Hippocampus						
Volume						
FA						
AD	−	+	<0.001	0.989	0.989	0.985–0.992
MD	−	+	<0.001	0.988	0.988	0.985–0.991
RD	+	−	<0.001	0.988	0.988	0.985–0.992
Pallidum						
Volume						
FA	−	+	<0.001	0.943	0.943	0.925–0.961
AD	−	+	<0.001	0.954	0.954	0.944–0.963
MD	−	+	<0.001	0.981	0.981	0.976–0.986
RD	−	+	0.018	1.016	1.016	1.003–1.029
Putamen						
Volume	+	−	0.026	1.013	1.013	1.001–1.024
FA	(+)	−	(0.063)	(1.012)	(1.012)	(0.999–1.025)
AD	−	+	<0.001	0.971	0.971	0.967–0.975
MD	−	+	<0.001	0.969	0.969	0.966–0.973
RD	−	+	<0.001	0.968	0.968	0.965–0.972
Thalamus						
Volume	+	−	<0.001	1.032	1.032	1.025–1.038
FA						
AD						
MD						
RD						

Italicized values highlight only close to be significant ($p > 0.05$ but $p < 0.1$) results.
(+) highlights only close to be significant ($p > 0.05$ but $p < 0.1$) results.
p_0 = p value with 1-sample T-test. $Mean_0$ = mean Left/Right ratio. $Mean_{Boot}$ = mean Left/Right ratio of the bootstrapped sample. 95% CI($Mean_{Boot}$) = two-tailed (1-alpha) confidence interval of the Left/Right ratio values from the bootstrapped sample.

According to the diffusion parameters of the trigeminal root entry zone, there were no significant differences between patients or controls, or between the ipsilateral and contralateral measures. Total brain volume and grey and white matter volumes did not differ between groups either.

Significance levels and bootstrap confidence intervals are presented in Table 3.

Correlation of the volumes and diffusion parameters with clinical parameters

The head size normalized volume of the total brain and cortical grey matter showed positive correlation with the cumulative number of headache days in the *CH* patients. Similar correlation was found in the LHS-CH patients. Also total grey matter and white matter

Table 3. The volume and diffusion parameters of the subcortical gray matter structures compared to healthy controls.

	CH (all)				RHS-CH				LHS-CH			
	P_0	t_0	t_{Boot}	95% CI (t_{Boot})	P_0	t_0	t_{Boot}	95% CI (t_{Boot})	P_0	t_0	t_{Boot}	95% CI (t_{Boot})
Left												
Amygdala												
Volume												
FA					**0.042**•	1.744	0.877	(−1.324)–3.328				
AD												
MD												
RD												
RIGHT												
Amygdala												
Volume												
FA	**0.022** •	2.035	1.557	(−0.708)–4.291					**0.032** •	1.875	1.238	(−1.267)–3.962
AD	*(0.076)*	*(1.443)*	*(0.843)*	*((−1.360)–2.941)*								
MD	**0.021**	2.064	1.263	(−0.908)–3.408	*(0.062)*	*(1.550)*	*(0.776)*	*((−1.586)–2.933)*	**0.048**	1.677	0.844	(−1.573)–3.484
RD	**0.012**	2.301	1.417	(−0.742)–3.567	*(0.051)*	*(1.647)*	*(0.892)*	*((−1.371)–3.041)*	**0.027**	1.944	1.007	(−1.318)–3.599
Caudatus												
Volume												
FA					*(0.055)*	*(1.611)*	*(1.279)*	*((−1.142)–3.946)*				
AD	**0.006**•	2.483	2.044	(−0.113)–4.560	**0.034** •	1.846	1.646	(−0.655)–4.502	**0.026** •	1.946	1.507	(−0.773)–4.469
MD	**0.026**•	1.834	1.581	(−0.596)–4.047					*(0.056* •*)*	*(1.605)*	*(1.258)*	*((−1.089)–3.851)*
RD	*(0.065)*	*(1.527)*	*(1.378)*	*((−0.761)–3.523)*					*(0.092* •*)*	*(1.337)*	*(1.001)*	*((−1.296)–3.456)*
Pallidum												
Volume												
FA	**0.048**	2.167	1.853	(−0.238)–4.078	**0.013**	2.255	1.535	(−0.808)–4.051	**0.049**	1.673	1.275	(−1.066)–3.706
AD												
MD												
RD	*(0.056*•*)*	*(1.597)*	*(1.275)*	*((−0.948)–3.592)*					*(0.079* •*)*	*(1.419)*	*(1.185)*	*((−1.266)–3.838)*

• Higher values in the CH group.

Bold values highlight significant and italics highlight close to be significant results.

CH (all): RHS-CH and LHS-CH patient together; RHS-CH: cluster headache patients with pain on the right side. LHS-CH: cluster headache patients with pain on the left side.

P_0: p value from the original GLM. t_0: t value from the original GLM. t_{Boot}: mean t value of the bootstrapped sample. 95% CI(t_{Boot}): two-tailed (*1-alpha*) confidence interval of the t values from the bootstrapped sample.

showed similar, but not significant tendency in the CH patients.

The head size normalized volume of the left and right hippocampus and right caudatus showed positive correlation, and the AD of the left and right thalamus, the MD and RD of the left hippocampus showed negative correlation with the cumulative number of headache days in the CH patients. The head size normalized volume of the left pallidum, left and right thalamus showed positive correlation, but the AD of the left hippocampus and the MD of the left pallidum showed negative correlation with the cumulative number of headache days in the RHS-CH patients.

The head size normalized volume of the left hippocampus showed positive correlation with the cumulative number of headache days in the LHS-CH patients. Significance levels and bootstrap confidence intervals are presented in Table 4.

Discussion

In this MRI study, we demonstrated an altered interictal microstructure of the subcortical structures in CH. Some of these microstructural changes were dependent on the lifetime disease burden. Demonstrating the lateralisation of diffusion parameters of the subcortical structures in a large cohort of healthy subjects, we showed that headache side dependent pooling of the data to boost the number of observations is not recommended.

In neuroimaging studies investigating unilateral processes, such as in CH and migraine, to boost the number of observations it is common to flip the data about the midsaggital axis to have hemispheres/structures aligned according to the headache side (24–26). This approach is used despite the fact that it was shown that there is a normal asymmetry in the white matter diffusion parameters (27). The most consistent asymmetry was found in the arcuate fasciculus and in the cingulum (27–29). Similarly, diffusion parameters of the subcortical structures were reported to be asymmetric in healthy subjects (30). While Fabiano's findings are important and consistent with our findings, in their study the mean of diffusivity from only three directions were examined in a small cohort of healthy subjects, and circular regions of interests were used in some of the structures (30). In our study, we used a larger cohort of healthy subjects and found asymmetries of various diffusion parameters estimated from diffusion measurements from 60 different directions. Based on these results, we concluded that we cannot pool data from the different hemispheres of CH patients. In our analysis, we treated CH patients as one group regardless of the side of the headache. Only as a secondary test, we compared the RSH-CH and LSH-CH patients to healthy subjects. Because of the small size of the

Table 4. Correlation of the volume and diffusion parameters of the subcortical gray matter structures with lifetime attack number in in CH.

	CH (all)				RHS-CH				LHS-CH			
	P_0	R_0	R_{Boot}	95% CI (R_{Boot})	P_0	R_0	R_{Boot}	95% CI (R_{Boot})	P_0	R_0	R_{Boot}	95% CI (R_{Boot})
LEFT												
Hippocampus												
Volume	**0.045**	**0.432**	0.398	(−0.076)−0.725	**0.035**	**−0.667**	−0.684	(−0.921)−(−0.413)	**0.025**	**0.641**	0.592	(−0.088)−0.901
FA												
AD	**0.017**	**−0.505**	−0.503	(−0.692)−(−0.256)	(0.073)	(−0.589)	(−0.608)	((−0.882)−(−0.236))				
MD	**0.022**	**−0.485**	−0.491	(−0.670)−(−0.249)								
RD	**0.041**	**−0.439**	−0.445	(−0.649)−(−0.184)								
Pallidum												
Volume					**0.039**	**0.658**	0.601	(−0.041)−0.903				
FA												
AD												
MD	(0.083)	(−0.378)	(−0.356)	((−0.687)−0.056)	**0.003**	**−0.835**	−0.837	(−0.992)−(−0.603)				
RD												

(continued)

Table 4. Continued.

	CH (all)				RHS-CH				LHS-CH			
	P0	R0	R_Boot	95% CI (R_Boot)	P0	R0	R_Boot	95% CI (R_Boot)	P0	R0	R_Boot	95% CI (R_Boot)
Thalamus												
Volume												
FA												
AD	**0.023**	**−0.483**	−0.453	(−0.776)–0.022	**0.011**	**0.756**	0.752	0.382–0.947	(0.073)	(−0.535)	(−0.427)	((−0.902)–0.711)
MD												
RD												
RIGHT												
Caudatus												
Volume	**0.007**	**0.562**	0.548	0.134–0.817	**0.041**	**0.653**	0.589	(−0.215)–0.961	(0.060)	(0.557)	(0.562)	((−0.103)–0.912)
FA												
AD												
MD												
RD												
Hippocampus												
Volume	**0.045**	**0.431**	0.449	0.111–0.752	(0.091)	(0.562)	(0.560)	(0.179–0.853)				
FA												
AD												
MD												
RD												
Pallidum												
Volume												
FA												
AD												
MD	(0.092)	(−0.368)	(−0.325)	((−0.698)–0.279)								
RD												
Thalamus												
Volume												
FA												
AD	**0.038**	**−0.445**	−0.405	(−0.769)–0.127	**0.020**	**0.717**	0.748	0.432–0.960				
MD												
RD												

Bold values are higher values in the CH group.

Bold values highlight significant and italics highlight close to be significant results.

CH (all): RHS-CH and RHS-CH patient together. RHS-CH: cluster headache patients with pain on the right side. LHS-CH: cluster headache patients with pain on the left side. p0: p value from the original Pearson-correlation. t0: t value from the original Pearson-correlation. R_0: original Pearson-correlation. R_{Boot}: mean correlation coefficient of the bootstrapped sample 95% CI(R_{Boot}): two-tailed (1-alpha) confidence interval of the correlation coefficients from the bootstrapped sample.

groups, the results of these later comparisons have to be handled cautiously even though the stability of the findings were evaluated by a bootstrap sampling. Furthermore, it has to be pointed out that the size of the subgroups of CH patients in our analysis does not allow us to investigate headache side dependent alterations of parameters or alterations of the lateralisation of these parameters.

Macro- and microstructural alterations are well-known features of pain-related disorders (24,31). Regarding CH, the seminal paper by May et al. (32) described an increased grey matter volume in the inferior and posterior hypothalamus in CH, but no other changes in grey matter density in either the cortex or the subcortical structures. In contrast, another VBM analysis indicated a decreased grey matter volume in the right thalamus, in the head of the right caudate nucleus and in several pain-processing-related cortical structures, such as the right precentral gyrus, right posterior cingulate cortex, bilateral middle frontal gyrus, right middle temporal gyrus, left inferior parietal lobule and left insula (13). Importantly, the decrease in the grey matter volume did not depend on the side of the pain. While slightly smaller subcortical structures were found, no subcortical volume alteration was identified with our surface-based analysis approach (except the right pallidum, which was smaller in RHS-CH than in healthy subjects). A recent VBM style investigation also called attention to the fact that the cortical and subcortical volumetric alterations are dynamic in relation to the pain state (e.g. in and out of bouts and in chronic CH) (25).

Alterations in the diffusion parameters in the white matter in primary headache disorders such as migraine and CH are already known (24,31), but the microstructural alterations in the subcortical structures described here have not been investigated previously in CH. Only a few studies have dealt with the pain-related changes in the diffusion parameters in the subcortical structures. An increased fractional anisotropy has been reported in the thalamus contralateral to the affected body side in multiple sclerosis patients with extremity pain (33). In irritable bowel syndrome, decreased FA has been found in the thalamic regions, and a reduced MD in the globus pallidus and a higher MD were described in the thalamus (34). The apparent diffusion coefficient (ADC) in the red nucleus of patients with migraine has been shown to be increased relative to healthy subjects (35). In migraineurs without aura, FA was reported to be higher and MD to be lower in the bilateral thalami compared to controls in the interictal phase (36). The diffusivity parameters have also been found to be similar to those in controls in the ictal phase (36). While the diffusion parameters of the trigeminal nerve or the root entry zone have been investigated in trigeminal neuralgia (37), there have been no

prior investigations published in CH. Our results did not find CH-specific alterations of the diffusion parameters of the trigeminal root entry zone, but one possible source of this negative result might be the high variability in the data. On average, the neural and vascular structures of the prepontine fossa range between 0.5 and 3.0 mm in diameter. This small diameter has to be considered in diffusion-tensor imaging studies in terms of the limited spatial resolution of the sequences used (38).

The FA of the bilateral amygdala was found to be increased in our study. The amygdala is known for being an important centre of emotional and affective aspects of pain. It is an important hub in the processing of noxious stimuli, and it has been shown to have structural and functional connections to cortical and subcortical structures involved in pain processing (39,40). It has been shown by several studies that there is a significant pain-related plasticity in the amygdala in chronic pain conditions, and amygdalar plasticity was suggested to be the key factor in the establishment of fear memory (41,42). We propose that the increased FA in CH patients might have a similar background. Interestingly, the pain related activation of the amygdala is heavily lateralised to the right (43), but no such lateralisation of diffusion parameters or size was found in our patients. While it is known that basal ganglia structures – such as the pallidum and caudate nucleus, which was found to have altered diffusion parameters in CH in our study – are activated in response to painful stimuli (5), and structural alterations are related to chronic pain conditions (11), the exact role of these structures in the processing of noxious stimuli is not well understood yet.

In a prior study, we showed diffusion parameter alterations in the white matter of CH patients (31). In the white matter, the pattern of diffusion parameter alterations may be related to the underlying pathological microstructural changes. In mouse models (44), the changes observed in AD and RD have been suggested to relate to axon or myelin damage, respectively. However, the background of the diffusion parameter changes in the subcortical grey matter is not so clear. Nevertheless, the subcortical grey nuclei have a well-defined microstructure, which – as we have shown – is altered by CH. There can be a few processes leading to the alteration of the diffusion parameters of the subcortical structures. The contribution of the extracellular and intracellular water fraction to the diffusion signal is not even. A combination of diffusion parameter changes could be explained by the change in the ratio of the extra and intracellular water fractions (e.g. global shrinkage of the structure or intracellular oedema) or, for example, protein deposits limiting the water diffusion. Alterations can also be caused by the change of the myelin or axon content or fibre orientation.

Recent studies suggest that neurodegeneration could result in diffusion changes in related basal ganglia. In movement disorders, in which the basal ganglia play a crucial role in the pathomechanism, altered diffusivity parameters were detected (in Huntington's disease (45); in Parkinson's disease (46); and in blepharospasm (47)). We consider that this pattern points to the co-occurrence of degenerative changes, presenting in the form of microstructural disintegration and compensatory or pain-related maladaptive plastic changes in CH.

Limitations

This analysis has some essential drawbacks. First of all, it is a cross-sectional assessment of the focal shrinkage of the subcortical and cortical volumes; also, we do not have exact information about the time elapsed from the last attack. A further drawback is the relatively low power of the secondary analyses (RHS-CH and LHS-CH) due to the limited number of patients. Finally, while only patients with no history of other neurological conditions were recruited/involved, we did not have any information about additional risk factors (e.g. diabetes mellitus) that the patients may have had. In order to acquire an in-depth understanding of the dynamics of brain atrophy and diffusion parameters, longitudinal studies are needed. Given the central role of the hypothalamus in CH, it would be crucial to investigate its size and microstructure. Unfortunately, our approach in its current form is not able to segment the hypothalamus, segmentation of the structure being limited by the low difference in intensity from the surrounding structures.

Key findings

- The diffusion parameters of the subcortical structures are lateralised in healthy subjects.
- Headache side dependent pooling of the imaging data to boost the number of observations is not recommended.
- The diffusion parameters of some subcortical structures are altered in cluster headache.
- The diffusion parameter changes of the subcortical structures in cluster headache are related to the lifetime disease burden.

References

1. Headache Classification Subcommittee of the International Headache Society. The International Classification of Headache Disorders: 2nd edition. *Cephalalgia* 2004; 24: S9–160.
2. Russell MB. Epidemiology and genetics of cluster headache. *Lancet Neurol* 2004; 3: 279–283.
3. Borsook D, Upadhyay J, Chudler EH, et al. A key role of the basal ganglia in pain and analgesia – insights gained through human functional imaging. *Mol Pain* 2010; 6: 27.
4. Juri C, Rodriguez-Oroz M and Obeso JA. The pathophysiological basis of sensory disturbances in Parkinson's disease. *J Neurol Sci* 2010; 289: 60–65.
5. Bingel U, Glascher J, Weiller C, et al. Somatotopic representation of nociceptive information in the putamen: An event-related fMRI study. *Cereb Cortex* 2004; 14: 1340–1345.
6. Chudler EH. Response properties of neurons in the caudate-putamen and globus pallidus to noxious and nonnoxious thermal stimulation in anesthetized rats. *Brain Res* 1998; 812: 283–288.
7. Baumgartner U, Buchholz HG, Bellosevich A, et al. High opiate receptor binding potential in the human lateral pain system. *Neuroimage* 2006; 30: 692–699.
8. Braz JM, Nassar MA, Wood JN, et al. Parallel "pain" pathways arise from subpopulations of primary afferent nociceptor. *Neuron* 2005; 47: 787–793.
9. Hagelberg N, Jaaskelainen SK, Martikainen IK, et al. Striatal dopamine D2 receptors in modulation of pain in humans: A review. *Eur J Pharmacol* 2004; 500: 187–192.

10. Starr CJ, Sawaki L, Wittenberg GF, et al. The contribution of the putamen to sensory aspects of pain: Insights from structural connectivity and brain lesions. *Brain* 2011; 134: 1987–2004.

11. Schmidt-Wilcke T, Leinisch E, Ganssbauer S, et al. Affective components and intensity of pain correlate with structural differences in gray matter in chronic back pain patients. *Pain* 2006; 125: 89–97.

12. Maleki N, Becerra L, Nutile L, et al. Migraine attacks the Basal Ganglia. *Mol Pain* 2011; 7: 71.

13. Absinta M, Rocca MA, Colombo B, et al. Selective decreased grey matter volume of the pain-matrix network in cluster headache. *Cephalalgia* 2012; 32: 109–115.

14. Patenaude B, Smith SM, Kennedy DN, et al. A Bayesian model of shape and appearance for subcortical brain segmentation. *Neuroimage* 2011; 56: 907–922.

15. Efron B. Missing data, imputation, and the bootstrap. *J Am Stat Assoc* 1994; 89: 463–475.

16. Hamilton M. A rating scale for depression. *J Neurol Neurosurg Psych* 1960; 23: 56–62.

17. Smith SM, De Stefano N, Jenkinson M, et al. Normalized accurate measurement of longitudinal brain change. *J Comp Assist Tomog* 2001; 25: 466–475.

18. Smith SM, Zhang Y, Jenkinson M, et al. Accurate, robust, and automated longitudinal and cross-sectional brain change analysis. *Neuroimage* 2002; 17: 479–489.

19. Smith SM, Jenkinson M, Woolrich MW, et al. Advances in functional and structural MR image analysis and implementation as FSL. *Neuroimage* 2004; 23: S208–219.

20. Smith SM. Fast robust automated brain extraction. *Hum Brain Map* 2002; 17: 143–155.

21. Jenkinson M, Bannister P, Brady M, et al. Improved optimization for the robust and accurate linear registration and motion correction of brain images. *Neuroimage* 2002; 17: 825–841.

22. Jenkinson M and Smith S. A global optimisation method for robust affine registration of brain images. *Med Image Analys* 2001; 5: 143–156.

23. Zhang Y, Brady M and Smith S. Segmentation of brain MR images through a hidden Markov random field model and the expectation-maximization algorithm. *IEEE Trans Med Imag* 2001; 20: 45–57.

24. Szabo N, Kincses ZT, Pardutz A, et al. White matter microstructural alterations in migraine: A diffusion-weighted MRI study. *Pain* 2012; 153: 651–656.

25. Naegel S, Holle D, Desmarattes N, et al. Cortical plasticity in episodic and chronic cluster headache. *NeuroImage Clin* 2014; 6: 415–423.

26. Teepker M, Menzler K, Belke M, et al. Diffusion tensor imaging in episodic cluster headache. *Headache* 2012; 52: 274–282.

27. Takao H, Hayashi N and Ohtomo K. White matter asymmetry in healthy individuals: A diffusion tensor imaging study using tract-based spatial statistics. *Neuroscience* 2011; 193: 291–299.

28. Buchel C, Raedler T, Sommer M, et al. White matter asymmetry in the human brain: A diffusion tensor MRI study. *Cereb Cortex* 2004; 14: 945–951.

29. Gong G, Jiang T, Zhu C, et al. Side and handedness effects on the cingulum from diffusion tensor imaging. *Neuroreport* 2005; 16: 1701–1705.

30. Fabiano AJ, Horsfield MA and Bakshi R. Interhemispheric asymmetry of brain diffusivity in normal individuals: A diffusion-weighted MR imaging study. *Am J Neuroradiol* 2005; 26: 1089–1094.

31. Szabo N, Kincses ZT, Pardutz A, et al. White matter disintegration in cluster headache. *J Headache Pain* 2013; 14: 64.

32. May A and Goadsby PJ. Hypothalamic involvement and activation in cluster headache. *Curr Pain Headache Rep* 2001; 5: 60–66.

33. Deppe M, Muller D, Kugel H, et al. DTI detects water diffusion abnormalities in the thalamus that correlate with an extremity pain episode in a patient with multiple sclerosis. *NeuroImage Clin* 2013; 2: 258–262.

34. Ellingson BM, Mayer E, Harris RJ, et al. Diffusion tensor imaging detects microstructural reorganization in the brain associated with chronic irritable bowel syndrome. *Pain* 2013; 154: 1528–1541.

35. Kara B, Kiyat Atamer A, Onat L, et al. DTI findings during spontaneous migraine attacks. *Clin Neuroradiol* 2013; 23: 31–36.

36. Coppola G, Tinelli E, Lepre C, et al. Dynamic changes in thalamic microstructure of migraine without aura patients: A diffusion tensor magnetic resonance imaging study. *Eur J Neurol* 2014; 21: 287–e13.

37. Lutz J, Thon N, Stahl R, et al. Microstructural alterations in trigeminal neuralgia determined by diffusion tensor imaging are independent of symptom duration, severity, and type of neurovascular conflict. *J Neurosurg* 2015: 124: 823–830.

38. Yousry I, Camelio S, Schmid UD, et al. Visualization of cranial nerves I-XII: Value of 3D CISS and T2-weighted FSE sequences. *Eur Radiol* 2000; 10: 1061–1067.

39. Bach DR, Behrens TE, Garrido L, et al. Deep and superficial amygdala nuclei projections revealed in vivo by probabilistic tractography. *J Neurosci* 2011; 31: 618–623.

40. Mishra A, Rogers BP, Chen LM, et al. Functional connectivity-based parcellation of amygdala using self-organized mapping: A data driven approach. *Hum Brain Map* 2014; 35: 1247–1260.

41. Ji G and Neugebauer V. Differential effects of CRF1 and CRF2 receptor antagonists on pain-related sensitization of neurons in the central nucleus of the amygdala. *J Neurophysiol* 2007; 97: 3893–3904.

42. Tsvetkov E, Carlezon WA, Benes FM, et al. Fear conditioning occludes LTP-induced presynaptic enhancement of synaptic transmission in the cortical pathway to the lateral amygdala. *Neuron* 2002; 34: 289–300.

43. Ji G and Neugebauer V. Hemispheric lateralization of pain processing by amygdala neurons. *J Neurophysiol* 2009; 102: 2253–2264.

44. Song SK, Yoshino J, Le TQ, et al. Demyelination increases radial diffusivity in corpus callosum of mouse brain. *Neuroimage* 2005; 26: 132–140.

45. Syka M, Keller J, Klempir J, et al. Correlation between relaxometry and diffusion tensor imaging in the globus pallidus of Huntington's disease patients. *PloS One* 2015; 10: e0118907.

46. Kim HJ, Kim SJ, Kim HS, et al. Alterations of mean diffusivity in brain white matter and deep gray matter in Parkinson's disease. *Neurosci Lett* 2013; 550: 64–68.

47. Blood AJ, Tuch DS, Makris N, et al. White matter abnormalities in dystonia normalize after botulinum toxin treatment. *Neuroreport* 2006; 17: 1251–1255.

III.

GRAY MATTER ATROPHY IN PRESYMPTOMATIC HUNTINGTON'S PATIENTS

András KIRÁLY[1]*, **Zsigmond Tamás KINCSES**[1, 2]*, **Nikoletta SZABÓ**[1, 2], **Eszter TÓTH**[1], **Gergő CSETE**[1], **Péter FARAGÓ**[1], **László VÉCSEI**[1, 3]

[1]Department of Neurology, Albert Szent-Györgyi Clinical Center, University of Szeged, Szeged, Hungary
[2]International Clinical Research Center, St. Anne's University Hospital Brno, Brno, Czech Republic
[3]Neuroscience Research Group of the Hungarian Academy of Sciences and University of Szeged, Szeged, Hungary
*These authors contributed equally

Background – Huntington's disease is a progressive disease in which neurodegeneration is on-going from the early presymptomatic phase. Development of sensitive biomarkers in this presymptomatic stage that are able to monitor the disease progression and test the efficacy of putative neuroprotective treatments are essential.
Methods – Seven presymptomatic Huntington mutation carriers and ten age-matched healthy controls were recruited. Six of the patients participated in a 24 months longitudinal study having MRI scans 12 and 24 months after the baseline measurements. High resolution T1 weighted images were carried out and voxel based morphometry was used to analyse the data. Apart of group differences, correlation of CAG repeat number with focal cortical thickness and with global gray matter volume was calculated.
Results – Focal cortical atrophy was found bilaterally in the superior temporal sulcus and in the left middle frontal gyrus in presymptomatic Huntington patients in whom no sign of cognitive or motor deterioration was detected. Global gray matter atrophy (p<0.048) and decreased total brain volume was found. The number of CAG triplets showed no correlation with the focal gray matter atrophy and total brain volume. Strong correlation between the CAG repeat number and global gray matter volume was found (p<0.016).
Conclusion – Cortical atrophy is apparent in the early, presymptomatic stage of the disease. With further validation in large patient sample atrophy measure could be biomarker of disease progression and putatively of neurodegeneration.

Keywords: cortical atrophy, gray matter, Huntington's disease, MRI; voxel based morphometry

Bevezetés – A Huntington-kór progresszív megbetegedés, melyben neurodegeneráció folyik már a korai preszimptomatikus fázistól kezdve. Különösen fontos a preszimptomatikus stádiumban a jelző biomarkerek megismerése, melyekkel a betegség progressziója monitorozható és tesztelhető a neuroprotektívnek vélt kezelés hatékonysága.
Módszer – Hét, preszimptomatikus Huntington-mutációt hordozó és tíz párosított egészséges kontroll volt a vizsgálatba bevonva. Hatan a betegekből 24 hónapos longitudinális tanulmányban vettek részt és a kezdeti mérést követően a 12. és 24. hónapokban MRI készült róluk. Nagy felbontású T1-súlyozott képek készültek és voxelalapú morfometriát használtak az adatok elemzésére. A csoportok közti különbségtől eltekintve korrelációt találtunk a CAG ismétlődési száma és a fokális corticalis vastagság, illetve a teljes szürkeállomány-terjedelem között.
Eredmények – Bilaterálisnak talált fokális corticalis atrófia volt jelen a superior temporalis sulcusban és a balközép frontális gyrusban olyan preszimptomatikus huntingtonos betegeknél, akik még nem mutatták jelét a kognitív vagy motoros hanyatlásnak. A teljes szürkeállomány-atrófia (p<0,048) és a csökkent teljes agyi volumen szintén igazolódott. A CAG-tripletek száma nem mutatott korrelációt a fokális szürkeállomány-atrófiával és a teljes agyi terjedelemmel. Erős korrelációt találtunk a CAG ismétlődési száma és a teljes szürkeállomány-terjedelem között (p<0,016).
Következtetés – A corticalis atrófia korán megjelenik, már a betegség preszimptomatikus fázisában. Nagyszámú betegmintán, az atrófia mérésével történő további megerősítés biomarkere lehet a betegség progressziójának és a feltételezett neurodegenerációnak.

Kulcsszavak: corticalis atrófia, szürkeállomány, Huntington-kór, MRI; voxelalapú morfometria

Huntington's disease (HD) is a neurodegenerative disorder with an autosomal dominant inheritance. CAG triplet expansion in the Huntingtin gene (IT15) coded on the 4th chromosome causes loss of neurons mainly in the striatum. The behaviour of the mutated *Huntingtin* protein is not completely understood, but it is seems to be toxic to certain cells in the brain and the possible toxic (or ineffective defensive) mechanisms may start to operate already in the intrauterine life[1]. Early symptoms are attributable to the function and connections of the striatum (movement control, mood, higher cognitive functions)[2–6]. Symptom onset, which is heavily dependent on the CAG repeat number, usually appears at the mid-adult life[7], but the neurodegerative changes begin years earlier[1, 8, 9]. The diagnosis is based on the symptoms and the family history confirmed by genetic testing. The length of CAG repeats accounts for 60% of the variation in the age symptom onset and the rate they progress. A longer repeat results in an earlier age of onset and a faster progression of symptoms[10]. The remaining variation is due to environmental factors and other genes that influence the mechanism of the disease.

Recently there have been a number of studies evaluating "extra-striatal" brain structure such as the morphology of the cerebral white matter and cortex in subjects with early HD or prodromal HD. As a whole, these studies support an interesting pattern in which the volume of cerebral white matter is substantially smaller than normal, while in contrast, the cerebral cortex is relatively "spared"[11–20]. One important contradiction for some of these analyses is the use of the global measure of cerebral cortex which is a gross one and may miss regional variation of structure within the cortex, as the cortex is divided up into many small structurally and functionally distinct regions.

Few studies have evaluated regional morphology of the cerebral cortex in HD. Rosas et co-workers showed that cortical thinning in presymptomatic HD patients was gradual in onset and regionally specific[21]. In more recent studies, cortical thickness maps of both small[22] and large[23] samples of prodromal HD subjects show an interesting pattern in which cortical thinning occurs in an unexpected havily superior-posterior pattern what appears to be frontal lobe sparing. This is surprising given the fact that, although the striatum receives input from all over the cortex, the output of the striatum (via basal ganglia and thalamic connections) is predominantly to the frontal cortex.

Furthermore, longitudinal MRI examinations have revealed that the rate of GM loss in HD patients is higher than that in the controls[24, 25]. Interestingly, while significant atrophy was observed in the subcortical nuclei, no cortical atrophy was detected during one or two year follow-up in presymptomatic carriers.

Currently there is no method to reliably follow up the progression of neurodegeneration *in vivo* before the onset of symptoms, which could be used to assess the efficacy of therapeutic intervention.

The aim of this study was to investigate in presymptomatic HD patients the volumetric changes of GM and the correlation of these with the length of CAG repeats. Furthermore, in a longitudinal investigation, we describe the rate of atrophy over 24 months.

Methods

SUBJECTS

Seven presymtomatic HD mutation carriers and ten healthy control subjects were recruited (for demographic data see in **Table 1**). Data from six patients were available for the longitudinal analysis. MRI measurements were repeated three times: baseline, 12 months, 24 months. Patients had no motor symptoms (as measured with the motor section of the Unified Huntington's Disease Rating Scale) or cognitive disturbance over the period of the study (as measured by Mini Mental State Examination, Digit

Table 1. *Demographic and clinical data of subjects (baseline data)*

	Huntington's patients	Healthy subjects
Age (mean years +/- SD)	36.43 (±10.29)	37.1 (±9.23)
N (male)	7 (4)	10 (4)
CAG repeat number (range)	42.29 (37-50)	N.A.
UHDRS	0	N.A.
Total brain volume (mm³)	1429401.17 (±62471.60)	1484013.59 (±78294.76)
Gray matter volume (mm³)	764580.46 (±61652.68)	825978.75 (±45992.47)
White matter volume (mm³)	664820.70 (±31501.88)	658034.84 (±43967.29)

Table 2. *Cognitive performance of the patient population. Follow-up results of the cognitive tests and partial brain volumes of the patient population*

	1st year	2nd year	Difference (p<)
Digit Span	6.50 (±1.04)	6.83 (±1.69)	0.360
Corsi Block Tapping	5.33 (±1.36)	4.83 (±0.41)	0.450
Backward Digit Span	5.16 (±0.989	5.00 (±1.41)	0.740
Listening Span	3.55 (±1.02)	3.49 (±0.69)	0.810
Letter fluency	13.75 (±4.29)	14.5 (±4.96)	0.650
Semantic fluency	24.42 (±4.68)	24.58 (±4.39)	0.900
Total brain volume (mm³)	1413375.53 (±81595.20)	1421300.50 (±63705.59)	0.130*
Gray matter volume (mm³)	762267.06 (±57706.04)	766153.37 (±54792.38)	0.048*
White matter volume (mm³)	651108.46 (±36691.40)	655147.13 (±28895.09)	0.760*

*Compared to the baseline data of control subjects – see in Table 1.

Span Test[26], Backward Digit Span[27], Listening Span Task[28] Semantic Fluency Task[29]. The controls have no neurological or psychiatrical disorders. The study was approved by the local ethics committee (authority number: 86/2009), and all the subjects provided written consent.

IMAGE ACQUISITION

MR imaging were carried out on a 1.5T GE Signa Excite HDxt MR scanner. During the examination, each subject laid supine in the scanner with eyes closed. Scanner noise was attenuated with earplugs, and head motion was restricted with foam padding around the head, and the necessity of head immobility was explained to each subject. 3D spoiled gradient echo (FSPGR: TE: 4.1ms, TR: 10.276ms, matrix: 256×256, FOV: 25×25cm, Flip angle: 15 degree, in-plane resolution: 1×1mm, slice thickness: 1mm) were acquired for all subjects.

GLOBAL ATROPHY

The total brain volume was calculated with SIENAX[30], part of FSL[31, 32]. SIENAX starts by extracting brain and skull images from the single whole-head input data[30]. Next, tissue-type segmentation with partial volume calculation is carried out[33] in order to calculate total volume of brain tissue (including separate estimates of volumes of GM, white matter). Volumetric comparisons were performed using the Statistical Package for Social Sciences (SPSS 17).

VOXEL-WISE ANALYSIS OF THE CORTICAL ATROPHY

We employed an "optimised" VBM-style protocol[34, 35] using FSL[32]. Non-brain parts were removed from all structural images[36], and tissue-type segmentation was carried out by FAST4[33]. The resulting GM par-

tial volume images were registered to a standard space (MNI152) using linear transformation[37], followed by a non-linear registration[38]. The resulting images were averaged to create a study-specific template, to which the native GM images were then non-linearly re-registered. The registered partial volume images were then modulated (to correct for local expansion or contraction) by dividing by the Jacobian of the warp field. The modulated segmented images were then smoothed with an isotropic Gaussian kernel with a sigma of 2mm in the case of group comparison. Finally, voxel-wise General Linear Model (GLM) was applied using permutation-based non-parametric testing. Modell coded group membership to identify HD related brain atrophy. CAG repeat numbers were used to identify atrophy correlated with disease burden. In the longitudinal study design coded for time and within-subject variance was incorporated in the design. Thresholding was carried out by novel method of cluster-free cluster enhancing technique (TFCE)[39].

Results

CLINICAL AND COGNITIVE CHANGES DURING THE THREE YEARS OF OBSERVATION

The patients were asymptomatic as measured on the UHDRS and remained so throughout the three-year of observation period. Nor were any significant changes detected in the cognitive performance measured on a wide variety of dimensions **(Table 2)**.

CORTICAL AND BRAIN ATROPHY IN PRECLINICAL HUNTINGTON'S DISEASE

GM atrophy in patients was observable in bilateral superior temporal sulcus and in the left middle
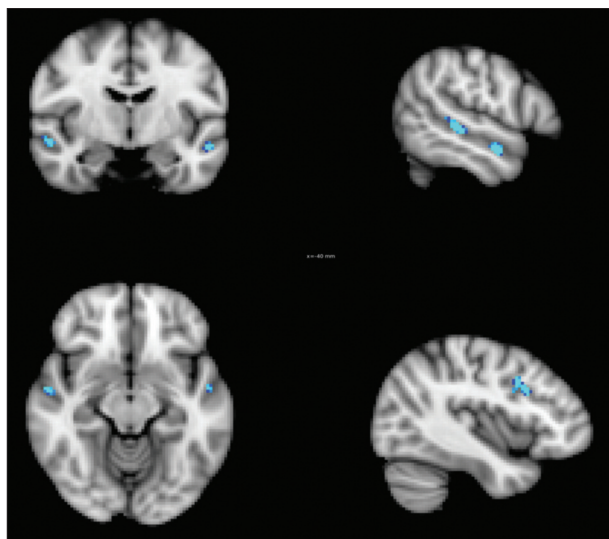
Figure 1. *Gray matter atrophy of bilateral superior temporal sulci and left frontal middle gyrus in patients compared to control group (blue-light blue, p<0.05)*

frontal gyrus **(Figure 1)**. No GM thickening was found.

Global decreased GM was found in Huntington's patients (p<0.048). No difference was found between the white matter (p<0.76) and total brain volume (p<0.13).
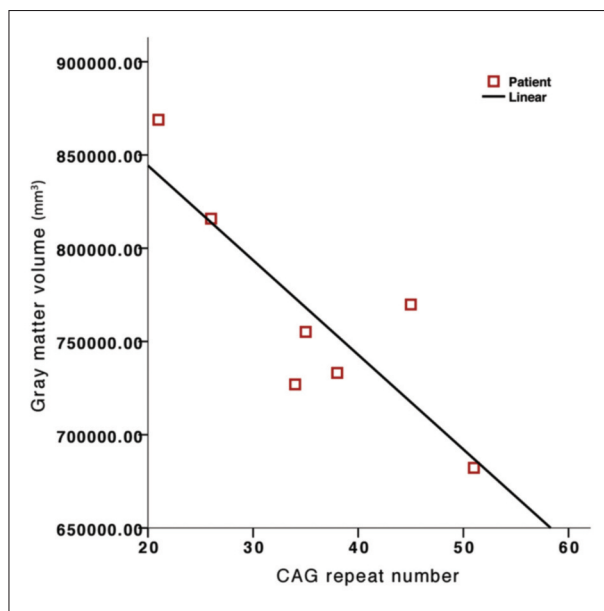
GM ATROPHY AND CAG REPEAT NUMBER

Using VBM style analysis no correlation was found between the CAG repeat number of the patients and the cortical thickness (p<0.3). Nevertheless strong correlation was shown between CAG repeat number and global GM volume (R=0.849, p<0.016, see in **Figure 2**). Total brain volume or white matter volume showed no correlation with the number of CAG triplets (R=0.615, p<0.14).

LONGITUDINAL FOLLOW-UP OF CORTICAL ATROPHY

Gradual GM atrophy development during the two years of the investigation was observed in the bilateral frontal regions, the temporal and insular cortices and in the anterior and posterior cingulate cortices **(Figure 3)**. As regards the subcortical structures, the GM density of the head of the left caudate nucleus was reduced during the study period.

Discussion

In presymptomatic HD patients local GM atrophy was found in the bilateral superior temporal sulcus

Figure 2. *Strong correlation between CAG repeat number and global gray matter volume in patients (R=0.849, p<0.016) was detected*
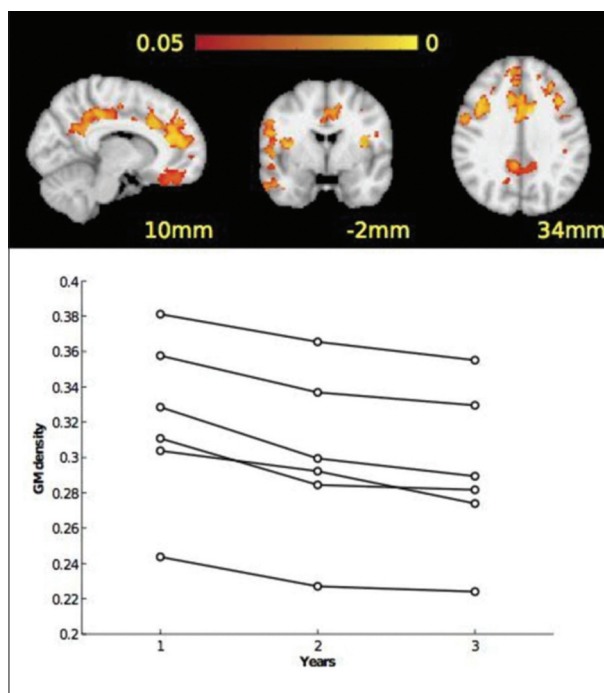
Figure 3. *Gray matter atrophy in preclinical HD during a two-year follow-up. Red-to-yellow color indicate p values (TFCE, corrected for multiple correlations). The graphs depict the voxel densities in each of the individual patients during the three consecutive years, at a frontal location of x=–28 mm, y=20 mm, z=4 mm*

and in the left middle frontal gyrus. We identified negative correlation between the CAG repeat num-

ber and of the total GM volume in presymptomatic mutation carriers. Furthermore gradual GM loss was identified over a 24 months of observation period in the frontal GM.

Halliday and colleagues in symptomatic HD patients found significant brain atrophy in both cortical and subcortical GM[40]. Atrophy of the cortex was relatively uniform, although the medial temporal lobe structures were spared. The size of the caudate nucleus and putamen were strikingly reduced in all cases and this atrophy correlated with the severity of cortical atrophy, suggesting an associated disease process. The rate of cortical but not subcortical atrophy correlated with CAG repeat numbers. The loss of frontal white matter correlated with both cortical and striatal atrophy[40]. As well as subcortical regions – striatum[2, 3, 14, 17, 41–45], globus pallidus[9, 14], thalamus[3, 14], hypothalamus[2, 42], substantia nigra[2, 9, 14] – some VBM studies have shown GM loss in the cortex in subjects with HD, although the location of the cortical loss varies greatly across studies and it is typically less prominent than the subcortical GM loss. A couple of structures that have been relatively consistently identified are the insular cortex[2, 9, 14, 17, 44, 46] and the sensorimotor and premotor region[14, 41, 42, 44]. Frontal lobe regions have also been identified, although the location of the atrophy was variable[2, 17, 41, 43, 44, 47]. *Peinemann* and collegues[2] found GM loss in the subcallosal gyrus, whereas *Muhlau* and co-workers[17] identified GM loss in the dorsolateral prefrontal cortex, but interestingly identified apparent GM gain in the orbitofrontal cortex and concluded that this region was relatively spared by the disease process. Regions of GM loss have also been identified in the parietal lobes[9, 17, 41], occipital lobes[17, 41, 47], amygdala[14] and parahippocampal gyrus[48]. Cross-sectional analyses, investigating HD patients who already display clinical evidence of the disease, have revealed a variable, but somewhat more extensive GM loss than in preclinical patients that observed in our study[14, 49, 50].

Higher CAG repeat numbers are associated with faster clinical progress[51] and earlier onset of symptoms[52]. In the current analysis we found impact of the CAG repeat number on brain atrophy in presymptomatic HD patients. A former neuropathological study described correlation of the CAG repeat and cortical atrophy, but there was no association with the volume of the subcortical struc-

tures[53]. In cross-sectional studies striatal atrophy was found to correlate with CAG repeat[54–57]. Furthermore, frontal-, occipital-, parietal- and cerebellar atrophy was found to correlate with CAG repeat in HD patients[47, 58]. Contrary, in early HD patients increased rate of brain atrophy was found as compared to controls, but no correlation was found between CAG repeat number and the rate of brain atrophy over six months[59]. However, in larger cohort of patients, a CAG repeat number increase by 1, resulted in brain atrophy increment by 0.12% per year[60]_ENREF_56. Earlier longitudinal VBM studies on preclinical carriers indicated only subcortical, and not cortical atrophy[25].

Our study certainly suffers from the limitation that only a relatively low number of patients were recruited. However, acquiring significant results when fewer subjects are measured might indicate larger effect size[61]. Moreover, the observation of continuous changes at three consecutive time points may well lend support to our hypothesis.

Conclusion

Cortical atrophy is apparent in the early, presymptomatic stage of the disease. Since brain structural changes are started in the very early, presymptomatic phase of the HD, sensitive biomarkers are needed. With further validation in large patient sample atrophy measure could be biomarker of disease progression and putatively of neurodegeneration.

REFERENCES

1. *Gardian G, Vecsei L.* Huntington's disease: pathomechanism and therapeutic perspectives. Journal of Neural Transmission 2004;111:1485-94.
http://dx.doi.org/10.1007/s00702-004-0201-4

2. *Peinemann A, et al.* Executive dysfunction in early stages of Huntington's disease is associated with striatal and insular atrophy: A neuropsychological and voxel-based morphometric study. J Neurol Sci 2005;239:11-9.
http://dx.doi.org/10.1016/j.jns.2005.07.007

3. *Kassubek J, Juengling FD, Ecker D, Landwehrmeyer GB.* Thalamic atrophy in Huntington's disease co-varies with cognitive performance: A morphometric MRI analysis. Cereb Cortex 2005;15:846-53.
http://dx.doi.org/10.1093/cercor/bhh185

4. *Antal A, et al.* Perceptual categorization is impaired in Huntington's disease: An electrophysiological study. Dement Geriatr Cogn 2003;16:187-92.
http://dx.doi.org/10.1159/000072801

5. *Nemeth D, et al.* Language deficits in pre-symptomatic Huntington's disease: evidence from Hungarian. Brain Lang 2012;121:248-53.
http://dx.doi.org/10.1016/j.bandl.2012.04.001

6. *Papp KV, Kaplan RF, Snyder PJ.* Biological markers of cognition in prodromal Huntington's disease: a review. Brain Cogn 2011;77:280-91.
http://dx.doi.org/10.1016/j.bandc.2011.07.009

7. *Quarrell OW, et al.* Reduced penetrance alleles for Huntington's disease: a multi-centre direct observational study. J Med Genet 2007;44:e68.
http://dx.doi.org/10.1136/jmg.2006.045120

8. *Vonsattel JP, et al.* Neuropathological classification of Huntington's disease. J Neuropathol Exp Neurol 1985;44:559-77.
http://dx.doi.org/10.1097/00005072-198511000-00003

9. *Thieben MJ, et al.* The distribution of structural neuropathology in pre-clinical Huntington's disease. Brain 2002;125:1815-28.
http://dx.doi.org/10.1093/brain/awf179

10. *Andrew SE, et al.* The relationship between trinucleotide (CAG) repeat length and clinical features of Huntington's disease. Nat Genet 1993;4:398-403.
http://dx.doi.org/10.1038/ng0893-398

11. *Aylward EH, et al.* Frontal lobe volume in patients with Huntington's disease. Neurology 1998;50:252-8.
http://dx.doi.org/10.1212/WNL.50.1.252

12. *Beglinger LJ, et al.* White matter volume and cognitive dysfunction in early Huntington's disease. Cogn Behav Neurol 2005;18:102-7.
http://dx.doi.org/10.1097/01.wnn.0000152205.79033.73

13. *Ciarmiello A, et al.* Brain white-matter volume loss and glucose hypometabolism precede the clinical symptoms of Huntington's disease. J Nucl Med 2006;47:215-22.

14. *Douaud G, et al.* Distribution of grey matter atrophy in Huntington's disease patients: a combined ROI-based and voxel-based morphometric study. Neuroimage 2006;32:1562-75.
http://dx.doi.org/10.1016/j.neuroimage.2006.05.057

15. *Fennema-Notestine C, et al.* In vivo evidence of cerebellar atrophy and cerebral white matter loss in Huntington disease. Neurology 2004;63:989-95.
http://dx.doi.org/10.1212/01.WNL.0000138434.68093.67

16. *Jernigan TL, Salmon DP, Butters N, Hesselink JR.* Cerebral structure on MRI .2. Specific changes in Alzheimers and Huntingtons diseases. Biol Psychiat 1991;29:68-81.
http://dx.doi.org/10.1016/0006-3223(91)90211-4

17. *Muhlau M, et al.* Voxel-based morphometry indicates relative preservation of the limbic prefrontal cortex in early Huntington disease. Journal of Neural Transmission 2007;114:367-72.
http://dx.doi.org/10.1007/s00702-006-0571-x

18. *Rosas HD, et al.* Evidence for more widespread cerebral pathology in early HD – An MRI-based morphometric analysis. Neurology 2003;60:1615-20.
http://dx.doi.org/10.1212/01.WNL.0000065888.88988.6E

19. *Paulsen JS, et al.* Preparing for preventive clinical trials. The predict-HD study. Arch Neurol-Chicago 2006;63:883-90.
http://dx.doi.org/10.1001/archneur.63.6.883

20. *Paulsen JS, et al.* Striatal and white matter predictors of estimated diagnosis for Huntington disease. Brain Res Bull 2010;82:201-7.
http://dx.doi.org/10.1016/j.brainresbull.2010.04.003

21. *Rosas HD, et al.* Regional and progressive thinning of the cortical ribbon in Huntington's disease. Neurology 2002;58:695-701.
http://dx.doi.org/10.1212/WNL.58.5.695

22. *Rosas HD, et al.* Regional cortical thinning in preclinical Huntington disease and its relationship to cognition. Neurology 2005;65:745-7.
http://dx.doi.org/10.1212/01.wnl.0000174432.87383.87

23. *Tabrizi SJ, et al.* Biological and clinical manifestations of Huntington's disease in the longitudinal TRACK-HD study: cross-sectional analysis of baseline data. Lancet Neurol 2009;8:791-801.
http://dx.doi.org/10.1016/S1474-4422(09)70170-X

24. *Aylward EH, et al.* Longitudinal change in regional brain volumes in prodromal Huntington disease. J Neurol Neurosurg Psychiatry 2011;82:405-10.
http://dx.doi.org/10.1136/jnnp.2010.208264

25. *Tabrizi SJ, et al.* Biological and clinical changes in premanifest and early stage Huntington's disease in the TRACK-HD study: the 12-month longitudinal analysis. Lancet Neurol 2011;10:31-42.
http://dx.doi.org/10.1016/S1474-4422(10)70276-3

26. *Racsmány M, Németh D, Pléh C.* A verbális munkamemória magyar nyelvű vizsgálóeljárásai (Hungarian Diagnostic Tools of Verbal Working Memory Functions). Magyar Pszichológiai Szemle (Hungarian Review of Psychology) 2005;60(4):479-506.

27. *Isaacs EB, Vargha-Khadem F.* Differential course of development of spatial and verbal memory span: A normative study. British Journal of Developmental Psychology 1989;7:377-80.
http://dx.doi.org/10.1111/j.2044-835X.1989.tb00814.x

28. *Janacsek K, Tánczos T, Mészáros T, Nemeth D.* The Hungarian version of Listening Span task. Magyar Pszichológiai Szemle (Hungarian Review of Psychology) 2009;64:385-406.
http://dx.doi.org/10.1556/MPSzle.64.2009.2.5

29. *Troyer AK, Moscovitch M, Wincour G, Alexander MP, Stuss D.* Clustering and switching on verbal fluency: The effects of focal frontal- and temporal-lobe lesions. Neuropsychologia 1998;36:499-504.
http://dx.doi.org/10.1016/S0028-3932(97)00152-8

30. *Smith SM, et al.* Accurate, robust, and automated longitudinal and cross-sectional brain change analysis. Neuroimage 2002;17:479-89.
http://dx.doi.org/10.1006/nimg.2002.1040

31. *Jenkinson M, Beckmann CF, Behrens TE, Woolrich MW, Smith SM.* Fsl. Neuroimage (in press).
http://dx.doi.org/10.1016/j.neuroimage.2011.09.015

32. *Smith SM, et al.* Advances in functional and structural MR

image analysis and implementation as FSL. Neuroimage 2004;23(Suppl 1):S208-19.
http://dx.doi.org/10.1016/j.neuroimage.2004.07.051

33. *Zhang Y, Brady M, Smith S.* Segmentation of brain MR images through a hidden Markov random field model and the expectation-maximization algorithm. IEEE transactions on medical imaging 2001;20:45-57.
http://dx.doi.org/10.1109/42.906424

34. Good CD, et al. A voxel-based morphometric study of ageing in 465 normal adult human brains. Neuroimage 2001;14:21-36.
http://dx.doi.org/10.1006/nimg.2001.0786

35. *Ashburner J, Friston KJ.* Voxel-based morphometry – the methods. Neuroimage 2000;11:805-21.
http://dx.doi.org/10.1006/nimg.2000.0582

36. *Smith SM.* Fast robust automated brain extraction. Hum Brain Mapp 2002;17:143-55.
http://dx.doi.org/10.1002/hbm.10062

37. *Jenkinson M, Smith S.* A global optimisation method for robust affine registration of brain images. Med Image Anal 2001;5:143-56.
http://dx.doi.org/10.1016/S1361-8415(01)00036-6

38. *Andersson JLR, Jenkinson M, Smith S.* Non-linear optimisation. FMRIB technical report. Oxford, 2007.

39. *Smith SM, Nichols TE.* Threshold-free cluster enhancement: addressing problems of smoothing, threshold dependence and localisation in cluster inference. Neuroimage 2009;44:83-98.
http://dx.doi.org/10.1016/j.neuroimage.2008.03.061

40. *Halliday GM, et al.* Regional specificity of brain atrophy in Huntington's disease. Exp Neurol 1998;154:663-72.
http://dx.doi.org/10.1006/exnr.1998.6919

41. *Muhlau M, et al.* Striatal gray matter loss in Huntington's disease is leftward biased. Movement Disord 2007;22:1169-73. http://dx.doi.org/10.1002/mds.21137

42. *Kassubek J, et al.* Topography of cerebral atrophy in early Huntington's disease: a voxel based morphometric MRI study. J Neurol Neurosur Ps 2004;75:213-20.

43. *Lambrecq V, et al.* Evolution of brain gray matter loss in Huntington's disease: a meta-analysis. Eur J Neurol 2013;20:315-21.
http://dx.doi.org/10.1111/j.1468-1331.2012.03854.x

44. *Stoffers D, et al.* Contrasting gray and white matter changes in preclinical Huntington disease An MRI study. Neurology 2010;74:1208-16.
http://dx.doi.org/10.1212/WNL.0b013e3181d8c20a

45. *Wolf RC, et al.* Brain structure in preclinical Huntington's disease: A multi-method approach. Neurodegener Dis 2013;12:13-22.
http://dx.doi.org/10.1159/000338635

46. *Thieben MJ, et al.* The distribution of structural neuropathology in pre-clinical Huntington's disease. Brain 2002;125:1815-28.
http://dx.doi.org/10.1093/brain/awf179

47. *Gomez-Anson B, et al.* Prefrontal cortex volume reduction on MRI in preclinical Huntington's disease relates to vi-suomotor performance and CAG number. Parkinsonism Relat D 2009;15:213-9.
http://dx.doi.org/10.1016/j.parkreldis.2008.05.010

48. *Barrios FA, et al.* Olfaction and neurodegeneration in HD. Neuroreport 2007;18:73-6.
http://dx.doi.org/10.1097/WNR.0b013e3280102302

49. *Henley SM, et al.* Pitfalls in the use of voxel-based morphometry as a biomarker: examples from huntington disease. AJNR Am J Neuroradiol 2010;31:711-9.
http://dx.doi.org/10.3174/ajnr.A1939

50. *Kassubek J, et al.* Topography of cerebral atrophy in early Huntington's disease: a voxel based morphometric MRI study. J Neurol Neurosurg Psychiatry 2004;75:213-20.

51. *Rosenblatt A, et al.* The association of CAG repeat length with clinical progression in Huntington disease. Neurology 2006;66:1016-20.
http://dx.doi.org/10.1212/01.wnl.0000204230.16619.d9

52. *Aziz NA, et al.* Normal and mutant HTT interact to affect clinical severity and progression in Huntington disease. Neurology 2009;73:1280-5.
http://dx.doi.org/10.1212/WNL.0b013e3181bd1121

53. *Halliday GM, et al.* Regional specificity of brain atrophy in Huntington's disease. Exp Neurol 1998;154:663-72.
http://dx.doi.org/10.1006/exnr.1998.6919

54. *Rosas HD, et al.* Striatal volume loss in HD as measured by MRI and the influence of CAG repeat. Neurology 2001;57:1025-8.
http://dx.doi.org/10.1212/WNL.57.6.1025

55. *Aylward E, et al.* Association between Age and Striatal Volume Stratified by CAG Repeat Length in Prodromal Huntington Disease. PLoS currents 2011;3:RRN1235.
http://dx.doi.org/10.1371/currents.RRN1235

56. *Henley SM, et al.* Relationship between CAG repeat length and brain volume in premanifest and early Huntington's disease. Journal of neurology 2009;256:203-12.
http://dx.doi.org/10.1007/s00415-009-0052-x

57. *Aylward E.H, et al.* Longitudinal change in basal ganglia volume in patients with Huntington's disease. Neurology 1997;48:394-399.
http://dx.doi.org/10.1212/WNL.48.2.394

58. *Ruocco HH, Bonilha L, Li LM, Lopes-Cendes I, Cendes F.* Longitudinal analysis of regional grey matter loss in Huntington disease: effects of the length of the expanded CAG repeat. J Neurol Neurosurg Psychiatry 2008;79:130-5. http://dx.doi.org/10.1136/jnnp.2007.116244

59. *Henley SM, et al.* Increased rate of whole-brain atrophy over 6 months in early Huntington disease. Neurology 2006;67:694-6.
http://dx.doi.org/10.1212/01.wnl.0000230149.36635.c8

60. *Henley SM, et al.* Whole-Brain Atrophy as a Measure of Progression in Premanifest and Early Huntington's Disease. Movement Disord 2009;24:932-6.
http://dx.doi.org/10.1002/mds.22485

61. *Friston K.* Ten ironic rules for non-statistical reviewers. Neuroimage 2012;61:1300-10.
http://dx.doi.org/10.1016/j.neuroimage.2012.04.018

IV.

PLoS one

Target Identification for Stereotactic Thalamotomy Using Diffusion Tractography

Zsigmond Tamás Kincses[1,2]*, Nikoletta Szabó[1], István Valálik[3], Zsolt Kopniczky[4], Lívia Dézsi[1], Péter Klivényi[1], Mark Jenkinson[5], András Király[1], Magor Babos[6], Erika Vörös[7], Pál Barzó[4], László Vécsei[1]

1 Department of Neurology, Albert Szent-György Clinical Center, University of Szeged, Szeged, Hungary, 2 International Clinical Research Center, St. Anne's University Hospital Brno, Brno, Czech Republic, 3 Department of Neurosurgery, St. John's Hospital, Budapest, Hungary, 4 Department of Neurosurgery, Albert Szent-György Clinical Center, University of Szeged, Szeged, Hungary, 5 FMRIB Centre, Department of Clinical Neurology, John Radcliffe Hospital, University of Oxford, Oxford, United Kingdom, 6 Euromedic Diagnostic Hungary Ltd, Szeged, Hungary, 7 Department of Radiology, Albert Szent-György Clinical Center, University of Szeged, Szeged, Hungary

Abstract

Background: Stereotactic targets for thalamotomy are usually derived from population-based coordinates. Individual anatomy is used only to scale the coordinates based on the location of some internal guide points. While on conventional MR imaging the thalamic nuclei are indistinguishable, recently it has become possible to identify individual thalamic nuclei using different connectivity profiles, as defined by MR diffusion tractography.

Methodology and Principal Findings: Here we investigated the inter-individual variation of the location of target nuclei for thalamotomy: the putative ventralis oralis posterior (Vop) and the ventral intermedius (Vim) nucleus as defined by probabilistic tractography. We showed that the mean inter-individual distance of the peak Vop location is 7.33 mm and 7.42 mm for Vim. The mean overlap between individual Vop nuclei was 40.2% and it was 31.8% for Vim nuclei. As a proof of concept, we also present a patient who underwent Vop thalamotomy for untreatable tremor caused by traumatic brain injury and another patient who underwent Vim thalamotomy for essential tremor. The probabilistic tractography indicated that the successful tremor control was achieved with lesions in the Vop and Vim respectively.

Conclusions: Our data call attention to the need for a better appreciation of the individual anatomy when planning stereotactic functional neurosurgery.

Introduction

Thalamotomy was introduced in the treatment of tremor by Hassler in 1954 [1], the selective stereotactic lesioning of the ventralis intermedius nucleus of the thalamus (Vim) was described by Narabayashi [2] and later the electrical stimulation of Vim in 1987 by Benabid [3]. The precise targeting within the brain is of crucial importance for successful surgical intervention. Targeting the desired thalamic nucleus is usually carried out by using stereotactic coordinates specified in relation to a point on the anterior commissure – posterior commissure (AC-PC) line [4,5,6]. Other methods try to establish population-based stereotactic coordinates of the target nuclei based on postmortem histological data or intraoperative stimulation techniques [7,8,9]. While achieving reasonable results, these methods neglect individual anatomical variations.

Since the identification of thalamic nuclei on conventional imaging modalities is difficult, several novel approaches were proposed to aid the visualisation of the functionally important thalamic nuclei. It is now possible to segregate the major thalamic structures using MR relaxometry, even in a clinically acceptable time [10,11]. Recently, probabilistic tractography was successfully used to investigate the connectivity profile of two major thalamic target nuclei for functional neurosurgery: ventralis intermedius (Vim) and ventralis oralis posterior (Vop) [12]. In addition, it is possible to segment the thalamic nuclei based on connectivity patterns defined by MR diffusion tractography [13,14]. This approach has been suggested by others [12,15,16], but the benefit of such a method has not been evaluated systematically so far.

In the current investigation we calculated the interindividual variability of the target thalamic nuclei, (Vop and Vim) location in healthy controls. We also present the retrospective DTI identification

of the target thalamic nuclei in two patients that underwent stereotactic Vim and Vop thalamotomy.

Methods

Participants

Nine healthy individuals, with no history of neurological or psychiatric diseases were included in the study (mean age: 28.3±7.09, male: 3). Furthermore, two patients were also included, who underwent stereotactic thalamotomy.

Ethics

The study was approved by the Ethics Committee of University of Szeged (authority number: 87/2009), and all subjects provided written consent.

Image acquisition

Imaging was carried out using a 1.5 T GE Signa Excite scanner. High resolution T1 weighted images (3D IR-FSPGR: TR/TE/TI: 10.3/4.2/450ms, flip angle: 15°, ASSET: 2, FOV: 25*25 cm, matrix: 256*256, slice thickness: 1mm) and diffusion-weighted images (DTI: TR/TE: 16000/93.8ms, flip angle: 90°, FOV: 23*23cm, matrix: 96*96, slice thickness: 2.4mm, ASSET: 2, NEX: 2) were acquired. Diffusion weighting was performed along 60 independent directions, with a b-value of 1000 s/mm^2. Six reference images, with no diffusion weighting were also obtained. The preoperative scans of the patients were obtained using identical acquisition sequences to those used for control subjects. Postoperative scans were carried out three months after the surgery. High-resolution-T1 weighted images (with parameters identical to the preoperative ones) and sagittal 3D FLAIR images (3D FLAIR: TR/TE/TI: 6000/134.6/1839ms, flip angle: 90°, FOV: 23*23cm, matrix: 256*256, slice thickness: 2mm) were acquired to localise the thalamotomic lesion.

Image processing

Data were processed using the tools from the FMRIB Software Library (FSL, version 5.0; Oxford Centre for Functional MRI of the Brain (FMRIB), UK; www.fmrib.ox.ac.uk/fsl [17]) according to the method reported by Behrens and colleagues [14]. Initially the raw diffusion data was corrected for eddy-currents and motion artefacts with FMRIB's Diffusion Toolbox (FDT [18]). The images were then skull stripped using the Brain Extraction Tool (BET [19]) and the diffusion-weighted images were registered to the high-resolution T1-weighted image with a 6 degree-of-freedom linear registration using the FMRIB Linear Image Registration Tool (FLIRT [20]). Probability distributions of fiber orientation were estimated for each brain voxel in the acquired diffusion space using a multi-fiber extension [21] of the probabilistic tractography available in FDT [18].

Probabilistic diffusion tractography can estimate the pathways that originate at any given seed voxel, as well as the probability that such a pathway will pass through any other voxel in the brain [18]. Binary masks of the thalamus and the cortical targets were drawn manually for each subject. Probabilistic multi-fiber diffusion tractography was initiated from every voxel inside the thalamic mask: 5000 times for each voxel. Counters were increased every time an individual streamline reached the cortical target region. Hence, the values stored in thalamic voxels in one of the resulting images represent the probability of those voxels being connected to the particular target cortical mask assigned to that image [14].

To investigate the inter-subject variability of the target nuclei, a specific distance reserving registration method was used: the high-resolution T1-weighted images were registered to the standard

MNI brain with a 6 degree-of-freedom transformation (rotations and translations only) that was based on landmark points in a way that kept the position of the anterior commissure fixed, while aligning the ACPC line and the mid-sagittal plane between images.

The Euclidean distance, given by the equation:

$$d(p,q) = \sqrt{\sum_{i=1}^{3}(q_i - p_i)^2}$$

was calculated for each subject between points representing the thalamic voxel with peak connection probability to the premotor cortex (for Vop) and to the motor cortex (for Vim) and the standard space voxel with peak connectivity as indicated by the Oxford Thalamic Connectivity Map [13]. The mean pair-wise distance was also calculated: the distance between the voxel with peak connection probability to the premotor (for Vop) and to the motor (for Vim) cortex was calculated between all possible pair of subjects and this inter-subject distance was averaged for Vop and Vim separately.

The connectivity images for the thalamus were thresholded at 10% of individual connectivity maximum and binarised in order to create masks of the thalamic regions connected to the premotor or motor cortex. To assess the similarity of positions the overlap between each pair of masks (between subjects) were calculated according to the method proposed by Crum and colleagues [22]. Overlap was measured by the Tanimoto Coefficient (TC), which is defined as the ratio of the number of voxels in the intersection of the two regions to the number of voxels in the union:

$$TC = \frac{N(A \bigcap B)}{N(A \bigcup B)}.$$

We also took further steps to exclude possible registration bias between the DTI and T1-weighted images that might originate from the EPI distortions. We manually compared the high-resolution T1-weighted image and the first volume of the diffusion data (no diffusion gradient applied) registered to the T1-weighted image for each subjects. The positions of the following landmarks were compared: AC, PC, the maximal width of the third ventricle at the level AC and the highest point of the corpus callosum in the midsagittal line.

Results

Inter-subject variability of the position of thalamic nuclei

As found with the manual comparison the shape and the position of the thalamus was not affected by EPI distortions. The largest misregistrations were found along the anterior-posterior axis, but even that was minimal (for AC and for PC 0.6±0.5mm). The width of the third ventricle was not different, and the position of the highest point of the corpus callosum differed only in case of a single subject with 1 mm.

The premotor thalamus was consistently localised in all subjects, however, since the individual brain shapes differed, the exact location of the Vop and Vim nucleus varied substantially across subjects (Fig 1). The mean distance of the peak connection probability of Vop from the peak probability indicated by the Oxford Thalamic Connectivity map was 5.08mm. The equivalent distance was 6.26mm for the Vim. The mean pair-wise inter-subject
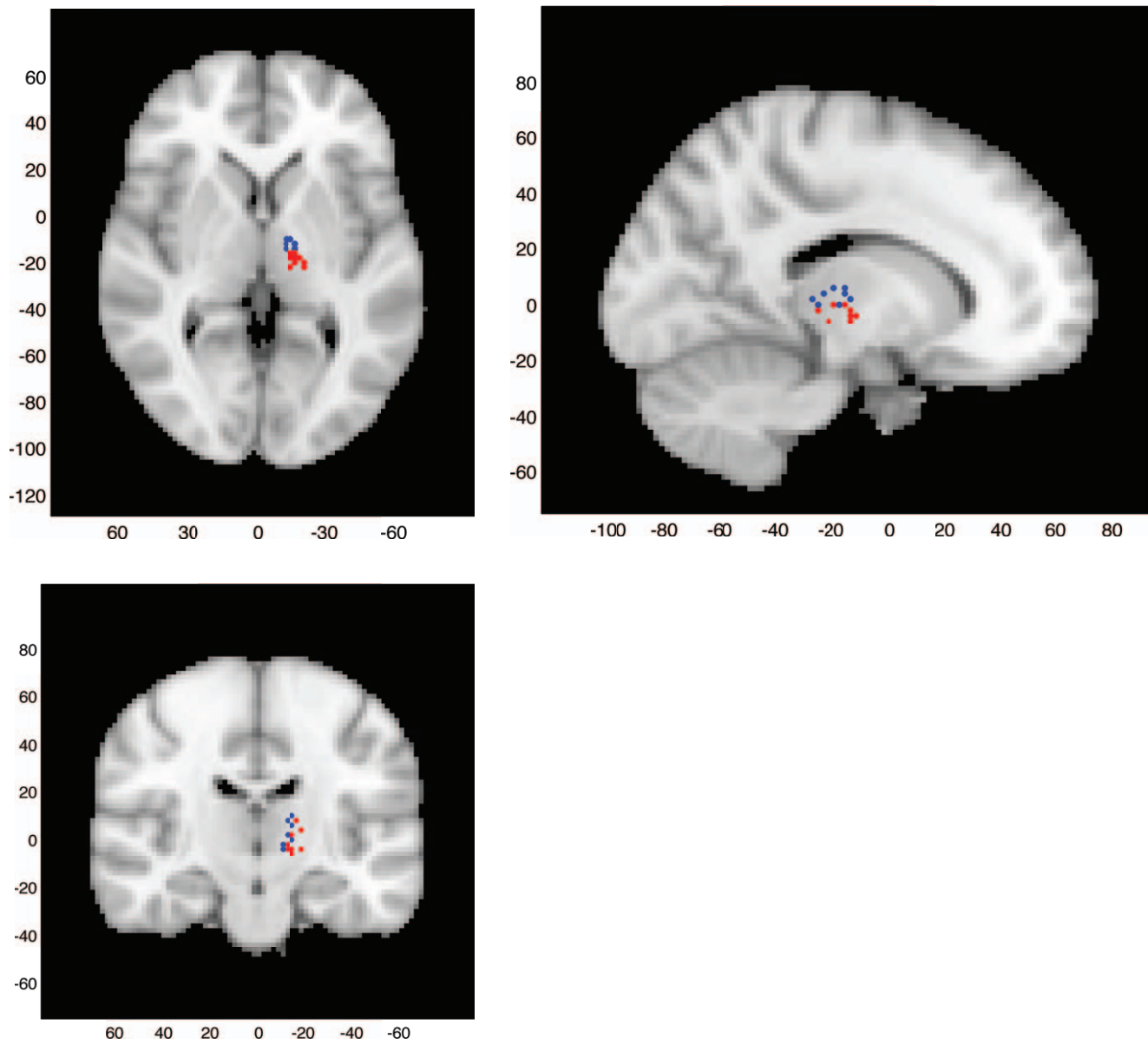
Figure 1. Spatial localisation of peak Vop and Vim voxels as defined by probabilistic tractography. Individual images were realigned to standard space with a 6 DOF transformation in a way to match the location of the AC and align the AC-PC line and the midsagittal plane. The registered peak connectivity voxels for the primary motor (Vim - in red) and for the premotor cortex (Vop – in blue) are shown on three orthogonal slices.

doi:10.1371/journal.pone.0029969.g001

distance of the peak connectivity voxel of Vop was 7.33±3.37mm (range: 0–14.56mm) and 7.42±3.35 mm (range: 2–14.28mm) for Vim. The mean distance of the tractography defined Vop and Vim coordinates from the Stereotactic target point defined by Hyam's method [12] was 7.19±4.36mm (range: 2.45–14.89mm) for Vim and 9.58±4.82mm (range: 3.0–17.12mm) for Vop.

The mean pair-wise overlap for Vop as calculated by the Tannimoto Coefficient was 40.2% (range: 15.5%–66.2%) and 31.8% (range: 3.2%–66.2%) for Vim.

Case #1: Vop thalamotomy for posttraumatic tremor

A left-handed, 32 year-old male, after having a motorbike accident that caused brainstem bleeding (at the level of the red nucleus; Fig 2), developed a tremor having resting, postural, as well

as intention components, bradykinesia, rigidity and a slight paresis of the left arm. Seven years after the accident, because of ineffective tremor control by various medication regimes, functional neurosurgery was offered. Because the patient has not accepted deep-brain-stimulation implantation stereotactic thalamotomy was carried out on the right side in the region of Vop/Vim border with target coordinates according to Guiot's method [5,23] that is, given the AC-PC length of 24.9mm, was 8mm anterior of PC and 12.7mm lateral from the mid-sagittal line on the AC-PC plane. During the standard surgical procedure the final position of the lesion along the selected trajectory was adjusted according to the tremor control of the intraoperative stimulation. After surgery the patient had an immediate relief from his left upper extremity tremor (his score on the part A of the Fahn-Tolosa-Marin tremor rating
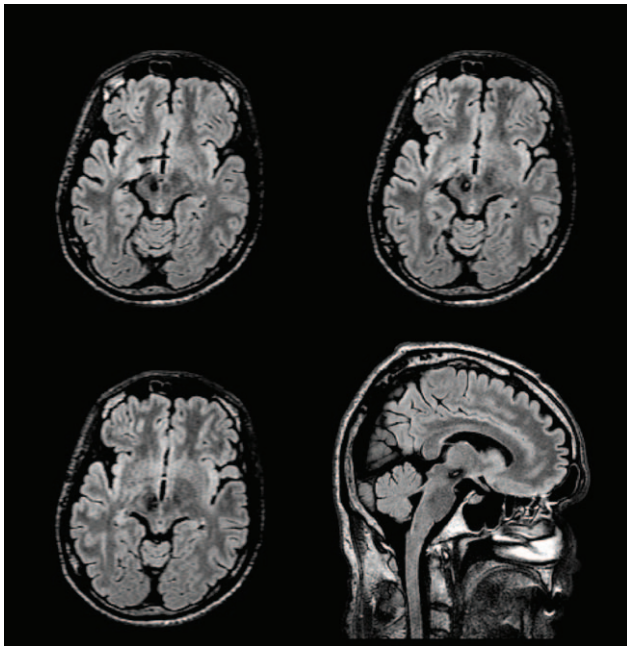
Figure 2. Preoperative FLAIR images show the right perirubral mesencephalic traumatic haemorrhage. Images are presented in radiological convention.
doi:10.1371/journal.pone.0029969.g002

scale (FMT) reduced form 16 to 4 points). Neither the muscle strength, nor the bradykinesia improved. At the three-month checkup these findings had not changed for the left upper extremity, however a small amplitude flexion-extension tremor appeared in the left toes.

As shown by the connectivity-based segmentation of the thalamus, regions connected with highest probability to the prefrontal, premotor, motor and sensory, parietal, occipital and temporal cortices were clearly delineated (Fig 3). The operative lesion of the thalamus, identified on the postoperative FLAIR images (registered to the preoperative T1-weighted structural image with 6 DOF linear registration) was situated in the region of the thalamus connected with the highest probability to the premotor cortex (Fig 3).

Probabilistic multi-fiber tractography initiated from the thalamic lesion showed, on one hand, connection to the medial premotor - prefrontal cortex and, on the other hand, to the brain stem particularly to the rubral/perirubral mesencephalic post-haemorrhagic lesion and some fibres travelling further on to the cerebellum (Fig 4).

Case #2: Vim thalamotomy for essential tremor

A right-handed, 50-year-old women had developed tremor ten years earlier. The tremor was most prominent in the hands but also appeared in the head, having postural and action components, and was also present when walking. Her family history was unremarkable. Medication regimes that had been tried over the years were ineffective, and the tremor severely affected the quality of life of the patient. Stereotactic Vim thalamotomy was carried out with target coordinates according to Guiot [5,23] that correspond well with the coordinates defined by Hyam's method [12]. After surgery the tremor of the right hand improved significantly and on the three-month control examination this effect was found to be enduring (FMT score reduced from 17 to 11 points). No significant change was detected in the head-tremor or in the tremor of the left hand.

The postoperative T1-weighted image was registered to the preoperative T1-weighted image in order to identify the position of the lesion in relation to the diffusion–based connectivity results. The connectivity-based segmentation of the thalamus indicated that the surgical lesion was in the putative Vim nucleus, the region that showed the highest probability of connection to the primary motor cortex (Fig 5). Postoperative probabilistic tractography from the lesion showed that the lesioned thalamus was connected to the primary motor cortex, mainly to the medial structures, and downstream to the ipsilateral cerebellar hemisphere (Fig 6).

Discussion

In the current study we investigated the inter-individual variability of the position of the thalamotomic target nuclei Vim
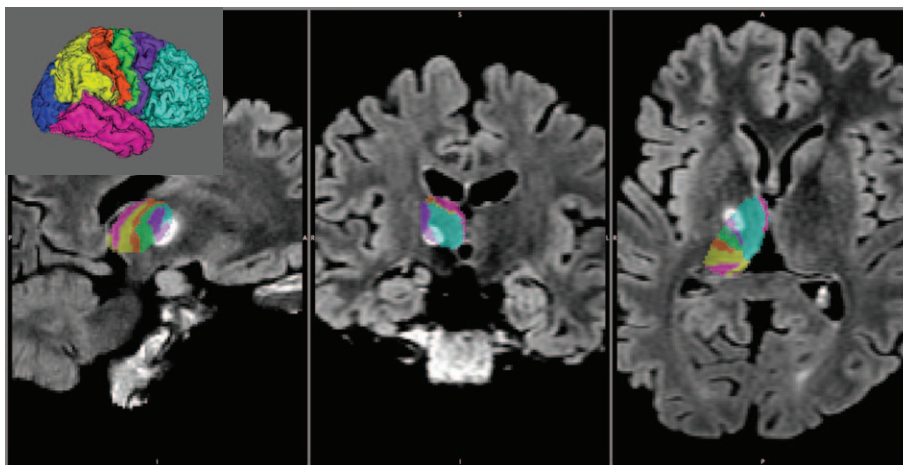
Figure 3. Connectivity-based segmentation of the right thalamus of the patient operated on for tremor caused by traumatic mesencephalic bleeding. Results are overlaid on the postoperative FLAIR images. The bright area represents the Stereotactic thalamotomy. The key to the colour coding of the thalamic segmentation is shown in the inset. The colour in each thalamic voxel represents the colour of the cortical area that has the highest connection probability to that voxel.
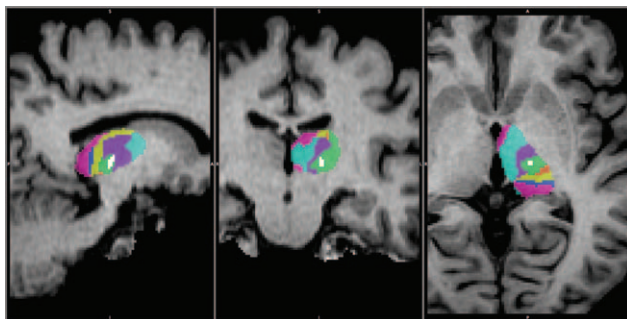doi:10.1371/journal.pone.0029969.g003
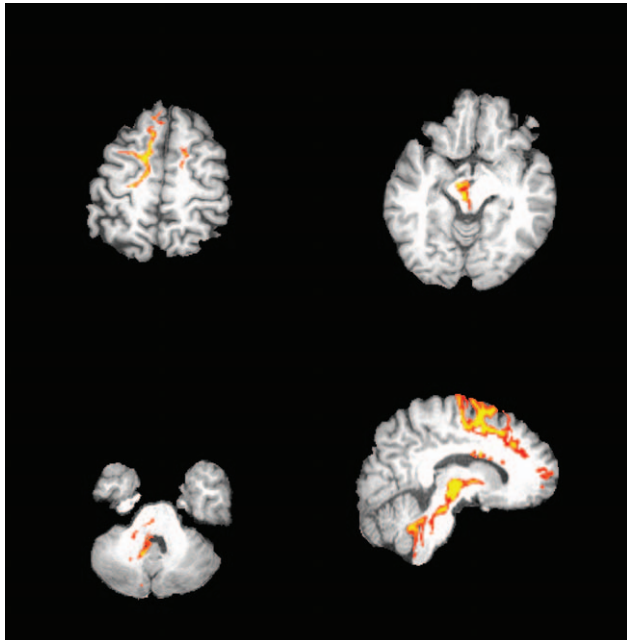
Figure 4. Connectivity of the thalamic lesion, evaluated using multi-fiber probabilistic tractography. The tracts reach the premotor cortex, on one hand, and the nucleus ruber and the perirubral mesencephalon, on the other hand, with some travelling further to the cerebellum. The image is thresholded at 500 particles (10%).
doi:10.1371/journal.pone.0029969.g004

Figure 6. Connectivity of the thalamic lesion of the essential tremor patient, evaluated using multi-fiber probabilistic tractography. The tracts reach the primary motor cortex, on one hand, and travelling to the cerebellum on the other hand. The image is thresholded at 250 particles (5%).
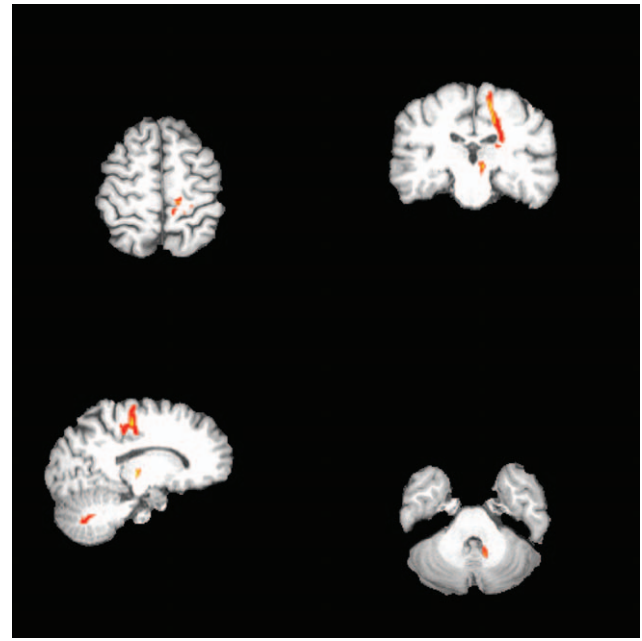doi:10.1371/journal.pone.0029969.g006

and Vop as defined by probabilistic diffusion tractography. We found that, compared to the size of the nucleus, the variability of its position is substantial. Our results call attention to the importance of defining the thalamotomic lesion target individually. We also showed that the lesion in two successful thalamotomic cases was in fact in the target nuclei as defined by tractography based segmentation.

Despite the accurate stereotactic atlases [7,24] that guide the standard methods for targeting, significant intersubject variability still exists [7]. The differences in gross thalamic morophology is already conspicuous: the medio-lateral aspect as defined by the

Figure 5. Connectivity-based segmentation of the left thalamus of the patient having essential tremor. Results are overlaid on the postoperative T1-weighted image. White voxels represent the location of the Stereotactic lesion. The colour coding of the thalamic segmentation is the same as that using in Figure 3. The lesion is in the area of the thalamus connected most strongly to the primary motor cortex: the putative Vim.
doi:10.1371/journal.pone.0029969.g005

position of the internal capsule, as well as the height of the thalamus vary between subjects [7]. The position of the pulvinar system varies even between subjects with the same AC-PC distance [7]. Moreover, as emphasized by Morel, these variations are not even homogenous within the thalamus, particularly along the mediolateral axis [7]. Our results, using a different modality, also indicate significant variability of the position of the Vop and Vim nuclei, especially when the size of the nucleus and the surgical lesion is considered. The distance between peak-probability Vop voxels was 7 mm on average and is similar for Vim, but in certain cases the distance was as much as one and a half centimetres. The overlap between Vops on average was around only 40% and varies from 15% to 60%. Similar overlap values were found for Vim. It is also important to emphasize that in the current variability estimation only young, healthy individuals were included. Brain pathology may further increase the variability.

One possible caveat of our analysis that cannot be neglected is the misregistration when aligning the high resolution T1-weighted and diffusion weighted images. The diffusion-weighted images suffer significant distortions because of susceptibility artefacts, however our analysis indicated that this distortions was minimal in the region of thalamus.

The high inter-subject variability should be accounted for during surgery. The first approach is to standardise the position of the lesion according to internal reference distances such as the length of the AC-PC line, the height of the thalamus and the width of the third ventricle [5,24]. Instead of using the histology-based stereotactic atlas derived from a limited number of brains, recently a population based-probabilistic functional atlas was developed from data gathered from pre-, intra- and postoperative neuroimaging and electrophysiological investigations [8,9]. The extension of this approach is the physiological control of lesion depth during

awaken surgery by monitoring patients complains while trying different stimulation positions.

It follows from the discussion above that, ideally, individual anatomy should be respected when performing stereotactic thalamotomy. Recently, Yamada and colleagues suggested a diffusion-based method for identification of the ventral thalamic nucleus [15]. Their approach incorporates tracking of the cerebello-thalamo-cortical and the spino-thalamic tracts that cross the thalamus, and the identification of anatomical landmarks on short tau inversion recovery (STIR) and fractional anisotropy images [15]. Sedrak and co-workers used the fractional anisotropy weighted color-coded diffusion direction maps to manually segment the thalamus from the surrounding white matter and identify the ventral intermedius nucleus [16] to define target for deep-brain-stimulation (DBS). The connectivity of effective electrode location investigated by tractography showed connections to the sensory-motor cortex and to the cerebellum. Compared to these deterministic approaches our method offers further advantages by utilising probabilistic tractography [14,18]. This method is able to give statistical evaluation of connection probabilities to cortical targets for every thalamic voxel that - by appropriate selection of the cortical targets – are then able to delineate thalamic regions that correspond well to thalamic nuclei as defined by histology [14,18,25]. This approach shows a high intra-subject reproducibility in terms of repeated analysis as well as repeated data acquisitions [25].

Within the ventral thalamic nuclear complex the ventralis oralis anterior/posterior (Voa/Vop) and the ventralis intermedius nucleus (Vim) can be delineated. The true connectivity of these nuclei is debated, and it is hard to mach different nomenclatures [26], but as a rule of thumb it can be said that Vim is the cerebellar receiving area while Vop is the pallidal receiving area of the thalamus [27,28]. More importantly, from our point of view, cortical connectivity of the putative Vim and Vop was recently investigated using diffusion imaging [12]. It was found that Vop seeded tractograms connected to the supplementary motor area (SMA) and to the dorsolateral prefrontal cortex (DLPFC) with higher probability than Vim-seeded tractograms; while the Vim was more likely to connect to the primary motor cortex (M1) and contralateral cerebellum, although significant cerebellar connections were found for Vim as well as for Vop [12]. Here we provide a confirmation of Hyam's pioneering analysis by showing that the Vop and Vim coordinates selected for thalamotomy were indeed effective. The connectivity profile of our patients' thalamotomic lesions were strikingly similar to those described as Vop and Vim connectivity profiles by Hyam [12].

Lesioning or stimulation of the ventral thalamic nuclei is a frequently considered option for the treatment of tremor of various causes including post-traumatic Holmes tremor [29,30,31,32,33,34]. Within the ventral nuclei, Vim is the optimal target in essential tremor [35,36]. It is less and less frequently used in the treatment of Parkinsonian tremor because of the poor benefits for bradykinesia and rigidity [37]. In multiple sclerosis, beside targeting Vim some authors prefer to target Vop suggesting better control of the ataxic component of the tremor [4,38]. In tremor cases developed after injury of the superior cerebellar peduncules or the rubrocerebellar connections (e.g. traumatic brain injury, tumour) tremor control usually is difficult. Reports about the stimulation/lesion of the Vim [32,33,39] and Voa/Vop [40] indicated positive outcome. Foote and colleagues also reported three posttraumatic tremor cases and one MS tremor case that responded to dual Vim-Voa/Vop stimulation [41]. Based on the connectivity profile, the thalamic lesion in our patient was in the Vop. This lesion resulted in excellent tremor control, however the rigidity and the bradykinesia of the affected extremity did not improve significantly. It also has to be mentioned that probabilistic tractography was recently also successfully used in defining connectivity of the pedunculo-pontine nucleus, a novel target for neurosurgical treatment of Parkinson's disease [42].

Conclusions and limitations

Atlas-based targeting for stereotactic functional neurosurgery is a frequently considered option for the treatment of movement disorders. While the overall outcome is reported to be positive, the failures and side effects might be related to the unaccounted inter-individual variability of the target localisation. To overcome such limitations we suggest incorporating information about individual anatomy from diffusion imaging, using connectivity-based segmentations of the thalamic nuclei. However, it has to be pointed out that in the two cases we reported in current analysis we did not plan the targeting with tractography based segmentation a priori of the surgery. Extension of this study to compare the result of the stereotaxic neurosurgery with and without tragtography based targeting is crucial. Further improvements might be expected if additional imaging modalities (e.g. relaxometry, fMRI) could also be utilised.

Author Contributions

Conceived and designed the experiments: ZTK EV PB LV. Performed the experiments: NS LD ZTK PK IV ZK AK MB. Analyzed the data: ZTK NS AK MJ. Contributed reagents/materials/analysis tools: MJ. Wrote the paper: ZTK NS LV. Carried out surgical intervention: ZK IV.

References

1. Hassler R, Riechert T (1954) [Indications and localization of stereotactic brain operations.]. Nervenarzt 25: 441–447.
2. Narabayashi H, Ohye C (1980) Importance of microstereoencephalotomy for tremor alleviation. Appl Neurophysiol 43: 222–227.
3. Benabid AL, Pollak P, Louveau A, Henry S, de Rougemont J (1987) Combined (thalamotomy and stimulation) stereotactic surgery of the VIM thalamic nucleus for bilateral Parkinson disease. Appl Neurophysiol 50: 344–346.
4. Bittar RG, Hyam J, Nandi D, Wang S, Liu X, et al. (2005) Thalamotomy versus thalamic stimulation for multiple sclerosis tremor. J Clin Neurosci 12: 638–642.
5. Dormont D, Cornu P, Pidoux B, Bonnet AM, Biondi A, et al. (1997) Chronic thalamic stimulation with three-dimensional MR stereotactic guidance. AJNR Am J Neuroradiol 18: 1093–1107.
6. Alusi SH, Aziz TZ, Glickman S, Jahanshahi M, Stein JF, et al. (2001) Stereotactic lesional surgery for the treatment of tremor in multiple sclerosis: a prospective case-controlled study. Brain 124: 1576–1589.
7. Morel A, Magnin M, Jeanmonod D (1997) Multiarchitectonic and stereotactic atlas of the human thalamus. J Comp Neurol 387: 588–630.
8. Nowinski WL, Belov D, Thirunavuukarasuu A, Benabid AL (2005) A probabilistic functional atlas of the VIM nucleus constructed from pre-, intra- and postoperative electrophysiological and neuroimaging data acquired during

the surgical treatment of Parkinson's disease patients. Stereotact Funct Neurosurg 83: 190–196.
9. Nowinski WL, Belov D, Benabid AL (2002) A community-centric internet portal for stereotactic and functional neurosurgery with a probabilistic functional atlas. Stereotact Funct Neurosurg 79: 1–12.
10. Deoni SC, Rutt BK, Parrent AG, Peters TM (2007) Segmentation of thalamic nuclei using a modified clustering algorithm and high-resolution quantitative magnetic resonance imaging at 1.5 T. Neuroimage 34: 117–126.
11. Deoni SC, Josseau MJ, Rutt BK, Peters TM (2005) Visualization of thalamic nuclei on high resolution, multi-averaged T1 and T2 maps acquired at 1.5 T. Hum Brain Mapp 25: 353–359.
12. Hyam JA, Owen SL, Kringelbach ML, Phd NJ, Stein JF, et al. (2011) Contrasting Connectivity of the Vim and Vop Nuclei of the Motor Thalamus Demonstrated by Probabilistic Tractography. Neurosurgery.
13. Johansen-Berg H, Behrens TE, Sillery E, Ciccarelli O, Thompson AJ, et al. (2005) Functional-anatomical validation and individual variation of diffusion tractography-based segmentation of the human thalamus. Cereb Cortex 15: 31–39.
14. Behrens TE, Johansen-Berg H, Woolrich MW, Smith SM, Wheeler-Kingshott CA, et al. (2003) Non-invasive mapping of connections between human thalamus and cortex using diffusion imaging. Nat Neurosci 6: 750–757.

15. Yamada K, Akazawa K, Yuen S, Goto M, Matsushima S, et al. (2010) MR imaging of ventral thalamic nuclei. AJNR Am J Neuroradiol 31: 732–735.
16. Sedrak M, Gorgulho A, Frew A, Behnke E, Desalles A, et al. (2011) Diffusion Tensor Imaging (DTI) and Colored Fractional Anisotropy (FA) Mapping of the Ventralis Intermedius (VIM) Nucleus of the Thalamus. Neurosurgery.
17. Smith SM, Jenkinson M, Woolrich MW, Beckmann CF, Behrens TE, et al. (2004) Advances in functional and structural MR image analysis and implementation as FSL. Neuroimage 23(Suppl 1): S208–219.
18. Behrens TE, Woolrich MW, Jenkinson M, Johansen-Berg H, Nunes RG, et al. (2003) Characterization and propagation of uncertainty in diffusion-weighted MR imaging. Magn Reson Med 50: 1077–1088.
19. Smith SM (2002) Fast robust automated brain extraction. Hum Brain Mapp 17: 143–155.
20. Jenkinson M, Smith S (2001) A global optimisation method for robust affine registration of brain images. Med Image Anal 5: 143–156.
21. Behrens TE, Berg HJ, Jbabdi S, Rushworth MF, Woolrich MW (2007) Probabilistic diffusion tractography with multiple fibre orientations: What can we gain? Neuroimage 34: 144–155.
22. Crum WR, Camara O, Hill DL (2006) Generalized overlap measures for evaluation and validation in medical image analysis. IEEE Trans Med Imaging 25: 1451–1461.
23. Guiot G, Arfel G, Derome P, Kahn A (1968) [Neurophysiologic control procedures for sterotaxic thalamotomy]. Neurochirurgie 14: 553–566.
24. Gallay MN, Jeanmonod D, Liu J, Morel A (2008) Human pallidothalamic and cerebellothalamic tracts: anatomical basis for functional stereotactic neurosurgery. Brain Struct Funct 212: 443–463.
25. Traynor C, Heckemann RA, Hammers A, O'Muircheartaigh J, Crum WR, et al. (2010) Reproducibility of thalamic segmentation based on probabilistic tractography. Neuroimage.
26. Hamani C, Dostrovsky JO, Lozano AM (2006) The motor thalamus in neurosurgery. Neurosurgery 58: 146–158; discussion 146–158.
27. Macchi G, Jones EG (1997) Toward an agreement on terminology of nuclear and subnuclear divisions of the motor thalamus. J Neurosurg 86: 670–685.
28. Molnar GF, Pilliar A, Lozano AM, Dostrovsky JO (2005) Differences in neuronal firing rates in pallidal and cerebellar receiving areas of thalamus in patients with Parkinson's disease, essential tremor, and pain. J Neurophysiol 93: 3094–3101.
29. Chen H, Zhuang P, Miao SH, Yuan G, Zhang YQ, et al. (2010) Neuronal firing in the ventrolateral thalamus of patients with Parkinson's disease differs from that with essential tremor. Chin Med J (Engl) 123: 695–701.
30. Franzini A, Cordella R, Messina G, Marras CE, Romito LM, et al. (2011) Deep brain stimulation for movement disorders.Considerations on 276 consecutive patients. J Neural Transm.
31. Hooper AK, Okun MS, Foote KD, Fernandez HH, Jacobson C, et al. (2008) Clinical cases where lesion therapy was chosen over deep brain stimulation. Stereotact Funct Neurosurg 86: 147–152.
32. Kim MC, Son BC, Miyagi Y, Kang JK (2002) Vim thalamotomy for Holmes' tremor secondary to midbrain tumour. J Neurol Neurosurg Psychiatry 73: 453–455.
33. Sanborn MR, Danish SF, Ranalli NJ, Grady MS, Jaggi JL, et al. (2009) Thalamic deep brain stimulation for midbrain tremor secondary to cystic degeneration of the brainstem. Stereotact Funct Neurosurg 87: 128–133.
34. Blomstedt P, Hariz GM, Hariz MI, Koskinen LO (2007) Thalamic deep brain stimulation in the treatment of essential tremor: a long-term follow-up. Br J Neurosurg 21: 504–509.
35. Flora ED, Perera CL, Cameron AL, Maddern GJ (2010) Deep brain stimulation for essential tremor: a systematic review. Mov Disord 25: 1550–1559.
36. Zesiewicz TA, Elble R, Louis ED, Hauser RA, Sullivan KL, et al. (2005) Practice parameter: therapies for essential tremor: report of the Quality Standards Subcommittee of the American Academy of Neurology. Neurology 64: 2008–2020.
37. Pahwa R, Lyons KE, Wilkinson SB, Simpson RK, Jr., Ondo WG, et al. (2006) Long-term evaluation of deep brain stimulation of the thalamus. J Neurosurg 104: 506–512.
38. Critchley GR, Richardson PL (1998) Vim thalamotomy for the relief of the intention tremor of multiple sclerosis. Br J Neurosurg 12: 559–562.
39. Broggi G, Brock S, Franzini A, Geminiani G (1993) A case of posttraumatic tremor treated by chronic stimulation of the thalamus. Mov Disord 8: 206–208.
40. Broggi G, Franzini A, Tringali G, Ferroli P, Marras C, et al. (2006) Deep brain stimulation as a functional scalpel. Acta Neurochir Suppl 99: 13–19.
41. Foote KD, Seignourel P, Fernandez HH, Romrell J, Whidden E, et al. (2006) Dual electrode thalamic deep brain stimulation for the treatment of posttraumatic and multiple sclerosis tremor. Neurosurgery 58: ONS–280-285; discussion ONS-285-286.
42. Muthusamy KA, Aravamuthan BR, Kringelbach ML, Jenkinson N, Voets NL, et al. (2007) Connectivity of the human pedunculopontine nucleus region and diffusion tensor imaging in surgical targeting. J Neurosurg 107: 814–820.
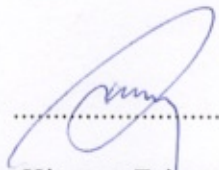
Társszerzői lemondó nyilatkozat

Alulírott **Dr. Kincses Zsigmond Tamás** (felelős társszerző) kijelentem, hogy **Dr. Király András** (pályázó) PhD értekezésének tézispontjaiban bemutatott - közösen publikált - tudományos eredmények elérésében a pályázónak meghatározó szerepe volt, ezért ezeket a téziseket más, a PhD fokozat megszerzését célzó minősítési eljárásban nem használta fel, illetve nem kívánja felhasználni.

Szeged, 2019. 01. 03.

....

dátum

Dr. Kincses Zsigmond Tamás

felelős társszerző

A pályázó tézispontjaiban érintett, közösen publikált közlemények:

Target identification for stereotactic thalamotomy using diffusion tractography.
Zsigmond Tamás Kincses, *Nikoletta Szabó, István Valálik, Zsolt Kopniczky, Lívia Dézsi, Péter Klivényi, Mark Jenkinson,* **András Király***, Magor Babos, Erika Vörös, Pál Barzó, László Vécsei*
PLoS One. 2012 Jan 4; 7(1)